Transient Liquid Phase Bonding of an Oxide Dispersion Strengthened Superalloy

A thesis submitted for the degree of Doctor of Philosophy

by

Suwan Wei

Department of Design, Brunel University

July 2002

Abstract.

Oxide dispersion strengthened (ODS) alloys have been developed with unique mechanical properties. However, in order to achieve commercial application an appropriate joining process is necessary which minimizes disruption to the alloy microstructure. Transient liquid phase (TLP) bonding is a promising joining method, but previous work has shown that the segregation of dispersoids within the joint region results in bonds with poor mechanical strengths. This research work was undertaken to further explore particulate segregation at the joint region when TLP bonding and to develop bonding techniques to prevent it.

A Ni-Cr-Fe-Si-B interlayer was used to bond an alloy MA 758. The effects of parent alloy grain size, bonding temperature, and external pressure on the TLP bonding process were investigated. Three melting stages were identified for the interlayer, and the bonding temperature was chosen so that the interlayer was in the semi-solid state during bonding. This novel bonding mechanism is described and applied to counteract the segregation of Y_2O_3 dispersoids. The grain size of the parent alloy does not alter the particulate segregation behaviour. It is concluded that a low bonding temperature with moderate pressure applied during bonding is preferable for producing bonds with less disruption to the microstructures of the parent alloy. Joint shear tests revealed that a near parent alloy strength can be achieved. This study also shed some light on choosing the right bonding parameters suitable for joining the complicated alloy systems.

A Ni-P interlayer was also used to bond the ODS alloy. Microstructural examination indicated that a thin joint width and less disruption to the parent grain structure were achieved when bonding the alloy in the fine grain state. The time for isothermal solidification was found to be shorter when compared with bonds made with the parent alloy in the recrystallized state. All these observations were attributed to the greater diffusivity of P along the grain boundaries than that of the bulk material. A high Cr content within the parent alloy changes the mechanism of the bonding process. The diffusion of Cr into the liquid interlayer has the effect of raising the solidus temperature, which not only accelerates the isothermal solidification process, but also reduces the extent of parent alloy dissolution.

Acknowledgements.

I would like to express my gratitude to my supervisor, Dr. Tahir Khan, for all his advice and help throughout the course of this work, always cheerfully given; to Dr. Bob Bulpett and everyone in the ETC, Brunel University, for the experimental and financial support; to those staff within the former Department of Materials Engineering, Brunel University, for the enjoyable life together with them; and finally to my wife for her understanding and patience during the time of producing this thesis.

Publications.

Work from this thesis has been presented at:

The Institute for the Joining of Materials conference "JOM-10" held in Helsingør, Denmark, on 16-20 May 2001. The paper was published in the proceedings of the International Conference on the Joining of Materials, JOM-10.

The Institute of Materials conference "The 1st Young Materials Scientist Research Forum" held in London on 22-23 June, 2001. The paper was published in the proceedings of the conference, IOM 2001.

Contents.

Abstract. I

Acknowledgements. II

Publications. III

Contents. IV

Chapter 1 Introduction. 1

Chapter 2 Literature review. 3

2.1 Introduction 3

2.2 Oxide-dispersion-strengthened (ODS) alloys. 4

2.2.1 Introduction. 4

2.2.2 Processing of ODS alloys. 5

2.2.3 Properties and applications of ODS alloys. 6

2.3 Joining methods for ODS alloys. 9

2.3.1 Introduction. 9

2.3.2 Mechanical bonding. 9

2.3.3 Fusion welding. 10

2.3.4 Solid-state welding. 14

2.3.4.1 Friction welding (FW). 14

2.3.4.2 Explosion welding (EXW). 15

2.3.4.3 Solid-state diffusion bonding (SDB) 15

2.3.5 Transient liquid phase (TLP) diffusion bonding 16

2.4 TLP bonding of ODS alloys. 21

2.4.1 Particulate segregation 21

2.4.2 Effect of bonding temperature. 24

2.4.3 Effect of external pressure. 25

2.4.4 Effect of the parent alloy grain size. 26

2.4.5 TLP bonding in a multiple-elemental system. 27

2.5 Summary **29**

Chapter 3 Materials and experimental techniques. 31

3.1 Introduction **31**

3.2 Materials used for TLP bonding. **32**

3.2.1 MA758 ODS alloy. 32

3.2.2 Interlayer alloys. 35

3.2.2.1 Ni-Cr-Fe-Si-B interlayer. 35

3.2.2.2 Ni-P interlayer. 35

3.3 Experimental Techniques **38**

3.3.1 Bonding equipment 38

3.3.2 Specimen preparation and bonding procedures. 39

3.3.3 Post-bond heat treatment. 40

3.3.4 Light microscopy. 41

3.3.5 Scanning electron microscopy. 41

3.3.6 Shear testing. 42

3.3.7 Microhardness test. 43

Chapter 4 TLP bonding using a Ni-Cr-Fe-Si-B interlayer. 45

4.1 Introduction **45**

4.2 The effect of grain size on bonding behaviour. **45**

4.2.1 TLP bonding with the ODS alloy in the fine-grained state. 46

4.2.1.1 Bond microstructure. 46

4.2.1.2 Composition profiles. 54

4.2.2 TLP bonding with the ODS alloy in the recrystallized state. 58

4.2.2.1 Bond microstructure. 58

4.2.2.2 Composition profiles. 63

4.2.3 Summary. 64

4.3 The effect of the bonding temperature on TLP bonding **67**

4.3.1 TLP bonding with the ODS alloy in the fine-grained state. 67

4.3.1.1 Bond microstructure. 67

4.3.1.2 Composition profiles. 73
4.3.2 TLP bonding with the ODS alloy in the recrystallized state. 76
4.3.2.1 Bond microstructure. 76
4.3.3 Summary. 78
4.4 The effects of pressure on bonding. 79
4.4.1 TLP bonding with the ODS alloy in the fine-grained state. 79
4.4.1.1 Bond microstructure. 79
4.4.1.2 Composition profiles. 82
4.4.2 TLP bonding with the ODS alloy in the recrystallized state. 85
4.4.2.1 Bond microstructure. 85
4.4.3 Summary. 86
4.5 Mechanical properties. 88
4.5.1 Shear strength. 88
4.5.2 Microhardness. 102
4.5.3 Summary. 105
4.6 Counteraction of Y_2O_3 dispersoids segregation. 106
4.6.1 Results and discussions. 106
4.6.2 Summary. 110
4.7 Summary. 116
Chapter 5 TLP bonding using a Ni-P interlayer. 117
5.1 Introduction. 117
5.2 The effect of grain size on bonding behaviour. 117
5.2.1 TLP bonding with the ODS alloy in the fine-grained state. 117
5.2.1.1 Bond microstructure. 117
5.2.1.2 Composition profiles. 122
5.2.2 TLP bonding with the ODS alloy in the recrystallized state. 126
5.2.2.1 Bond microstructure. 126
5.2.2.2 Composition profiles. 131
5.2.3 Summary. 134
5.3 The effect of external pressure on TLP bonding. 135

5.4 The effect of Cr on the TLP bonding process..... 139

5.5 Summary..... 144

Chapter 6 Conclusions and recommendations for further work. 145

6.1 Conclusions..... 145

6.1.1 TLP bonding using a Ni-Cr-Fe-Si-B interlayer. 145

6.1.2 TLP bonding using a Ni-P interlayer. 146

6.1.3 Particulate segregation during TLP bonding processes..... 147

6.2 Recommendations for further work. 147

References: 149

Chapter 1 Introduction.

ODS alloy exhibit excellent creep strength and resistance to corrosion at elevated temperatures [1, 2]. There is considerable interest in producing gas turbine vanes, turbine blades, and sheets for use in oxidizing/corrosive atmospheres using these materials. The development of joining techniques used for these alloys is essential and will increase the possibility of manufacturing more complex configurations compared with powder metallurgical techniques. However, joining procedures must be such that joints with optimum properties can be produced. This can only be achieved if the complex microstructure of these alloys, i.e. an even distribution of fine oxide particles and a coarse grain size with a high grain aspect ratio of 6-10 (GAR) can be retained across the joint region.

Fusion welding of ODS alloys has not proved successful because the high temperatures used cause excessive melting of the parent alloy [3]. This results in a weldment without dispersion strengthening and the unique grain structure [4].

Alternative joining methods that do not involve melting of the ODS alloy have also been used, these include friction welding and solid-state diffusion bonding techniques [5, 6]. Solid-state joints in ODS alloys exhibit properties superior to those of fusion weldments. However, joints show a disruption to the grain structures of the parent alloy and do not perform significantly better than a conventional fusion weld [7].

Transient liquid phase diffusion bonding process has considerable potential to join ODS alloys with minimum disruption to the parent microstructure [8]. The TLP bonding process is an isothermal bonding technology, which has been developed for high performance alloys. The application of TLP bonding to join some ODS alloys [9, 10, 11] has been successful. However, the segregation of oxide particles in regions adjacent to the bond-line was observed, and regions devoid of strengthening particles act as sites for failure. Furthermore, little work has been carried out to understand the true mechanisms of TLP bonding when complicated alloy systems are involved.

This study was undertaken to explore the mechanisms of the TLP bonding process in a multiple element system and to investigate the segregation of particles at the joint region. Parameters affecting the TLP bonding process have also been studied with the aim of optimizing the bonding conditions for joining ODS alloys.

The literature review in Chapter 2 considers the development of ODS alloys and some of the joining processes such as fusion welding and solid-state joining methods which have been used to join ODS alloys. The TLP bonding technique is described and the parameters which affect the bonding process are reviewed in detail. Chapter 3 contains the experimental procedures and describes the bonding equipment, bonding techniques and methods used to analyze the joints.

In Chapter 4, a description is given of MA 758 ODS alloy bonded using a Ni-Cr-Fe-Si-B interlayer. The effects of the parent alloy grain size and parameters on the TLP bonding process are discussed. The counteraction of the segregation of Y_2O_3 dispersoids during TLP bonding is explained and an optimized joining technique has been developed.

Chapter 5 describes bonding of the ODS alloy using a Ni-P interlayer. The effect of the parent alloy grain size on bonding behaviour is considered. It is suggested that the high Cr content diffuses from the parent alloy into the liquid interlayer and this alters the solidus temperature of the interlayer, which has a significant effect on the bonding mechanisms. Finally, Chapter 6 presents the conclusions of this study and possibilities for further research are outlined.

Chapter 2 Literature review.

2.1 Introduction.

In the most general sense, joining is a part of fabrication [12] and is the process of attaching one component or structural element to another to create an assembly, where the assembly of the component part is required to perform some function. Ideally, a structure should be designed without joints, because joints are generally a source of weakness or excess weight. In practice, limitations on component size imposed by manufacturing processes and the requirements of inspection, accessibility, repair, portability and assembly, mean that some load-carrying joints are inevitable in all large structures. The revolution which has occurred in materials science and engineering over the past two decades has not been matched by improvements in joining science and technology [13]. It is becoming increasingly apparent that the usefulness of many new materials is limited by our ability to manufacture products made from these materials economically, rapidly and reliably.

In this chapter, the development of ODS alloys is discussed with respect to the mechanical alloying process, properties and applications. The methods for joining ODS alloys are reviewed with particular emphasis on the use of diffusion bonding processes. Finally, the theory behind particulate segregation during the TLP bonding process is discussed and the bonding variables which influence segregation are outlined.

2.2 Oxide-dispersion-strengthened (ODS) alloys.

2.2.1 Introduction.

The term 'superalloy' appears to have been introduced in the late 1950s to describe those materials with a high mechanical strength at elevated temperatures, which are primarily used for the aircraft gas turbine engine [14]. A superalloy is an alloy developed for elevated temperature service, usually based on a group VIIIA element, where relatively severe mechanical stressing is encountered and where high surface stability is frequently required [15]. The key technical requirements for such materials are threefold:

1. mechanical strength at the required temperature;
2. resistance to attack by the environment;
3. ability to be produced in the required component form.

To the metallurgist the challenge was to develop alloys for operation at temperatures well above 1000 °C. These materials must be capable of exhibiting strength as well as resistance to corrosion at these extreme temperatures. Alloying can only partially meet these requirements. Simple alloys, even those solid solution strengthened and precipitation hardened alloys reach the limits of their use below the requirements of many applications. ODS alloys were developed around 1966 at INCO's Paul D. Merica Research Laboratory and made by mechanical alloying (MA) to fulfill this challenge [16].

ODS alloys are strong both at room and elevated temperature [17] (Table 2-1). The elevated temperature strength of these materials is derived from more than one mechanism. Firstly, the uniform dispersion (with a spacing of 1-100 nm) of very fine (5-50 nm) oxide particles (commonly used are Y_2O_3 and ThO_2), which are stable at high temperatures, inhibits dislocation motion in the metal matrix, and increases the resistance of the alloy to creep deformation [18]. Another function of these dispersoids is to inhibit the recovery and recrystallization processes, which allow a very stable large grain size to be obtained [19]. These large grains resist grain rotation during high temperature deformation. A stable large grain size can also be obtained by secondary recrystallization mechanisms [20, 21, 22]. The very

homogeneous distribution of alloying elements during MA gives both the solid-solution strengthened and precipitation hardened alloys more stability at elevated temperatures and an overall improvement in properties. Mechanically alloyed materials also have excellent oxidation and hot corrosion resistance. The increased resistance to oxidation-sulfidation attack is due to the homogeneous distribution of the alloying elements and the improved scale adherence due to the dispersoids themselves [23, 24].

Table 2-1 Room temperature and elevated temperature mechanical properties of commercial ODS nickel and iron-base alloys (after Ref. 25).

Alloy	Test Temperature, °C	0.2% Yield strength, MPa	Ultimate tensile strength, MPa	Elongation, %	Reduction in area, %
MA6000	Room temperature	1220	1253	7.2	6.5
	871	675	701	2.2	4.6
	982	445	460	2.8	1.9
MA754	Room temperature	586	965	21	33
	871	214	248	31	58
	982	169	190	18	34
MA956	Room temperature	517	655	20	35
	1000	97	100	--	--
	1100	69	72	12	30

2.2.2 Processing of ODS alloys.

ODS alloys all use raw materials, such as elemental powders, crushed master alloy (intermetallic) powders and pre-alloyed powders [26]. Oxide powder (i.e.Y_2O_3) lying within a narrow range of crystallite sizes (optimum strength of the alloy is achieved when the crystallite size is less than 30 nm) and metal powders are blended together to form a bulk pre-blended feed stock, the chemical composition of which is verified before actual processing. These ingredients are charged into large, horizontal axis ball mills containing alloy steel balls. Each ball mill is used for the production of one type of alloy. Cross contamination between different alloys is thus avoided, while pick-up from the through-hardened steel balls and the internal parts of the mill is prevented by the accumulation of a protective alloy coating. During milling, an equilibrium powder particle size distribution is established and each individual particle acquires the alloying constituents in the correct proportions. The process is

considered complete when the composite particles have a finely layered structure, not visible under an optical microscope.

The mechanical alloyed powder from the mill is then collected into stainless steel containers and powder from several different containers can be blended together at this stage. After a full chemical analysis, the blend is consolidated at elevated temperatures by either extrusion or hot isostatic processing (HIP). In most cases extrusion is preferred because it is less expensive than HIP and contributes to the work necessary for secondary recrystallization. The powder is loaded into mild steel extrusion cans measuring up to 300 mm in diameter and 900 mm in length and containing up to 28 kg powder. The powder is soaked for several hours in a furnace at the extrusion temperature, during which time homogenization of the powder and true alloying occur, if it has not already occurred during milling. Extrusion is carried out in commercial presses at temperatures, ratios, and speeds that are independent. The ODS alloys have a very fine equaxied submicron grain structure in the as-extruded condition.

Once consolidated, the MA billets are worked to final shape, such as sheet, plate, bar, tube, etc., using normal hot working methods such as extrusion and hot rolling. Virtually, all processing of the nickel-base alloy is performed hot, while cold working operations are possible with the iron-base alloys. The materials are then subjected to a secondary recrystallization anneal at temperatures at or above 1300 °C to produce a coarse grain structure. The combination of oxide dispersion strengthening and the coarse grain structure provides outstanding creep and stress rupture properties at elevated temperatures higher than 1000 °C [27, 28, 29].

2.2.3 Properties and applications of ODS alloys.

2.2.3.1 Nickel-base ODS alloys.

Typical compositions of the commercially available nickel-base ODS alloys are presented in Table 2-2. The most significant advantage of ODS alloys is the increased stress rupture properties. The MA 6000 alloy can maintain a given stress for a much longer time than a conventional alloy for similar vane applications [30]. This is mainly due to the benefits of the combined strengthening modes in the

mechanically alloyed materials.

Table 2-2 Nominal compositions (wt%) of nickel-base ODS alloys.

Alloy	Ni	Cr	Al	Ti	Mo	W	Y_2O_3	Ta
MA 754	Bal	20	0.3	0.5	--	--	0.6	--
MA 757	Bal	16	4.0	0.5	--	--	0.6	--
MA 758	Bal	30	0.3	0.5	--	--	0.6	--
MA 760	Bal	20	6.0	--	2.0	3.5	0.95	--
MA 6000	Bal	15	4.5	0.5	2.0	4.0	1.1	2.0

The nickel-base ODS alloys continue to find applications in a wide variety of industries and are considered mainly for three groups of applications: gas turbine vanes, turbine blades, and sheets for use in oxidizing/corrosive atmospheres. The largest use of MA 754 is as vanes and blades for aircraft gas turbine engines. For this type of application requiring good resistance to thermal fatigue, MA 754 is given a strong texture [31]. The majority of the grains are aligned so that their <100> axes are parallel to the principle working direction along the length of the bar. Such a texture results in low modulus of elasticity (149 GPa) in the longitudinal direction. The low modulus improves resistance to thermal fatigue by lowering stresses for given thermal strains. MA 758 alloy is used in a number of industries where its high chromium content makes it resistant to extremes of temperature and environment. The alloy is used in the glass industry for high temperature components requiring both high temperature strength and resistance to extremely corrosive molten glass. MA 758 alloy is also used for internal combustion engine components, mainly in critical fuel injection parts.

New product forms of the commercial alloys continue to be developed. Large diameter, thin wall tubing of alloy MA 754 has been produced and evaluated for radiant tube applications, and alloy MA 758 has been used as tubing in heat exchangers and process equipment operating at very high temperatures.

The MA 6000 ODS alloy is a more complex alloy developed as a blade material for advanced gas turbines [32]. It is used for first and second stage turbine vanes and blades machined from solid bar. Unlike cast alloys, MA 6000 alloy exhibits nearly flat-rupture-life curves at high temperatures due to the combination of

oxide-dispersion strengthening and high grain-to-width ratios (typically >100 to 1). The characteristics of this alloy allow blade cooling to be reduced or eliminated as the metal temperature can be increased by 100 °C or more in engines where the stresses are uniform or low.

2.2.3.2 Iron-base ODS alloys.

Table 2-3 lists the compositions of iron-base ODS alloys. These alloys combine high temperature strength and stability of oxide-dispersion strengthening with excellent resistant to oxidation, carburization, and hot corrosion. These alloys are suitable for use in gas turbine combustion chambers. The MA 956 [33] alloy is particular well suited for use in heat processing applications. For example, vacuum furnace fixtures made of MA 956 have shown excellent durability and are able to compete with wrought molybdenum, which is also used in these applications. In comparison to molybdenum, MA 956 is ~30% lower in density, providing weight savings and cost advantages. Further, since MA 956 has a lower vapour pressure than molybdenum, it will not coat the inside of the vacuum chamber or the parts being heat treated. Thus, MA 956 rods, flats, and sheets are used in numerous atmosphere and vacuum furnace applications including muffles, baskets, and trays. Alloy MA956 in tube form has also been used for high temperature, severe service applications such as coke injection lance pipes in steel making.

Table 2-3 Nominal compositions (wt%) of iron-base ODS alloys.

Alloy	Fe	Cr	Al	Ti	Mo	Y_2O_3
MA 956	Bal	20	4.5	0.5	--	0.5
MA 957	Bal	14	--	1.0	0.3	0.25

More recently, MA 967 [25] alloy has been evaluated for use as the fuel cladding in fast neutron, breeder reactors. Conventional austenitic alloys are unsuitable for this application due to the dimensional swelling phenomenon caused by the high neutron fluxes.

2.3 Joining methods for ODS alloys.

2.3.1 Introduction.

Joining ODS alloy components increases the possibility of manufacturing more complex configurations than powder metallurgy. However, very little comprehensive information is available regarding the application of joining practice to ODS alloys with considerably more references on the joining of wrought materials [34, 35]. Because of the complex nature of the ODS alloys structure, joining procedure must be carefully designed to produce joints with optimum properties and avoid degradation of the parent alloy properties. When joining ODS alloys, several things need to be considered.

Firstly, the stable oxides, or dispersoids, that are used in the ODS alloy systems have no equilibrium solubility in the liquid phase. If melting occurs, then the dispersoids rapidly agglomerate, and buoyancy floats the oxide to an upper surface. This results in the loss of the primary means of high-temperature strengthening. Agglomerated semi-continuous dispersoids in the partially melted zones are also suspected to contribute to early service failures.

Secondly, at very high temperatures, grain boundaries become a weak link and fracture becomes intergranular. In order to minimize such a grain boundary strength limitation, ODS alloys are produced with a micro-grain size, where the grain boundary areas normal to the principal stresses are minimized without incurring the difficulties inherent in producing single crystals. The elongated grain structure is often referred to as a high grain aspect ratio (GAR). Welds or joints that significantly interrupt this large interlocked grain structure will fail prematurely at extreme temperatures, even if they are produced by solid means.

2.3.2 Mechanical bonding.

Undoubtedly, the oldest method used to join materials together was mechanical means, i.e. mechanical fastening. Mechanical joining methods are often based on localized, point-attachment processes, in which the joint is provided by a nail, a rivet, a screw or a bolt. All such joints depend on residual tensile stresses in the attachment to hold the components in compression. Loads are transferred from one component

to another strictly through the development of mechanical forces from the physical interference or interlocking of component or fastener features at the macroscopic level or through friction arising from interlocking of material aspirates at the microscopic level, or both. In such instances, there is no dependence on the development of any primary or secondary atomic or molecular bonds between the components' materials, although some bonding may occur locally.

Table 2-4 Advantages and disadvantages of mechanical bonding.

Advantages	**Disadvantages**
Simplicity in assembly and disassembly	Creates significant stress concentrations
Can permit relative motion	Utility limited with some materials
Cause no change to chemical composition or microstructure	Allows fluid intrusion or leakage
Allows the joining of dissimilar materials	Installation labour is high
Provides damage tolerance	Often a weight penalty
Simple, no special joint preparation	Joints can loosen

Table 2-4 shows the advantages and disadvantages of mechanical bonding. First and foremost, for the advantages, many mechanical joints are designed for ease of assembly and disassembly without component damage while for the disadvantages, mechanical joints create significant stress concentration at the point of fastening, primarily because of the hole required for or produced by any fastener [36], which is most important when a fatigue-critical structure is involved. The efficiency of mechanical joints can vary considerably, depending on the materials making up the joint element, the design, the geometric factor. Mechanical fastening techniques such as riveting have been used to join MA 957 alloy [37]. However, this type of joint can only be used in relatively low temperature applications.

2.3.3 Fusion welding.

Next to mechanical bonding, welding is unquestionably the oldest method of joining

materials. In welding two components are joined by heating the region at the interface above the melting point of one or other of the components. Like other joining processes, welding offers several advantages and disadvantages. The most significant advantage is undoubtedly that welding provides exceptional structural integrity, producing joints with very high efficiencies. Almost all metals and many polymers glasses and ceramics, as well as the matrixes of many composites, can be welded using a variety of pressure or non pressure, fusion or non-fusion processes, with or without auxiliary filler. For further details see Table 2-5.

Table 2-5 Summary of advantages and disadvantages of welding.

Advantages	Disadvantages
Joints of exceptional structural integrity and efficiency	Prevents disassembly
Wide variety of processes	Heat of welding degrades base properties
Applicable to many materials within a class	Unbalanced heat input leads to disruption or residual stress
Manual or automated operation	Requires considerable operator skill
Can be highly portable	Can be expensive
Leak-tight joints for continuous weld	

The greatest disadvantage of welding is that it prevents disassembly. Often however, this permanency is the reason for its selection as a joining method. But, for joining ODS alloys, extensive heating and melting of the parent alloy presents the worst situation resulting in considerable microstructural disruption.

2.3.3.1 Gas-tungsten arc welding (GTA).

GTA uses a non-consumable tungsten electrode to establish a direct current arc that melts the materials to be welded, as seen in Figure 2-1 [35]. An inert gas shield of argon, helium, or various commercial mixtures is used to protect the electrodes and

weld pool from oxygen, nitrogen, and hydrogen contamination and to stabilize the arc characteristics for improved welding performance. Filler wire, if used, is usually added to the leading edge of the weld pool to fill the joint [38].

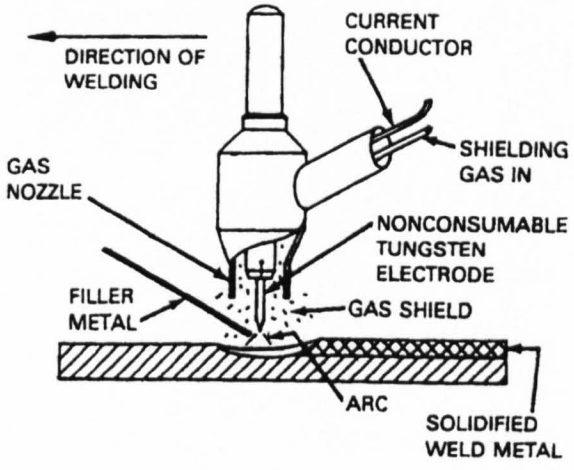

Figure 2-1 GTA welding operation.

GTA welding of ODS alloys is typically carried out using minimal welding current and techniques that are designed to minimize melting of the alloys. When welding alloys with significant aluminium content, such as MA 956, there is a high propensity for an aluminum-rich light grey oxide film to form on the weld-bead surface [35]. The dispersoids from the melted parent alloy also float to the weld-bead surface. These oxides should be removed by light abrasive techniques before subsequent weld beads are deposited, in order to prevent incomplete fusion defects or oxide inclusions. Slow cooling may be required for complex welding structures to avoid weld cracking [39]. The grain structure of the weldment is equaxied as compared with the elongated grain structure of the parent alloy [40]. A weld centre-line perpendicular to the direction of the original grain structure and a loss in dispersoids are seen and therefore result in weldments exhibiting strength well below that of the ODS alloy. Joint properties are only representative of conventional wrought alloys and the level of creep strength achieved at very high temperatures has not been matched. Attempts have been made to either design welds as attachments that are subjected to reduced stresses or place the welds in cooler locations where they can withstand the stress. GTA welding is also used for applications in which the alloy's resistance to corrosive attack at high temperature is required rather than the limits of its strength.

2.3.3.2 Gas-metal arc welding (GMAW/MIG).

Unlike GTA, GMAW/MIG uses a continuous wire electrode that establishes the arc and furnishes filler metal into the weld pool [35]. A shielding gas mixture is used where the composition of the mixture is dependent on the mode to protect the molten weld pool from atmospheric contamination and to provide the correct arc characteristics, as seen in Figure 2-2.

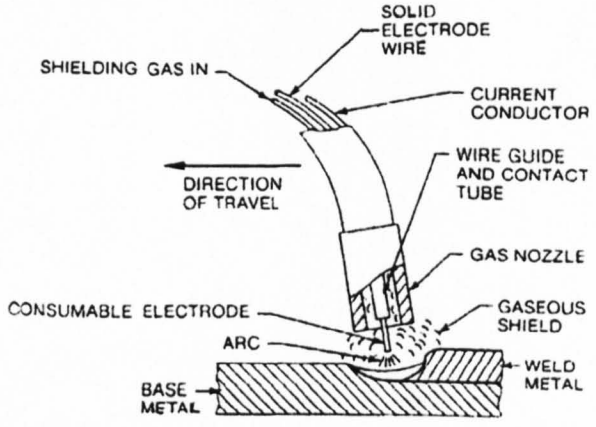

Figure 2-2 MIG welding operation.

GMA welding of ODS alloys is typically implemented with pulsed or synergic power sources and low-to-average current settings to minimize the melting of the base metals. This technique is most used in welding nickel-base ODS alloys. Similar to GTA welds, poor mechanical properties are achieved and the same precautions must be considered in the welding design [35].

2.3.3.3 Electron-beam (EBW) and laser-beam welding (LBW).

EBW is a sophisticated welding process that incorporates a beam of concentrated high-velocity electrons into a narrow, very intense source of heat. The weld is generally accomplished in a vacuum at pressures from medium to high vacuum. LBW is similar to EBW, but uses a focused laser to vaporize metal at the joint interface. Typically, CO_2 lasers are used with inert shielding gases such as helium [35].

EBW and LBW have been used to join MA 956, and the best results have been obtained in lap joints where the beam is oriented as close to parallel to the joint as possible. In butt joints, the best results can be obtained by inclining the joint and

beam as much as possible from 90 ° [41, 42]. LBW has been used in joining of MA756 alloy [43]. Due to the highly concentrated energy source and fast processing speed, LBW resulted in a small volume of the parent alloy being melted and solidified. Therefore the weldment is of better quality and dispersoids agglomeration is significantly reduced compared with TIG welding [44, 45]. However, similar to the TIG welding, LBW resulted in a loss of grain orientation, which further contributed to the loss of strength of the weldment.

2.3.3.4 Resistance projection welding (RPW).

During RPW, the joining surfaces are heated by the electrical currents generated in materials at the weld. The joint must be free of contamination to obtain uniform weld soundness.

RPW has been used to join MA 956 alloy. An RPW of ODS alloys is typically implemented with parameters designed to minimize the thickness of the weld nugget and solidification time (high current, tip pressure, and minimum weld time). Delayed hydrogen cracking can occur in iron-base ODS alloys, particularly in thicker restrained pieces if preheated, minimum inter-pass temperatures, and post-weld diffusion treatments are not employed. The grain growth in the weldment is opposite to the direction of the grain structure of the parent ODS alloy. Thus, the properties of the joint are less than the parent alloy's [46]. The commercial practicality and benefits of these techniques still need to be defined better.

2.3.4 Solid-state welding.

Solid-state joining processes involve no melting and joint formation relies on the application of pressure. Bonding is achieved by the introduction of mechanical, electrical, or thermal energy and/or diffusion.

2.3.4.1 Friction welding (FW).

FW, in its simplest form, involves two axially aligned parts, with one part rotating against a stationary part under an applied pressure. The pressure is increased to generate the frictional heat necessary for welding at the contacting surfaces in order

to form a solid-state joint.

FW is capable of creating sound solid-state joint in ODS alloys [47]. The plastic deformation and flow at the bond interface typically produce a relatively straight grain-boundary interface. Given sufficient high welding pressure and metal displacement, sound friction welds were made in MA754 ODS alloy [48]. The best results have been obtained by welding the ODS alloy in the fine-grained, unrecrystallized state and then subjecting the joint to a recrystallization anneal. This boundary interface normal to the principal stresses is undesirable, and it produces properties that are no better than most fusion processes [49].

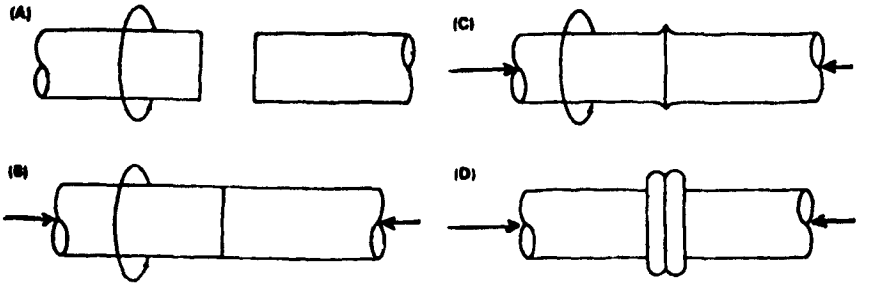

Figure 2-3 Basic steps in friction welding.

2.3.4.2 Explosion welding (EXW).

EXW is a solid-state metal-joining process that uses explosive force to create a metallurgical bond between two metal components. Although the explosive detonation generates considerable heat, there is no time for heat transfer to the metal components. Therefore, there is no appreciable increase in temperature to lead to any melting [35].

EXW generally creates a favorable grain structure by virtue of the lap joints used. In a limited study in which MA956 was joined, the best results were obtained by bonding coarse-grained alloy and then using a post-weld heat treatment at 1100 °C for 10 hours [50].

2.3.4.3 Solid-state diffusion bonding (SDB).

Diffusion bonding in the solid-state is a micro-deformation process which involves holding components under load at an elevated temperature usually in a protective

atmosphere or vacuum. A metal interlayer (diffusion aid) may or may not be used between the faying surfaces.

Moore and Glasgow [51] have shown that diffusion bonding of a nickel-base ODS alloy, MA 6000, is feasible. The process has also been applied to joining alloy MA956 [52], and the results show great potential for the fabrication of components for high temperature applications. Whether such a joint is sufficiently defect-free on the nano-metre scale to give parent alloy creep resistance remains to be seen, but they do offer the possibility of achieving good bonds.

2.3.5 Transient liquid phase (TLP) diffusion bonding.

2.3.5.1 Introduction.

TLP bonding is a joining process which relies on isothermal solidification for joint formation. This joining technique is capable of achieving an ideal bond, with the bonded zone showing a composition and microstructure which closely matches that of the components. TLP bonding has been applied to many metallic systems [53], and more recently TLP bonding has been developed by investigators working in the aerospace industry as a technique for joining high temperature materials, for example nickel and cobalt based alloys without having to apply substantial pressure during bonding [54]. TLP bonding is now finding use in applications which require high thermal, electrical, chemical and/or mechanical stability such as in electrical connectors, turbine vanes and metal matrix composites (MMCs).

During TLP bonding, a thin layer of liquid forms at the joint interface and wets the contacting surfaces, and then solidifies isothermally on holding at the bonding temperature. Liquid film formation during TLP bonding depends on the formation of a low melting point eutectic or peritectic at the joint interface. An interlayer is clamped between the contacting metal surfaces and entire assembly is heated to the bonding temperature. At the bonding temperature, which is normally slightly above the eutectic temperature, inter-diffusion between the interlayer and base metal causes a liquid layer to form. Because of the difference in diffusivities on either side of the solid/liquid interface, dissolution of the base metal into the liquid layer occurs much faster than diffusion of the solute out of the metal. Widening of the liquid layer

occurs until the concentration within the liquid becomes saturated throughout with the constituent of the base metal. Continued diffusion of elements from the interlayer into the base metal reduces the solute concentration within the joint to a value below that required to sustain the liquid-state and the joint region begins to solidify. A post-bond homogenisation reduces this concentration even further and the re-melt temperature of a joint is very near or equivalent to that of the melting temperature for the parent alloy. All stages of the TLP bonding process depend on solute diffusion from the joint centre-line region into the parent alloy.

The interlayers used for joining nickel based alloys are based on the use of chromium or nickel interlayers alloyed with melting depressants such as boron and silicon. The interlayer is held between the components to be bonded and the assembly is then heated in a protective atmosphere to a temperature above the melting point of the interlayer. The molten interlayer wets the components and the boron diffuses very rapidly into the bulk alloy. As the boron diffuses, so the melting point of the interlayer rises, until it exceeds the bonding temperature. At this point the interlayer will isothermally solidify to complete the joining process. The final microstructure is generally indistinguishable from that of the bulk components, and hence the mechanical properties tend to be similar to that of the parent alloys. For joining alloys, TLP bonding has some definite advantages. Firstly, joint formation is isothermal and no large scale melting of the parent alloy occurs so that the disruption to the parent microstructure is avoided. Since the joining technique depends on capillary flow, the joint preparation before bonding is relatively simple. The adjustment of the gap between the joining surfaces permits the repair of defects up to 100μm wide. By contrast with diffusion bonding [55, 56], the joining process is highly tolerant of the presence of a faying surface oxide layer. For this reason, and because of the absence of thermal stresses, TLP bonding is ideal when joining intermetallic parent alloys which have stable oxide surface films and are highly sensitive to microstructural changes, and have poor low temperature ductility [57, 58, 59]. This bonding process is also suitable for joining parent alloys which are inherently susceptible to hot cracking or post-weld heat treatment cracking problems [60]. Also, the process is suited to the fabrication of large and complex shaped components. However, some disadvantages include the need for rapid heat-up,

bonding times can be in the order of a few hours, a post-bond heat treatment for age hardening alloys is required [53], and also sometimes there is tendency of intermetallic compound formation [61, 62].

2.3.5.2 The transient liquid phase bonding process.

The mechanisms of the TLP bonding process can be divided into a number of stages although in reality there are competing reactions occurring on different time scales [63]. Duvall *et al.* [54] examined TLP bonding and suggested that the process comprised three stages: base metal dissolution, isothermal solidification of the liquid phase and joint homogenization. However, Tuah-Poku *et al.* [64], who TLP bonded silver using a pure copper interlayer suggested that the interlayer melting and widening of the liquid zone at the bonding temperature were separate stages. MacDonald and Eagar [53] pointed out that a further stage should be included to account for solute diffusion during the heating cycle to the bonding temperature. This is particularly important if thin interlayers are used, diffusion of the interlayer into the parent alloy during the heating stage results in insufficient liquid forming at the bonding temperature and a poor quality joint. It is also worth mentioning that a low heating rate between the eutectic temperature and the bonding temperature can have an important effect on process kinematics during TLP bonding [65]. The TLP bonding process is considered below in Figure 2-4 and Figure 2-5.

Stage 1 – Heating-up.

This is the heating stage, where the component is heated to the interlayer melting temperature. During heating, inter-diffusion occurs between the interlayer and the parent alloy so that the solute concentration $C^{\alpha S}$ at the parent alloy/interlayer interface changes with temperature following the solidus line in the binary diagram. This stage is particularly important when using a very thin interlayer, as found out by Niemann [66] and Li *et al.* [67], i.e. if heating rate is too slow then the interlayer will not melt due to insufficient melting depressant left within the interlayer.

Stage 2 – Melting of the interlayer and dissolution of the parent alloy.

Two pieces of the parent alloy, A, are to be joined by an interlayer of B. The melting of B results from a mixing of A and B atoms at the A/B interface and it starts when

the interface attains the concentration equal to $C^{\alpha L}$. Since there is a definite concentration gradient at the interface, the dissolution of B is very rapid. The diffusion at this stage is controlled by D_L, the diffusivity in the liquid. The total time required for the dissolution of the interlayer, B, may be of the order of seconds. The driving force for continuous dissolution of B is proportional to the difference $C^{L\beta}$ - $C^{L\alpha}$, which expresses the width of the eutectic depression. The resulting liquid has an average concentration of B greater than $C^{L\alpha}$ and therefore is not in equilibrium with the adjoining solid. The parent alloy dissolves into the liquid to dilute the liquid and hence the width of the liquid increases. The temperature increases from the melting temperature to the bonding temperature (T, in Figure 2-4) and the solute concentrations, $C^{L\alpha}$ and $C^{\alpha L}$, and $C^{L\beta}$ and $C^{\beta L}$ at the solid/liquid interfaces are changing with temperature following the solidus and liquidus lines in the binary phase diagram. When the samples are held at the bonding temperature, three metallurgical phases (α, β, and liquid) are present at the dissolution stage. At the end of this stage, the liquid zone has reached its maximum width.

Stage 3 – Isothermal solidification.

In this stage, the liquid zone isothermally solidifies as a result of solute diffusion into the parent alloy at the bonding temperature. The solid/liquid interface reverses direction and the liquid zone shrinks as the liquid becomes enriched in A and impoverished in B. The solute concentrations at the solid/liquid interface $C^{L\alpha}$ and $C^{\alpha L}$ are unchanged during this stage and the width of the liquid zone decreases continuously until the joint completely solidifies. The solute distribution in the liquid is uniform during almost all of the isothermal solidification stage. The rate of loss of solute B, from the liquid to the solid α-phase controls the interface displacement rate. Since this is determined by the rate of diffusion of B into the α-phase, the process is slow, because it relies on solid-state diffusion. Therefore, the isothermal solidification is generally considered to be the most important stage, because the time required for TLP bonding is determined by this stage.

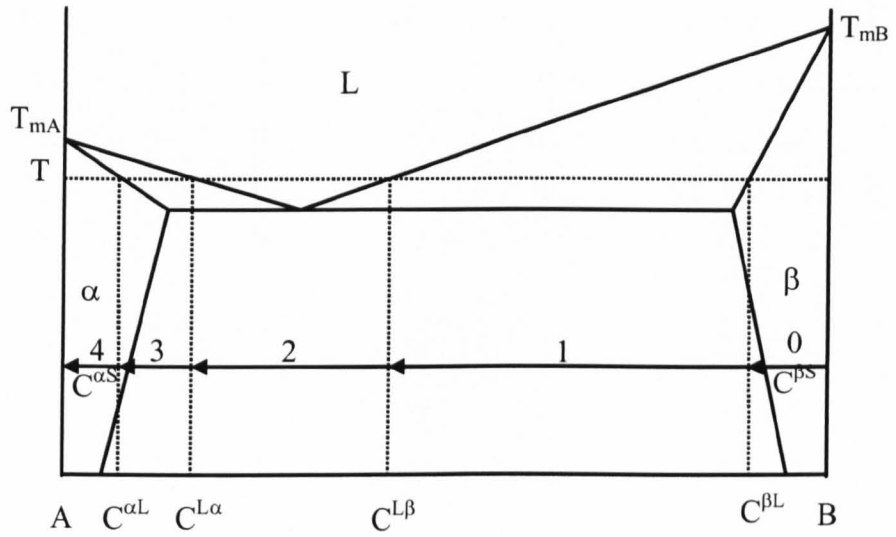

Figure 2-4 Schematic of a binary eutectic phase diagram showing the stages in TLP bonding.

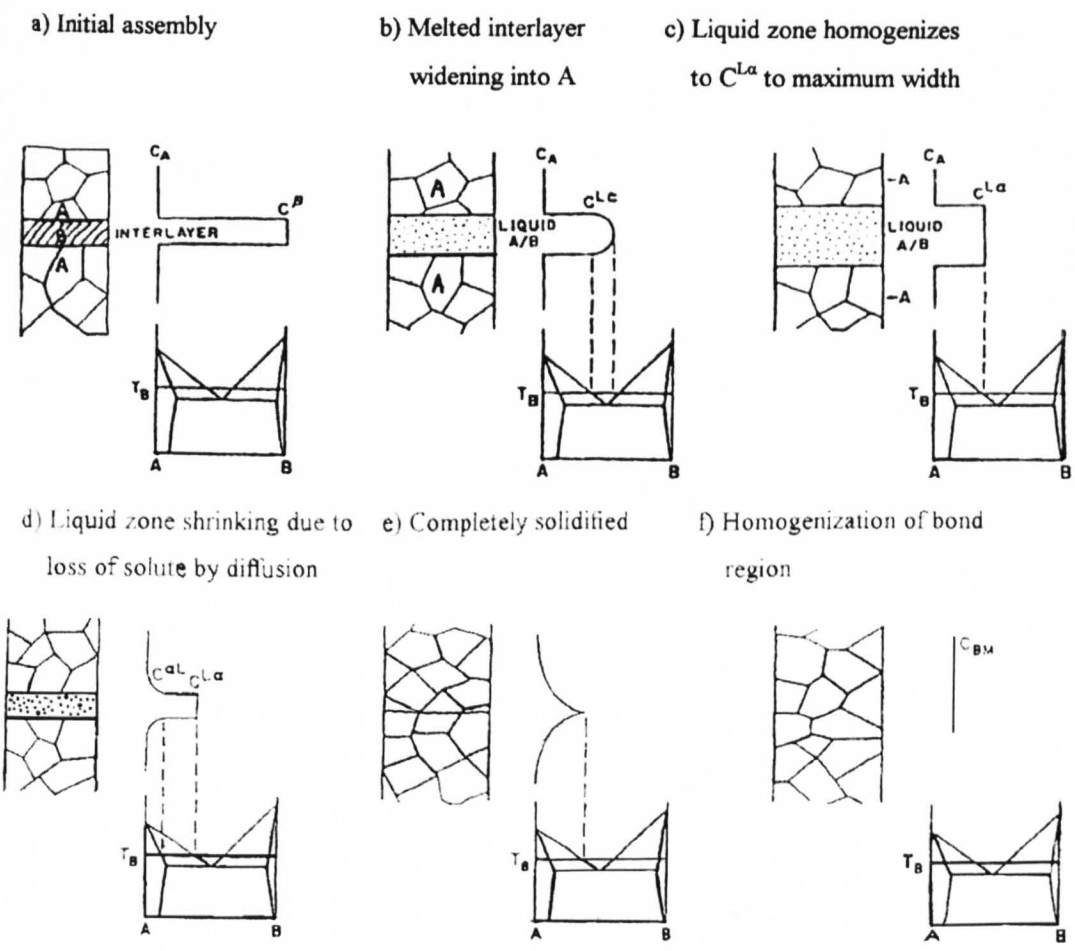

Figure 2-5 Schematic illustration of the TLP bonding process [64].

Stages 4 Homogenization of the joint.

In order to homogenize the bond region, further annealing may be done at an appropriate temperature. Again Ds, the diffusion rate in the solid, is the dominant parameter and the annealing time may be quite long. The bulk of the bonding time in the bonding process is therefore taken up by stages 3 and 4.

2.4 TLP bonding of ODS alloys.

With ODS alloys, if the parent alloy properties are to be achieved, it is essential to retain an even dispersion of reinforcing particles and a grain microstructure continuous across the joint region.

At the end of stage 2 of the TLP bonding process, the interlayer (solute) concentration in the liquid layer has homogenized to the equilibrium concentration $C^{L\alpha}$ and the liquid layer has attained its maximum width. Continued diffusion of the solute into the parent alloy results in isothermal solidification. The planar solid/liquid interface moves towards the middle of the joint.

2.4.1 Particulate segregation.

When a moving solidification front intercepts an insoluble particle, it can be pushed, engulfed or entrapped. Engulfment occurs through growth of the solid over the particle, followed by enclosure of the particle in the solid and these steps are required to achieve a uniform particle distribution. If the solidification front breaks down into cells, dendrites, or equaxied grains, as in a casting, two or more solidification fronts can converge on the particle, If the particles is not engulfed by one of the fronts, it will be pushed in between two or more solidification fronts and will finally be entrapped in the solid at the end of local solidification. It is considerably easier to understand particle behaviour at the solid/liquid interface in directional solidification processes where particles can only be pushed or engulfed and where a planar interface is maintained.

There are two basic theoretical approaches to the study of particle behaviour at a solid/liquid interface. The thermodynamic model [68] predicted engulfment when the net change in free energy due to engulfment was negative. The total energy for

engulfment has been calculated as 8.283 Nm^{-1} in Al-SiC MMCs [69]. This means that SiC particles will always be pushed in an Al-SiC system. Experimental observation revealed this was not necessarily true and the kinetic approach must also be considered [69].

The kinetic approach [70] was based on the simple idea that as long as a finite layer of liquid exists between the particle and the solid, the particle will not be engulfed. Pushing was said to take place due to repulsive forces between the particle and the solid and engulfment was due to the drag forces.

The concept of a critical interface velocity, Vc, was postulated [70] and at interface velocities below Vc the particles are pushed and velocities above Vc the particles are engulfed. This concept has now become widely accepted [71] and analytical models to explain the pushing or engulfment of insoluble particles by the advancing planar solid/liquid interface have been developed [72]. The critical velocity is given by the relationship:

$$Vc = \Delta\sigma a_0 / 12\eta\alpha R \tag{2.1}$$

where $\Delta\sigma$ is the relative surface energy difference $[(\sigma_{ps} - (\sigma_{pl} + \sigma_{sl}))]$, σ_{ps} is the interfacial energy between the particle and the solid; σ_{pl} is the interfacial energy between the particle and the liquid, σ_{sl} is the interfacial energy between the liquid and the solid]; a_0 is a dimensional constant; η is the viscosity; α is the thermal conductivity ratio of the particle and the melt; and R is the radius of particle. For a given rate of movement of the solid/liquid interface, V, particles having radii larger than Rc would be engulfed and the particles with radii less than Rc would be pushed, as shown in

$$Rc = \Delta\sigma a_0 / 12\eta\alpha V \tag{2.2}$$

It has been demonstrated that the critical rate of solid/liquid interface movement becomes extremely high when the particle radius is less than 10 μm [73]. Figure 2-6 shows the calculated relationship between the critical velocity, Vc, and the particle radius, R, when a 20% alumina reinforced aluminium-based MMCs was TLP bonded at a temperature of 580 °C. In these calculation, $\Delta\sigma$ = 1.0 Nm^{-1} (an estimated value taken from [71]), $a_0 = 2 \times 10^{-10}$ m, η = 0.005 Pa s and α = 0.146.

Additional variables, such as solid/liquid interface shape and the temperature gradient ahead of the interface must be considered in metal-ceramic systems of practical importance, such as in MMCs and ODS alloys.

Particle segregation has been observed when TLP bonding particle reinforced copper, [74], yttria-bearing ODS alloys such as MA956 [75], and during TLP bonding of aluminum-based MMCs materials containing alumina and silicon carbide particles [74]. Particles segregating towards the bond-line create a depleted zone between the region of higher particle density adjacent to the bond-line and the parent alloy which promotes preferential failure during tensile testing [74].

In experiments using an aluminium-magnesium alloy containing SiC particles directional-solidified at various cooling rates, increasing the rate of interface movement from 16 $\mu m\ s^{-1}$ (for a temperature gradient of 95 $^{\circ}C\ cm^{-1}$) to 40 $\mu m\ s^{-1}$ (for a temperature gradient of 117 $^{\circ}C\ cm^{-1}$) altered the behaviour from particle pushing to engulfment [69]. In the case of aluminium-nickel alloys containing SiC particles, particles were pushed when the rate of interface movement was up to 155 $\mu m\ s^{-1}$ and the temperature gradient was as low as 70 $^{\circ}C\ cm^{-1}$. For similar solidifying conditions, particle engulfment occurred in the aluminium-magnesium-SiC melts. This difference in behaviour was attributed to the flat solid/liquid interface profile and a lower viscosity in the aluminium-nickel-SiC melt.

The rate of interface movement during the isothermal solidification stage of TLP bonding is extremely slow. The average rate of interface movement was found to be $2 \times 10^{-4}\ \mu m\ s^{-1}$ when TLP bonding coarse grained nickel [76] and $5 \times 10^{-4}\ \mu m\ s^{-1}$ when silver was TLP bonded using a copper interlayer [64]. The average rate of interface movement was measured at approximately $1 \times 10^{-3}\ \mu m\ s^{-1}$ during the TLP bonding of an aluminium-based MMC using a copper interlayer at a bonding temperature of 580 $^{\circ}C$ [75].

The literature indicates that when particles have radii less than a critical value they tend to be pushed ahead of the moving solid/liquid interface and it is suggested that particulate segregation will occur during the isothermal solidification stage of TLP bonding.

Other variables affecting particulate segregation include bonding temperature, base metal grain size, interlayer thickness, heating rate and their combined effect on the liquid width at T_B.

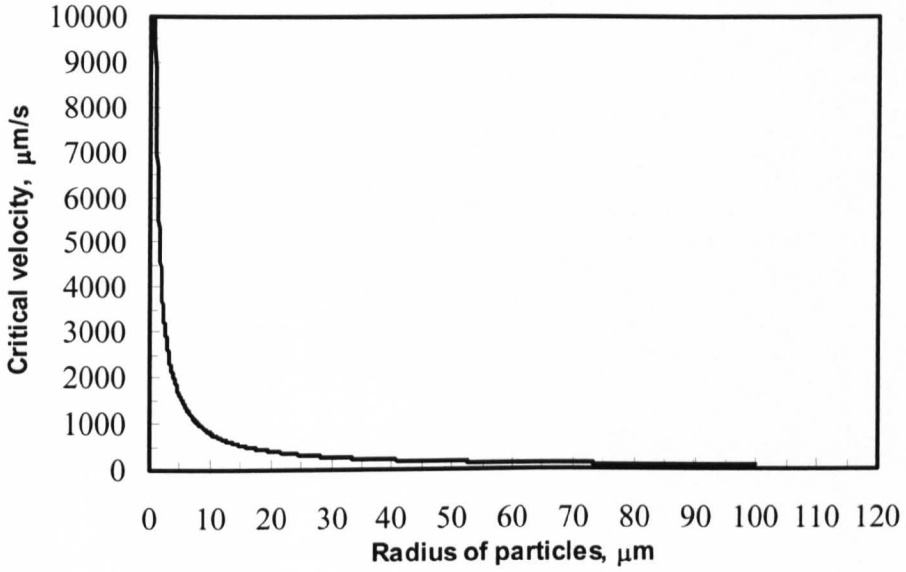

Figure 2-6 Relationship between the critical rate of solid/liquid interface movement and the particle radius during TLP bonding of alumina reinforced MMCs at a bonding temperature of 580 °C.

2.4.2 Effect of bonding temperature.

The bonding temperature selected is important because as the bonding temperature increases the liquid width increases. During the dissolution of the parent alloy, the parent alloy dilutes the solute-rich liquid interlayer until the concentration equals the equilibrium concentration, $C^{L\alpha}$, as seen in Figure 2-4. As the bonding temperature is increased, $C^{L\alpha}$ reduces following the liquidus line on the binary phase diagram. More parent alloy is required to dilute the liquid layer and consequently the width of the liquid layer is increased. This is important when joining ODS alloys because minimal parent alloy dissolution is necessary to avoid disruption to the microstructure of the parent alloy. Also, it has been indicated [67] that segregation will not occur during TLP bonding if the liquid width at the bonding temperature is less than some critical value. Therefore, it is important to be able to keep the width of the liquid interlayer/dissolution of the parent alloy as small as possible by choosing a low bonding temperature.

During the isothermal solidification the change in liquid width follows a parabolic law [75]:

$$W_{max} - W(t) = 4\beta t^{1/2} \qquad 2.3.$$

where β is the rate constant and W(t) is the liquid width at bonding time t. The rate constant, β, can be derived if the interface displacement, ΔX, is plotted against the square-root of the hold time, t, at the bonding temperature, i.e.

$$\Delta X = 2\beta t^{1/2} \qquad 2.4.$$

Constant β can be calculated numerically using the relation:

$$(C_{L\alpha} - C_{\alpha L})\beta\pi^{1/2} + \frac{D^{1/2}(C_{\alpha L} - C_M)}{1 - erf(\beta / D^{1/2})} \times \exp(-\frac{\beta^2}{D}) = 0 \qquad 2.5.$$

where C_M is the original solute concentration; D is the solute diffusion coefficient, $C_{L\alpha}$ is the solute concentration in liquid at the solid/liquid interface and $C_{\alpha L}$ is the solute concentration in solid at the solid/liquid interface.

Reducing the bonding temperature causes the solute diffusion coefficient and the rate constant value to decrease. Therefore, the time required for isothermal solidification will be longer. This will reduce the rate of movement of the solid/liquid interface, which is in favourable for particulate segregation.

It has been suggested that selection of the optimum bonding temperature during TLP bonding depends on the interplay of increasing solute diffusivity and decreasing equilibrium solute concentration in the solid [64].

2.4.3 Effect of external pressure.

Applying a moderate compressive load to the brazing method has been reported to compare favorably with the conventional TLP bonding process. Rabinkin and Pounds [77] found that when TLP bonding copper with a copper-phosphorous interlayer under an applied pressure of 9.8MPa, its Charpy impact energy was increased and the microstructure of the joint was changed. An ejection model had been proposed to explain the increase in the joint strength. According to this model, the liquid phase was enriched with melting temperature depressants and was ejected out of the joint region. This results in the loss of brittle intermetallic phases. A similar beneficial

effect from applied pressure during TLP bonding of an Al alloy was found by Dammer [78]. This mechanism has also been confirmed by Yeh and Chuang [79]. It was found out that the tensile strength and shear strength of the joint increased with applied pressure when TLP bonding INCONEL 718 alloys using a Ni-P interlayer.

The effect of pressure during TLP bonding of ODS alloys has not been reported. However, research on TLP bonding of MMCs has revealed that the joint shear strength increased with applied load [75, 80], which was attributed to a decrease in the mount of particulate segregation when using higher loads. In the meantime, some pressure is always necessary during TLP bonding to ensure adequate contact between the surfaces and the interlayer [81, 82]. Therefore, it is suggested that applying extra pressure during TLP bonding of ODS alloy could help in avoiding particle segregation and in increasing mechanical properties.

2.4.4 Effect of the parent alloy grain size.

The literature indicates that the parent alloy grain size affects the isothermal solidification rate during TLP bonding. This is because TLP bonding is a diffusion controlled process and any factor that affects diffusion will alter the process kinetics. When a polycrystalline parent alloy is TLP bonded, solute diffusion will depend on a number of factors, including grain size. When the grain size of the parent alloy is reduced, more grain boundaries are involved in the diffusion of solute. This means a faster diffusion rate of solute because diffusivity along grain boundaries is much greater than in the bulk materials, especially when the temperature is in the range $T \leq 0.5 - 0.75T_m$ (where T_m is the melting temperature, K) [83]. Therefore, dissolution of the parent alloy was less and a shorter time for completion of isothermal solidification was observed when bonding the parent alloy in the fine-grained state.

It has been observed that the rate constant, β, (see equation 2.4) increases when a fine grain size parent alloy was employed during TLP bonding of a nickel alloy [76]. The rate constant increased from 0.046 $\mu m\ s^{-1/2}$ to 0.074 $\mu m\ s^{-1/2}$ when the parent alloy grain size decreased from 4 mm to 40 μm.

The solidification rate increases due to liquid penetration along grain boundaries intersecting the bond region. This is in turn increased the solid/liquid interfacial area

increasing solute diffusion at the grain boundary region [76, 84]. A detailed explanation of the grain boundary grooving phenomenon was first proposed by Mullins [85, 86]. Grooving occurred as a result of surface/condensation, volume diffusion in the fluid and evaporation/condensation. The driving force for interface migration emanates from interfacial curvature. Consequently, a flat interface that has no intersection with a grain boundary will not migrate. This is a quite different situation from that during TLP bonding. The driving force for interface migration during TLP bonding results from the concentration gradient in each phase, and interface migration will occur even when the interface is flat and there is no grain boundary intersection (e.g. in a single crystal bonding situation). The material transport mechanisms comprise volume diffusion in each phase, interfacial diffusion, and grain boundary diffusion. Ikeuchi *et al.* [87] simulated solid/liquid interface migration in the grain boundary region during TLP bonding of a nickel-based alloys using a Ni-19at%P interlayer. Liquid penetration at the grain boundary was only apparent near the end of the dissolution process. Liquid penetration is more pronounced when the hold time increases during the isothermal solidification stage. These observations correspond well with the experimental results observed by Saida *et al.* [88]. Kokawa *et al.* [76] indicated that liquid penetration could not be observed during the dissolution process, but become more pronounced when the hold time increased during the isothermal solidification stage of TLP bonding.

However, the average rate of solid/liquid interface movement is still extremely slow when the fine grained parent alloy is TLP bonded. In this study, it will be answered whether the parent alloy grain size would affect particle segregation behaviour or alter the degree of disruption to microstructure of the parent alloy.

2.4.5 TLP bonding in a multiple-elemental system.

When an alloy is TLP bonded using an interlayer, assumptions are made to simplify the problem, e.g. no formation of intermetallic phases, only diffusion of one solute plays the key role, no metallic reaction during bonding. However, in most cases the TLP bonding process is far more complicated when joining alloys.

Direct experimental evidence for the formation of an intermediate phase at the bonding temperature has been presented by Gale and Wallach [89]. During TLP

bonding of a nickel-based alloy using a Ni-Si-B interlayer, Ni_3B is formed in the parent alloy immediately adjacent to the original solid/liquid interface. Boride formation was seen both above and below the eutectic temperature for the Ni-B binary eutectic system. When bonding at a temperature higher than the Ni-B binary eutectic temperature, extensive dissolution of the parent alloy was observed. Once formed, borides remained stable with further change in hold time. Following completion of isothermal solidification, the borides could be observed as a near continuous band demarcating the original position of the solid/liquid interface. This was attributed to the more rapid diffusion of B in nickel than Si in nickel, which resulted in a local, non-equilibrium composition profile. In NiAl/Ni-Si-B/Ni joints, Orel *et al.* [90] observed that boride formation and liquation within the nickel substrates proceeded in a similar manner. This was attributed to the lower B diffusivity in NiAl than Ni.

Information regarding the phase diagram and diffusivity data is an essential requirement for rigorous modelling of TLP bonding process. Unfortunately, this type of information is unavailable at present. This is why most of the research on TLP bonding has been focused on quite simple systems, e.g. a pure metal TLP bonded using a pure metal interlayer or a binary eutectic interlayer. Little research has been done on complex alloys containing more than three elements and bonds made using an interlayer containing more than three elements. When complex alloys are TLP bonded, researches concerning the mechanisms have been independently modelled to the detailed microstructural studies. This has resulted in some of the basic assumptions in modelling not being supported by direct microstructural observations in real joints. In particular, the key assumption that intermetallic phase formation does not occur during isothermal solidification is questionable. For example, it has been shown that an intermediate phase (Ni_3B) forms at the bonding temperature when Ni and NiAl/Ni parent alloys are TLP bonded using a Ni-Si-B interlayers. It is therefore difficult to understand the bonding process and not possible to optimize the conditions when joining commercial alloys using interlayers available in industry.

2.5 Summary.

ODS alloys exhibit excellent high temperature strength with good resistance to oxidation and corrosion. These alloys combine a stable large grain size, high grain aspect ratio, and an even dispersion of oxide particles to produce properties previously unattainable by conventional alloys. Developing a suitable joining technology is essential for ODS alloys because components with complicated designs, such as blades and vanes as well as combustion chambers, can not be made by other methods. The joint must exhibit properties suitable for service but must be produced without degrading the properties of the ODS alloy.

Fusion welding techniques have been used to join ODS alloys, but the melting process results in oxide agglomeration, so that the dispersion strengthening effect within the joint is no longer effective. Melting and re-solidification of the weld also produce an equaxied grain structure and a grain boundary perpendicular to the parent grain structure, resulting in a degradation of properties of the ODS alloy. While weldments exhibit strength properties significantly less than the parent alloy, components can be designed so that the weldment experiences a low stress region so that the alloys' excellent corrosion resistance can be utilized.

Solid-state joining processes seem to be good candidates for joining ODS alloys since no melting of the parent alloy takes place. Solid-state joints in ODS alloys exhibit properties superior to those of fusion weldments. However, joints showing a planar grain boundary normal to the principle stresses within the joint will not perform much better than a conventional fusion weld.

TLP bonding offers great promise in maintaining the parent alloy microstructure across the joint region. The application of TLP bonding in joining of ODS alloys, e.g. MA956, MA957, and MA 756, has potential for success. However, due to the complicated nature of this method, far more research needs to be carried out. For example, during the isothermal solidification stage of the TLP bonding process the solid/liquid interface moves towards the centre of the joint. Earlier investigators have discovered that the movement of the solid/liquid interface could push particles resulting in agglomeration at the bond interface. This has been widely investigated in

the TLP bonding of MMCs, but not in the joining of ODS alloys. Furthermore, the TLP bonding of more complicated systems containing multiple elements has not been thoroughly researched. The TLP bonding of real systems which are complex must be undertaken in order to understand the mechanisms of the joining processes and in turn to optimize the bonding techniques to join ODS alloys and other advanced materials.

Chapter 3 Materials and experimental techniques.

3.1 Introduction.

In this study, TLP bonds were produced using various specimen preparation techniques and bonding conditions and details are described in this chapter.

Firstly, specimens to be joined were cut from the alloy bar in a specific direction and with fixed dimensions, then polished to a fine surface finish (1 um diamond powder polish). Specimens were then bonded under various conditions. As-bonded specimens were metallographically examined in order to analyze joint microstructures. Scanning electron microscopy (SEM) combined with energy dispersive X-ray analysis (EDX) was applied to conduct a more detailed investigation of joint microstructures and to monitor compositional changes across the joint region. As-bonded specimens were also subjected to a post-bond heat treatment in order to homogenize both the composition and microstructure across the joints.

In order to assess the viability of a joining method, it is important to conduct mechanical tests to measure joint strengths and a number of methods for mechanical testing are available. Tensile test results can be misleading, recording high tensile strengths even though only a small percentage of the surface may have actually bonded successfully [91]. Fatigue testing of TLP bonded joints was attempted, but the specimens were difficult to manufacture due to the machining standards required and the high scatter of experimental data which required a volume of results which exceeded materials and time constraints. Shear testing is fairly standard and reliable, and other workers have used this method of testing to compare joint strengths [92]. Micro-hardness tests are also reliable and provide information on changes in plastic deformation of the joint region, the latter being influenced by solid solution strengthening due to solute distribution across the joint. Micro-hardness measurements can also indicate the formation of hard, intermetallic precipitates at joints which in turn affect joint properties.

3.2 Materials used for TLP bonding.

3.2.1 MA758 ODS alloy.

INCONEL alloy MA758 is a nickel-based (ODS) alloy, made by mechanical alloying. The nominal composition of the alloy is given in Table 3.1.

Table 3.1 Nominal composition of the MA758 ODS alloy, wt%.

Ni	Cr	C	Al	Ti	Y_2O_3	Fe
Balance	30	0.05	0.3	0.5	0.6	1.0

The MA758 ODS alloy was joined in the as-received, fine-grained structure and recrystallized elongated condition, as shown in Figure 3-1 and Figure 3-2. The fine-grained alloy has an equaxied grain structure of 1-2 μm in diameter and the recrystallized alloy has elongated grains with an aspect ratio of 5 - 10. Very fine Y_2O_3 particles, about 15 – 50 nm in diameter, were homogeneously distributed in the matrix, with a spacing of about 90 nm [93]. These two distinct microstructures were chosen in order to investigate the effect of grain size on the TLP bonding processes.

The alloy in the fine-grained state was received as a hot rolled circular plate with size of 305 mm in diameter and 12 mm in thickness. The plate was sectioned into four pieces and each of these was further sectioned into four more pieces, as shown in Figure 3-3. The specimens to be bonded were cut to a dimension of 10 × 10 × 5 mm and those were suitable for metallographic examination, whilst a dimension of 15 × 15 × 10 mm was bonded for shear testing.

Alloys in the recrystallized-elongated-grained state were received as an extruded round bar, which was machined and annealed with a size of 27.0 mm in diameter and 125 mm in length, as shown in Figure 3-4. The round bar was cut along the longitude direction with a thickness of 5 mm to make bonds for metallographic examination and 10mm for shear testing. The sectioned bar was then machined into a rectangular shape before joining.

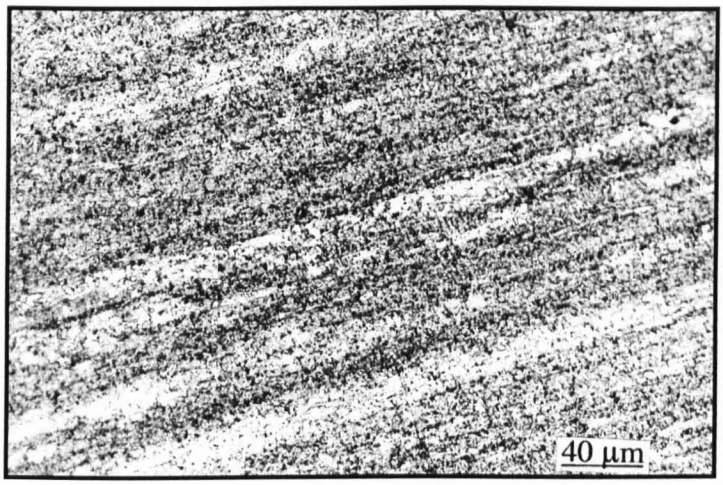

Figure 3-1 Microstructure of parent alloys in the fine-grained state (light micrograph).

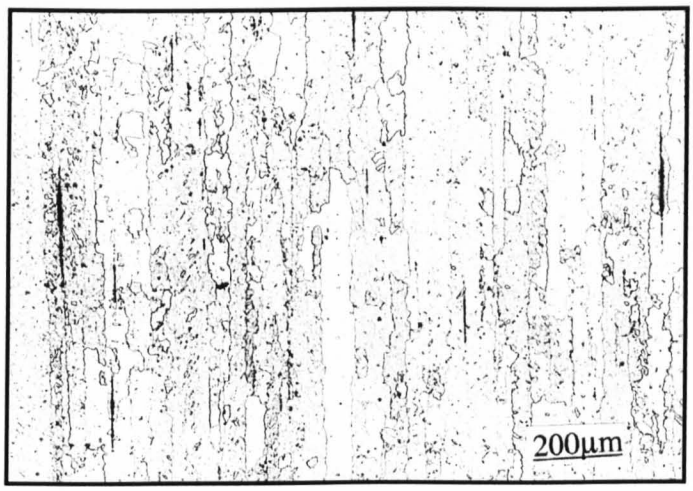

Figure 3-2 Microstructure of parent alloys in the recrystallized state (light micrograph).

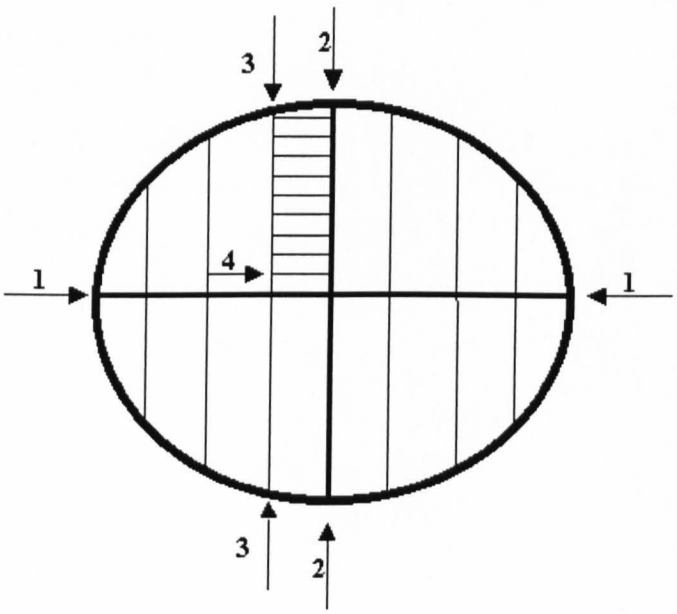

Figure 3-3 Sectioning of the specimen in the fine-grained state, plan view (1-4 indicates stages of preparation).

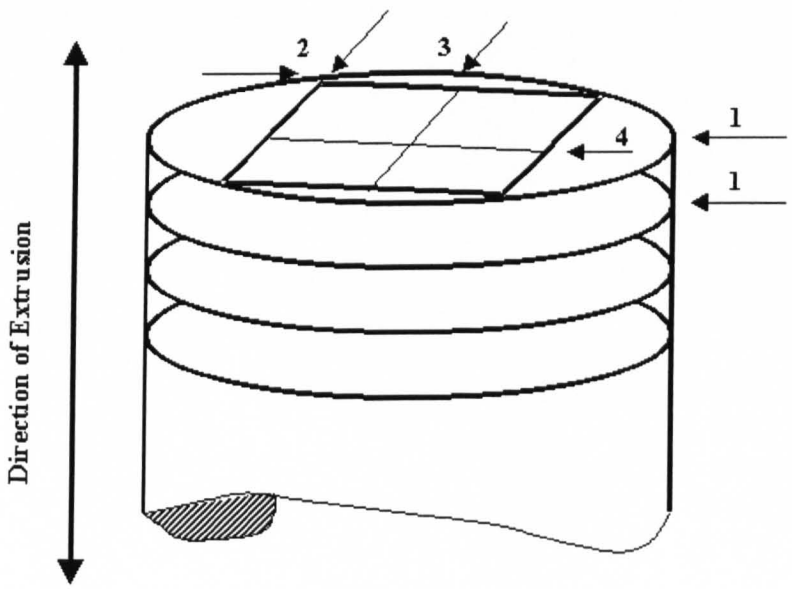

Figure 3-4 Sectioning of the specimen in the recrystallized state (1-4 indicates stages of preparation).

3.2.2 Interlayer alloys.

3.2.2.1 Ni-Cr-Fe-Si-B interlayer.

The commercially available interlayer Ni-Cr-Fe-Si-B was chosen as the interlayer for bonding MA758 alloy because it had a composition similar to the parent alloy. The composition of this interlayer is shown in Table 3.2. This product was manufactured by a melt-spinning technique and in this study it was used in the form of a thin foil (dimensions of 10 mm × 10 mm × 30 μm). The crystallization behaviour and melting stages of the interlayer upon heating are shown in Figure 3-5 and Figure 3-6. Three exothermal peaks were found during the crystallization process. Generally, this means there were three phases which crystallized from the amorphous metal matrix. This is why three endothermic peaks were found in the differential thermal analysis (DTA) trace for the interlayer on melting. The melting temperature for the Ni-Cr-Fe-Si-B interlayer was established as 1077 °C. Accordingly, the bonding temperature was chosen as 1100 and 1200 °C.

Table 3.2 Nominal compositions of the interlayers, wt%.

	Ni	Cr	C	Fe	Si	B	P
Ni-Cr-Fe-Si-B	Bal	14	0.03	4	4.5	3	------
Ni-P	91.72	------	------	------	------	-------	8.28

3.2.2.2 Ni-P interlayer.

In order to investigate the effect of elements from the parent alloy, e.g. Cr, on the TLP bonding process, a commercially available Ni-P interlayer was chosen to TLP bond the alloy. The nominal composition of the Ni-P interlayer is shown in Table 3.2. The Ni-P interlayer was received as an amorphous foil, 20 mm wide, 20 μm thick, and 1 m long. The Ni-P amorphous metal crystallized and then melted upon heating as shown in Figure 3-7 and Figure 3-8. Only one crystallized phase, Ni_3P, was detected, which has a melting temperature of 885 °C. Accordingly, a bonding temperature of 1000 °C was chosen when using this interlayer.

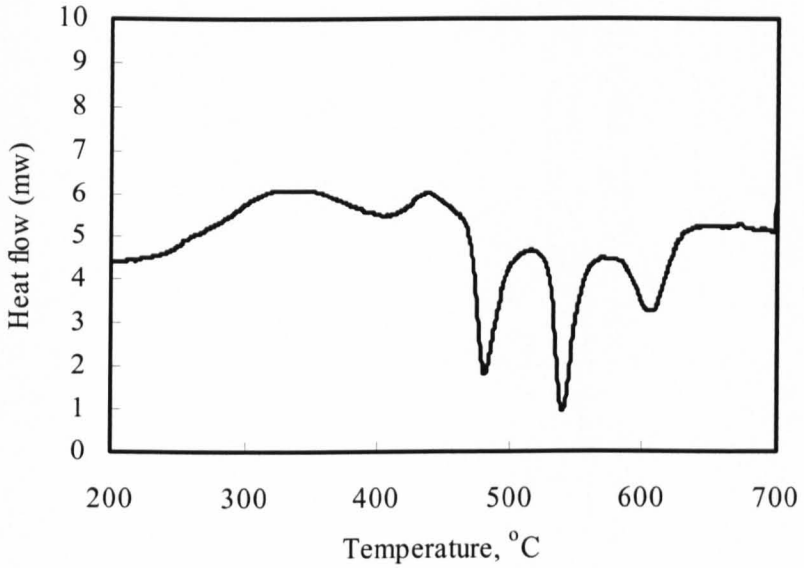

Figure 3-5 Crystallization of the Ni-Cr-Fe-Si-B interlayer (DSC trace).

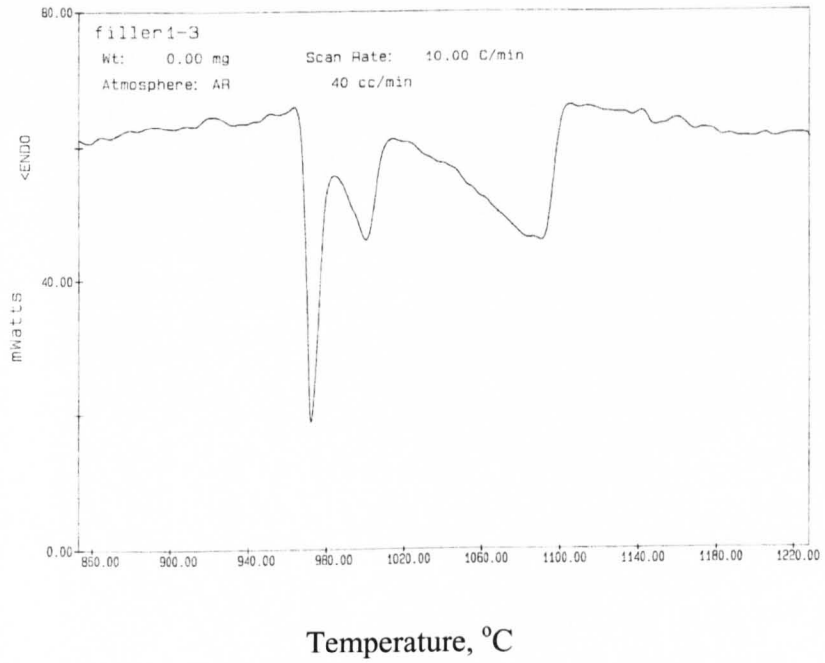

Figure 3-6 Melting of the Ni-Cr-Fe-Si-B interlayer (DTA trace).

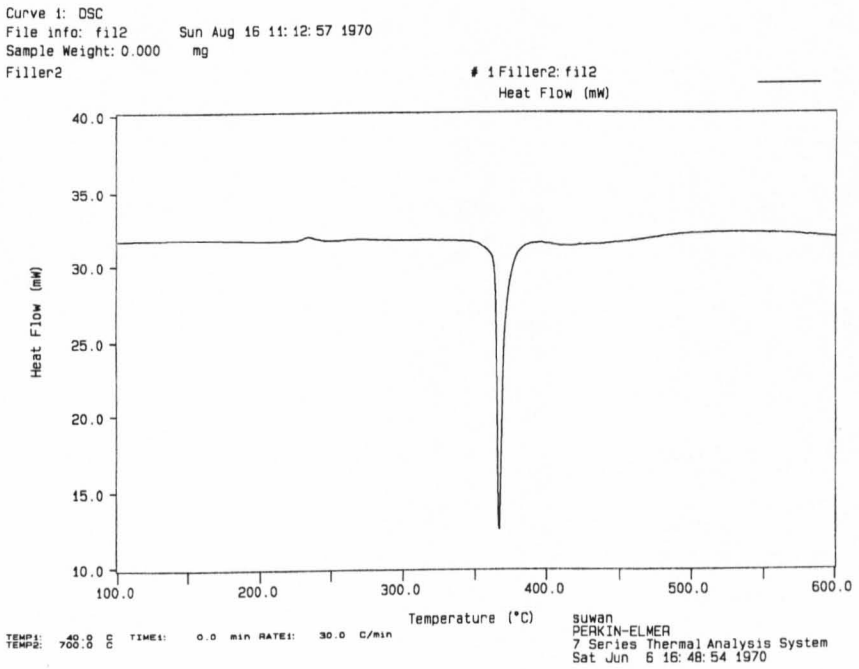

Figure 3-7 Crystallization of the Ni-P interlayer (DSC trace).

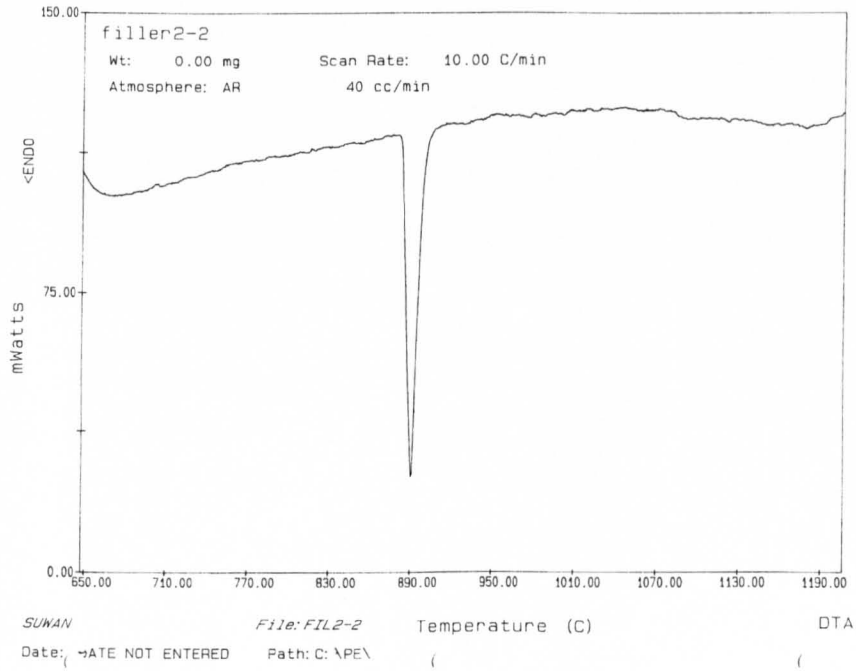

Figure 3-8 Melting of the Ni-P interlayer (DTA trace).

3.3 Experimental Techniques.

3.3.1 Bonding equipment.

TLP bonding was carried out in a purpose-built bonder, as shown in Figure 3-9. This was essentially a stainless steel capsule mounted in a vacuum system and coupled to an induction furnace.

The front door of the capsule was secured by four bolts and hinged to allow external access. A transparent view port was located in the centre of the door. On the right hand side of the capsule was the connection to a thermocouple unit. A water cooled, copper made induction coil with an inside diameter of 27 mm was fitted within the centre of the capsule.

Two steel rams were needed to position specimens for bonding within the induction coil. The upper ram was free to move through a bellow type seal in the top plate. Weight placed on the top ram allowed a force to be applied to the bonding couples. The lower ram was mounted on the base-plate of the capsule and fitted with a screw-jack mechanism that allowed the ram to be raised or lowered. The base plate contained three large holes drilled in it to allow the capsule to be evacuated by a vacuum system.

The vacuum system consisted of a rotary pump and a diffusion pump, which provided a vacuum of 4×10^{-4} torr. An air admittance valve was fitted to the pipe, which connect the rotary and diffusion pump.

The induction furnace was a Radyne C51 with a separated cooling system. The maximum power output is 20 kW. The furnace was fitted with a thyristor, which allowed a fine manual control over the power output.

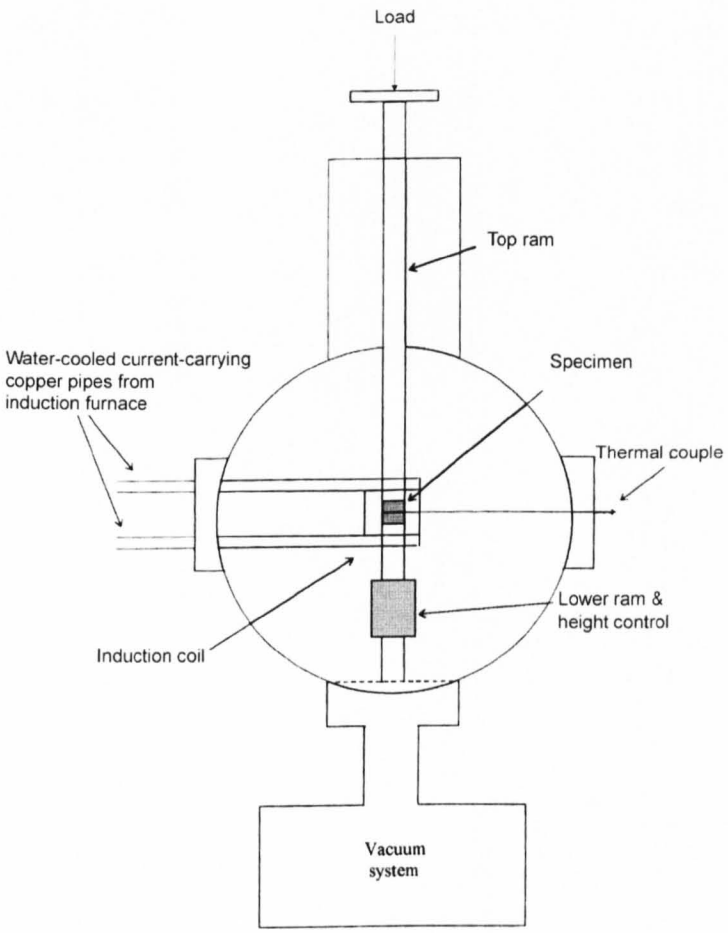

Figure 3-9 Schematic of the vacuum bonding chamber.

3.3.2 Specimen preparation and bonding procedures.

Specimens to be joined were prepared using SiC paper to a 1200 grit finish, and then ultrasonically cleaned in an acetone bath. All samples were stored in acetone before joining.

An interlayer was placed between the bonding surfaces of the samples positioned in the middle of induction coil. After placing the upper ram on top of the specimen assembly, the thermocouple was placed into a thermocouple hole, which was located close to the joining interface. After a vacuum of 4×10^{-4} torr was achieved, the samples were induction heated to the melting temperature of the interlayer using a heating rate of 50 °C/s, followed by a slower heating of 10 °C/s to bonding temperature. Finally, joints were kept at bonding temperature for a specific time, e.g. 30 minutes. After the hold time was completed, the specimen was furnace cooled to

room temperature in vacuum. Figure 3-7 shows the joining heat cycle.

When using the Ni-Cr-Fe-Si-B interlayer, specimens were bonded at 1100 °C with a hold time of 5, 15, 30, 60 minutes respectively. A higher bonding temperature, 1200 °C, was also used to investigate the effect of bonding temperature on bonding process. When investigating the effect of pressure on the bonding, the extra load was applied by placing weight, e.g. 2, 8, and 16 kg, on the top ram. The actual load applied to the bonding couple was measured under vacuum using a balance.

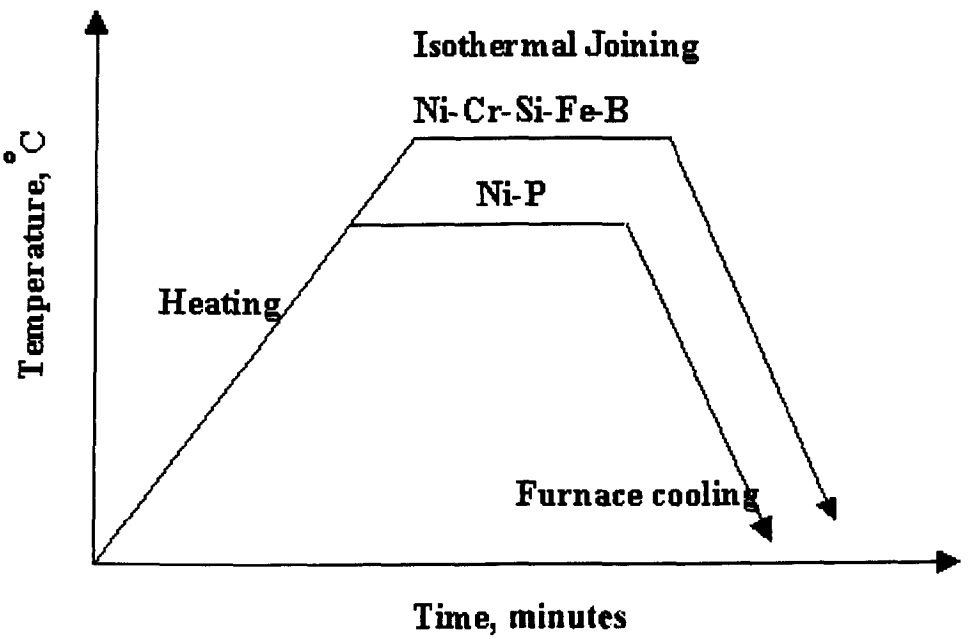

Figure 3-10 Heating cycle of TLP bonding.

When the Ni-P interlayer was used, the same set up used for the Ni-Cr-Fe-Si-B interlayer was applied. A bonding temperature of 1000 °C with a hold time of 5, 15, 30 and 60 minutes was employed. After the bonding cycle was completed, the specimen was furnace cooled to room temperature in a vacuum. The effect of pressure on the bonding was also investigated.

3.3.3 Post-bond heat treatment.

All bonded specimens were post bond heat-treated using a Lenton Thermal Designs-1700 furnace. The heating cycle incorporated a number of steps as follows:

- heated to 1000 °C at a heating rate of 5 °C minute^{-1};
- heated to 1360 °C at a heating rate of 2 °C minute^{-1};
- isothermally heat-treated for 120 minutes;
- cooled to room temperature at a cooling rate of 5 °C minute^{-1};
- all post bond heat treatments were applied in air.

3.3.4 Light microscopy.

Metallographic examination was carried out using light microscopy, which allowed rapid visual investigation of the microstructure of the joints. Each bonded sample was sectioned into two pieces. One piece was examined in the bonded condition and the other one was post-bond heat treated before examination.

All specimens were prepared using standard methods of metallographic preparation, which include: grinding using SiC paper down to 1200 grit and polishing using diamond paste to 1 μm finish. Between each step, ultrasonic cleaning in water for at least 5 minutes was needed to give a thorough cleaning.

The chemical enchant was made by mixing 1 part of H_2O_2, 2 parts of concentrated HCl (37 wt%), and 2 parts of distilled water just before etching. An etching time between 10 – 40 s was employed. It is worth noting that, before etching being applied, most of the bonded specimens have good microstructure contiguity so that no visible bond line can be detected under light microscopy.

3.3.5 Scanning electron microscopy.

In this study, a JEOL 840A SEM was used to study the morphology of the bond interfaces, to characterize the distribution of elements and to investigate fracture surfaces of the shear test specimens.

A quantitative analysis was obtained by using a LINK SYSTEMS ZAF4 system. The conditions under which the ZAF analysis was carried out in this study are as follows:

1. sample tilt: 35 °;

2. working distance: 39 mm;
3. accelerating voltage: 20 kV;
4. counting time: 100 seconds;
5. dead time: 15 – 20 %;
6. counting rate : 1800 – 2500 cps.

To minimize cumulative errors, calibration was carried out before each ZAF analysis by gaining calibration on a pure Cu standard specimen under the same conditions listed above. Elemental concentrations were measured at ranges of 0, 2, 4, 6, 8, 10, 12, 14, 16, 18, 20, 80 μm from the centre of the joint. The ZAF analysis in this study has a standard error of 0.1-0.4 wt% and dose not include content of Boron. So it is only considered as semi-quantitative measurement.

Knowledge of the chemical composition of the TLP bonded joint was important because assessing the interlayer concentration at the joint region after bonding was used as a means of determining when the bonding process was complete. Also, the homogeneity of the joint region after bonding has an important influence on the mechanical properties of the joint.

In order to investigate the distribution of the fine Y_2O_3 dispersoids, a Philips XL30 ESEM-FEG was used, which offers high resolution secondary electron imaging. The XL30 ESEM-FEG is the first Scanning Electron Microscope (ESEM®) to employ the stable, high brightness Schottky Field Emission Source for outstanding observation performance of potentially problematic samples for conventional high vacuum SEMs. Specifications of the XL30 ESEM-FEG is as follows,

Resolution	2 nm
Accelerating voltage	0.2 to 30 kV
Electron gun	Field-Emission
Magnification	15 to 500,000

3.3.6 Shear testing.

Bonded specimens to be tested were machined into a rod of 6 mm in diameter after

final polishing using SiC paper of grade 1200 finish and followed by a final polish using 6 μm diamond paste. The edge effects were eliminated and oxidation effects were avoided due to the large quantities of materials machined off. Then the polished rod was cut to only 10 mm in length with the bond-line in the centre. All test specimens were ultrasonically cleaned in an acetone bath before test.

The shear testing was performed using an Instron 4206 machine. Figure 3-11 shows a schematic set up of shear test. A cross head speed of 0.5 mm minute^{-1} and a load cell of 50 kN were used. A low cross head speed was chosen in order to minimize the experimental error because the as-bonded specimens could be brittle. An average of three bonded samples was tested per bonding condition at room temperature.

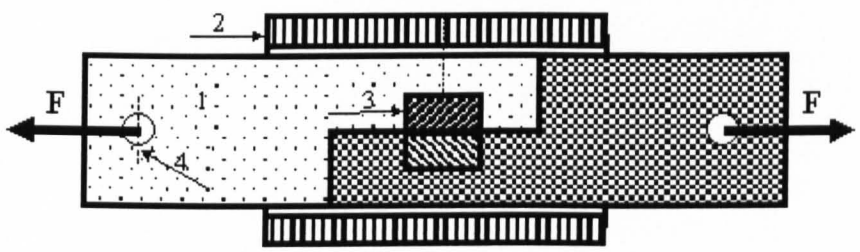

Figure 3-11 The shear testing fixture: 1) holder; 2) steel tube; 3) specimen; 4) bolt.

3.3.7 Microhardness test.

The hardness of a metal, defined as the resistance to penetration, gives an indication of its plastic deformation behaviour. Most hardness tests rely upon the accurate measurement of the diameter of an indentation formed on the surface of the metal, by forcing an indenter into the metal under a controlled load. The hardness may be related to the yield or tensile strength of the metal, since during the indentation, the materials around the impression are plastically deformed. In this study, a Vickers diamond pyramid indenter fitted to a Leitz Mini-load hardness tester was used to obtain microhardness results in Vickers hardness number, HV. The load of 100 g and duration time of 10 s were used throughout this study. These values were chosen not only by the requirement of accuracy but also to make the size of indentation not too big to carry out as many measurements as possible in one run. Calibration of the

hardness indenter was checked with reference to a standard block with a quoted hardness of 591 HV. It was found that for ten hardness measurements with a 100 g load, they underestimated the hardness by 3% with duration time of 10 s.

In this work, micro-hardness profiles were used to assess the homogeneity of the bond region and to give some indications of the compositional and microstructural changes during the TLP bonding process.

Chapter 4 TLP bonding using a Ni-Cr-Fe-Si-B interlayer.

4.1 Introduction.

MA758 alloy was bonded using a Ni-Cr-Fe-Si-B interlayer in order to establish the effects of the grain size, bonding temperature and external pressure on the bonding process. In this chapter, the quality of joints was assessed by the homogeneity of composition profile, continuity of microstructure, and mechanical properties. The particulate segregation behaviour was investigated in order to produce a homogenous particle distribution across the joint region and therefore make a strong joint.

4.2 The effect of grain size on bonding behaviour.

TLP bonding is a diffusion-controlled process, and therefore, any joining parameter that can affect diffusion will change the process during the bonding operation. When bonding a single crystal material, transport of solute depends on the volume diffusion in solid and in liquid. However, when polycrystalline materials are TLP bonded, solute diffusion will depend on a number of factors, such as grain boundary diffusion [83], bond interface curvature [85], changes in the solid/liquid interfacial area [76, 88], grain boundary migration [94], and segregation of elements to grain boundaries [95]. In this study, MA758 alloy was TLP bonded using the parent alloy in the equiaxed fine-grained and in the recrystallized states. It is well known that the alloy in the fine-grained state has a greater grain boundary area than the alloy in the recrystallized state. As a result, the diffusion rate of solutes in the parent alloy in the fine-grained state can be expected to be greater than that in the recrystallized state. This difference in diffusion behaviour will affect the dissolution and isothermal solidification stages of the bonding.

4.2.1 TLP bonding with the ODS alloy in the fine-grained state.

4.2.1.1 Bond microstructure.

The microstructure of bonds made with the parent alloy in the fine-grained state at a bonding temperature of 1100 °C for 5 minutes hold time is shown in Figure 4-1. Some eutectic phase was found within the joints, which implied that isothermal solidification had not been completed. Precipitates were found in the region close to the interlayer/parent alloy interface. These precipitates were also found in the joints made at 1100 °C with a longer hold time, for instance, 60 minutes, as shown in Figure 4-3. By increasing the hold time at 1100 °C these precipitates could not be removed from the interface. It was clear that precipitates were located close to the interfaces between the parent alloy and the centre-line of the joint, which implied that the formation of precipitates can be correlated to the diffusion of elements from the joints (e.g. diffusion of B). This micrograph also shows that the grains within the joint centre-line had a much larger grain size compared with those within the parent alloy. There was no recrystallization of the parent alloy from either side of the joint. In the bonds made with a hold time of 15 minutes, no residual eutectic phases were observed. This implied that a hold time of 15 minutes was sufficient to complete isothermal solidification.

As illustrated in Figure 4-2 and Figure 4-3, when the joints were isothermally bonded after a longer hold time (30 and 60 minutes), recrystallized grains were found on either side of the joints. With a longer hold time, the recrystallized grains increased in size. A similar observation was reported by Khan and Wallach [96] in the TLP bonding of ODS ferritic alloys. In this study, the recrystallized area can be divided into three different zones according to their grain morphologies, as shown in Figure 4-4 and illustrated in Figure 4-5. In zone 1, only very small equaxied grains, with a grain size of 5 μm, were present. In zone 2, much larger grains, with a grain size of 30 μm were found. Zone 3 had recrystallized elongated grains, which were parallel to the rolling direction. With a longer hold time, the elongated grain zone expanded into the parent alloy and finally, for hold time of 60 minutes, the whole sample recrystallized. In the present study, the indication was that recrystallization started

from the bond interface and expanded parallel to the rolling direction and towards the parent alloy. The direction of grain growth follows the route for B diffusion. Figure 4-6 shows the relationship between recrystallization distances from the interface and the hold time when joints were made at 1100 °C. However, when the fine-grained parent alloy was annealed at 1100 °C for 60 minutes, no recrystallization occurred. Therefore, recrystallization behaviour was attributed to the diffusion of boron from the interlayer into the parent alloy. It also correlated with the parent alloy grain microstructures. In fact, the mechanical alloying and extrusion process results in a cold worked microstructure with an ultra-fine, submicron sized grain structure. Therefore, most of the stored energy of the alloy is in the deformed grain structure. This stored energy is so large that moving grain boundaries can easily overcome the drag from the Y_2O_3 dispersoids.

In metallurgical terms, a good joint can be defined as one free from precipitates, free from porosity, and with a composition and microstructure as similar as possible to that of the parent alloy. One of the objectives in this study was to produce good joints for high temperature applications. Therefore, as-bonded specimens were heat treated at 1360 °C for 2 hours in order to homogenize the joint composition and encourage grain growth across the joint region.

Figure 4-7 and Figure 4-8 show the microstructures of the bonds made at 1100 °C for 5 and 30 minutes followed by a post bond heat treatment. Firstly, the precipitates, which were found at the joints in the as-bonded condition, were not detected, see Figure 4-7. Previous studies have reported these precipitate to be silicides and borides [97]. With reference to the binary phase diagrams [98] the possible eutectic temperatures of possible precipitates Ni-B, Ni-Si, Fe-B, and Cr-B are 1093, 1152, 1180, and 1620 °C respectively. This suggests that these precipitates are not chromium borides, which are stable above 1380 °C, but most probably borides and silicides of nickel and iron. However, later in this study, EDX analysis (in Figure 4-59) shows these precipitates are rich in Cr and without any trace of Si, Fe, Al, and Y. Therefore, these precipitates were thought to be Cr(Ni) borides. These observations are consistent with earlier work by Ekrami and Khan [99].

Directional recrystallization across the joint region was not achieved. As seen in Figure 4-8, the grains within the joint centre-line, instead of being consumed by the recrystallized grains from the parent alloy, recrystallized and grew into the parent alloy. It has been reported in the literature that when MA758 is isothermally annealed, it recrystallizes to produce a fine-grained structure, because fine Y_2O_3 dispersoids pin grain boundaries and inhibit grain growth [100, 101, 102]. The only way to produce directional recrystallization in MA758 ODS alloy is to apply a temperature gradient during heat treatment, e.g. zone annealing [103]. The use of a temperature gradient provides enough activation energy to overcome the drag force exerted by the Y_2O_3 dispersoids. Later in chapter four, section five, the results from this study further confirm the effect of the Y_2O_3 dispersion on the recrystallization behaviour of MA758 alloy. Therefore, the reasons why a homogenized microstructure with directional recrystallization across the joint was not produced by a post-bond heat treatment are:

1. grains within the joint were too large to be consumed during isothermal annealing;

2. a distribution of fine Y_2O_3 dispersoids within the joint centre-line prevented grain growth across the joints;

3. greater activation energy was necessary to encourage fine grains within the parent alloy to grow across the joint (e.g. through zone annealing).

The results show that grains within the joint seemed to consume more grains in recrystallized zone 1 than grains in zone 2 (see Figure 4-5). We must also point out that the grains adjacent to the joint are larger than grains further away in the parent alloy. This is because the original grain size in zone 2, was larger than that in the parent alloy before the post-bond heat treatment. As a result, grains in zone 2 grew faster.

A prolonged hold time had no effect on the grain structures within the joint centre-line. This implied that once isothermal solidification was complete, it was difficult for the grains within the joint centre-line to recrystallize at the bonding temperature. However, after a post-bond heat treatment at 1360 °C for 120 minutes

was applied, hold time at bonding temperature had a significant effect on grain growth within the joint centre-line. With a longer hold time, larger grains were produced during the post-bond heat treatment. The difference in the recrystallized grain size was attributed to the difference in the stored-energy within the parent alloy before the heat treatment. When joining MA758 ODS alloy at 1100 °C, the parent alloy with the fine-grained structure would recover and release stored-energy. The longer the hold time, the less stored energy remained for grain growth and recrystallization of the parent alloy. As discussed earlier, the recrystallization of grains within the joint centre-line consumes the grains in zone 1 which is competing with the recrystallization in zone 2. With a longer hold time and therefore a weaker competition from zone 2, the grains within the joint centre-line would consume more grains in zone 1 and grow larger. This is also confirmed by the fact that the grains adjacent to the joint centre-line with a hold time of 5 minutes are larger than those with a hold time of 30 minutes after the post bond heat treatment applied while the grains within the joint centre-line are smaller. This implied that hold time at the bonding temperature is vital regarding producing a homogeneous microstructure across the joint region. This study shows that a hold time of 30 minutes at a bonding temperature of 1100 °C can produce the best homogeneity in microstructure across the joint.

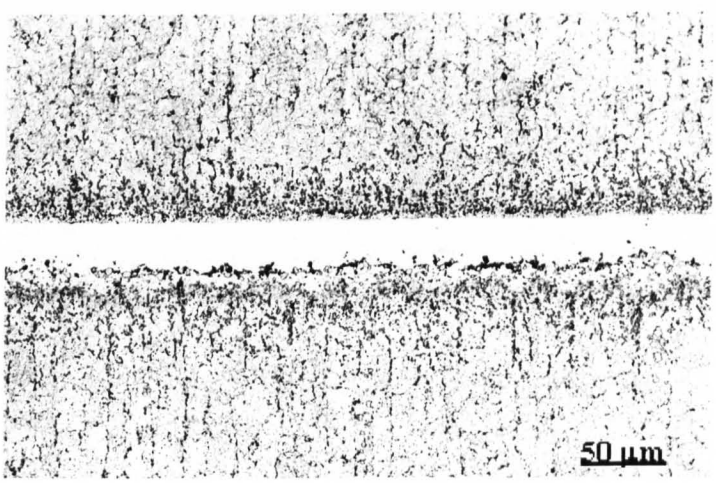

Figure 4-1 Microstructure of the joints made with the parent alloy in the fine-grained state at 1100 °C for a hold time of 5 minutes (light micrograph).

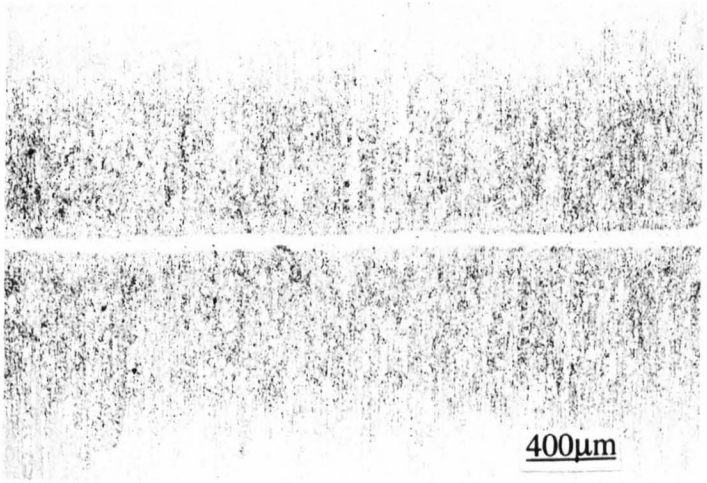

Figure 4-2 Microstructure of the joints made with the parent alloy in the fine-grained state at 1100 °C with a hold time of 30 minutes (light micrograph).

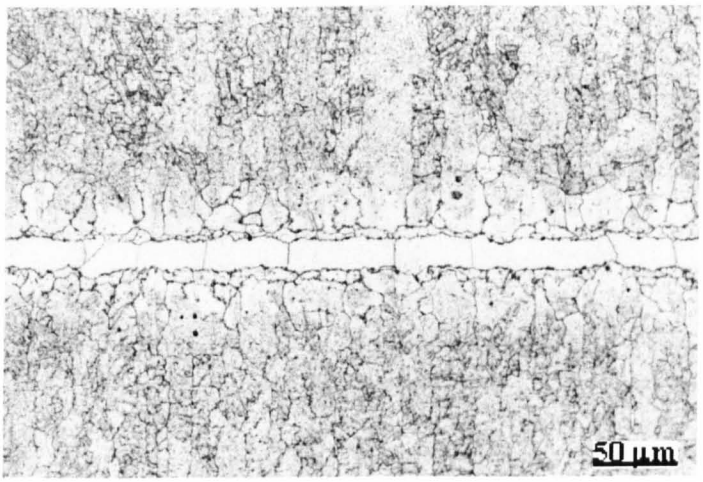

Figure 4-3 Microstructure of the joints made with the parent alloy in the fine-grained state at 1100 °C with a hold time of 60 minutes (light micrograph).

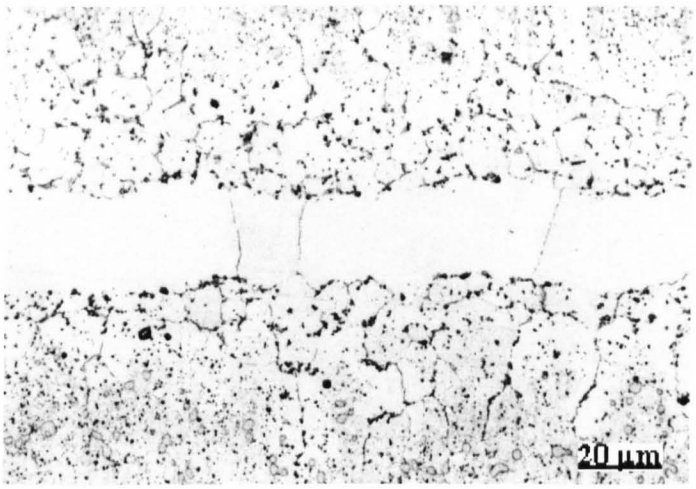

Figure 4-4 Recrystallization zones in the joints made with the parent alloy in the fine-grained state at 1100 °C with a hold time of 30 minutes (light micrograph).

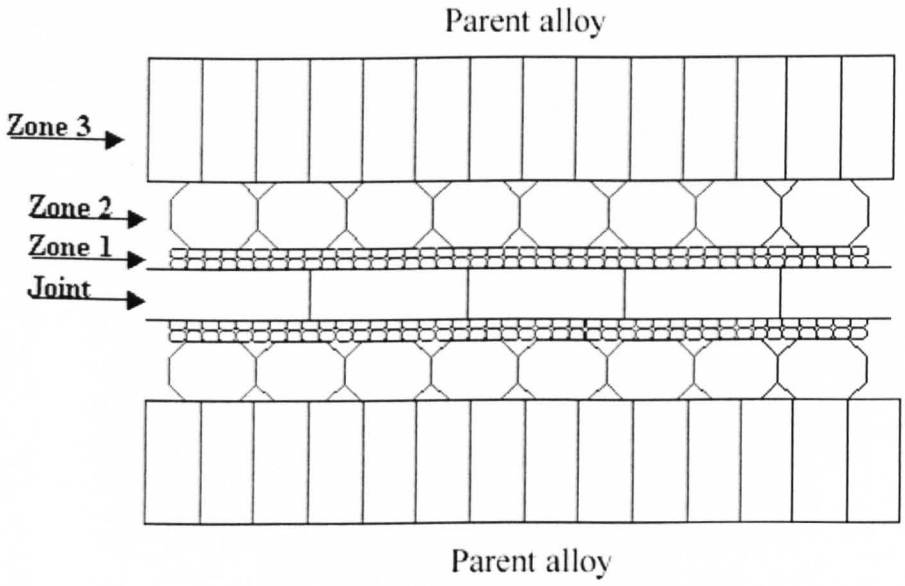

Figure 4-5 Schematic diagram of the recrystallization zones.

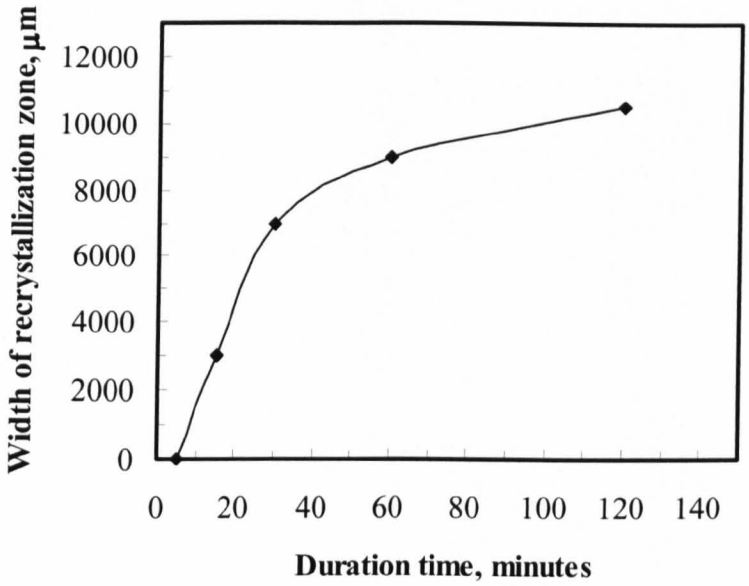

Figure 4-6 The expansion of the recrystallization zone towards parent alloy.

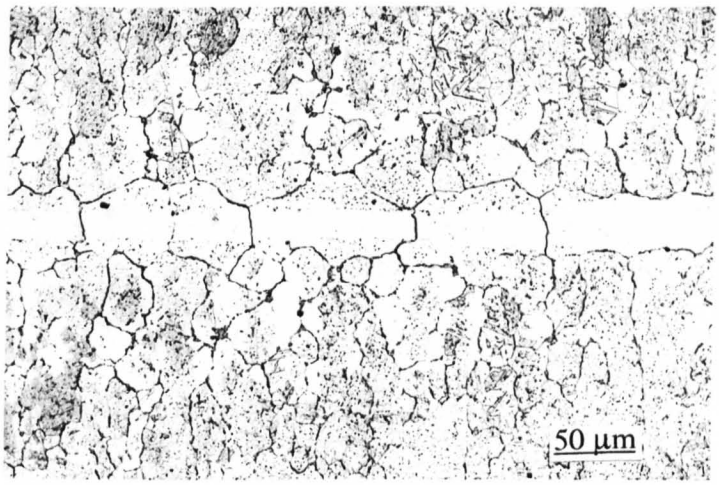

Figure 4-7 Microstructure of the bonds made with the parent alloy in the fine-grained state at 1100 °C with a hold time of 5 minutes and subjected to a post-bond heat treatment (light micrograph).

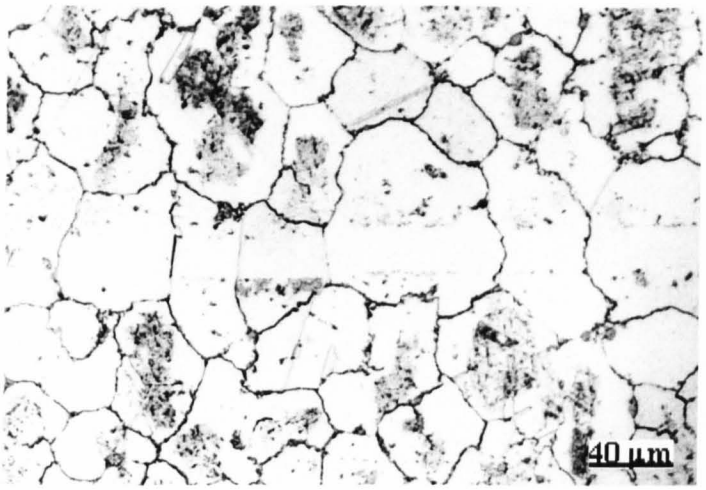

Figure 4-8 Microstructure of the bonds made with the parent alloy in the fine-grained state at 1100 °C for a hold time of 30 minutes and subjected to a post-bond heat treatment (light micrograph).

4.2.1.2 Composition profiles.

The composition profile of elements as a function of distance from the centre of the joint was investigated using a quantitative EDX, LINK SYSTEMS ZAF4 systems. The system used in this study could not detect any elements with an atomic number lower than 11. Therefore, the distribution of boron (atomic number of 5) was not included in the results presented here. Consider bonds in a two-dimensional case and assume boron was homogenously distributed. Due to the conservation of mass:

$$C_0 \times H_0 = C_1 \times H_1 \qquad (4.1)$$

Where C_0: the original content of boron; H_0: the thickness of the interlayer; C_1: the content of boron after bonding; H_1: the area of the bonding affected zone. The bonding-affected zone includes the thickness of the joint centre-line, about 20μm, and the width of the recrystallized zones on each side of the centre-line, about 1000 μm. Before bonding, there was 2-3 wt% boron in the amorphous interlayer. Therefore, (according to equation 4.1) the content of boron after bonding will be reduced to as low as about 0.06 wt%, which is negligible. As we know the diffusion rate of boron in solid Ni ($\sim 10^{-10}$ m^2s^{-1}) at 1100°C is much faster than all the other elements such as Cr and Fe, it is reasonable to assume that most of the boron will have been lost from the centre.

Figure 4-9 shows composition profiles of the bonds made at 1100 °C with a hold time of 30 minutes. Within the joint centre-line, there was a higher concentration of Ni (~69 wt%) and a lower concentration of Cr (~28.5 wt%) than that in the parent alloy. The distribution of both Ni and Cr was homogenous within the joint. There was a transition area, through which compositions with higher content of Ni and lower content of Cr within the joint centre-line changed to that with lower content of Ni and higher content of Cr in the parent alloy. A prolonged hold time did not alter the distribution of these two elements and the position of the transition area. As discussed in chapter four, section two, the isothermal solidification was complete after a hold time of 30 to 60 minutes at 1100 °C and therefore, the width of the area which has the different compositions to the parent alloy can be considered as the melt-back distance. If we compare this melt-back distance with the width of

recrystallized zone 1, they were identical. It is suggested that small grains in zone 1 were produced during isothermal solidification of the molten liquid but not the recrystallized grains from the parent alloy. This was confirmed by examining the microstructure of the joints in section 4.2.1.1, in which only the grains in zone 2 increased in size with a longer hold time.

The concentration profiles for Fe and Si show a gradual decrease away from the centre of the joint and these concentrations become constant within the parent alloy, see Figure 4-9. Both the Al and Ti concentrations increased with the distance from the centre of the joints. The Al concentration is high at the interface between the molten liquid and solid parent alloy, which is probably due to the Al segregating to the bond interface and also the break-up of surface oxides during the bonding process [104]. The EDX analysis also produced a peak for yttria which was detected within the joint and a homogenous distribution was recorded. Because the Y_2O_3 dispersoids are stable at 1100 °C, the peak of Y can be considered as the trace of Y_2O_3 particles. Therefore, the results show that the Y_2O_3 dispersoids were present homogenously in the joint. Further details regarding the distribution of Y_2O_3 dispersoids will be discussed in section 4.6.

Post-bond heat treatment homogenized the composition profiles of the joints, are as illustrated in Figure 4-10. The content of Ni and Cr was homogenously distributed across the joint region and had the same value as that within the parent alloy. The concentrations of Fe, Si, Al, and Ti were also detected to be present evenly across the joint.

Generally speaking, the bonds made at 1100 °C with a hold time of 30 minutes and subjected to a post-bond heat treatment at 1360 °C for 120 minutes have a homogenized microstructure and compositions across the joint region.

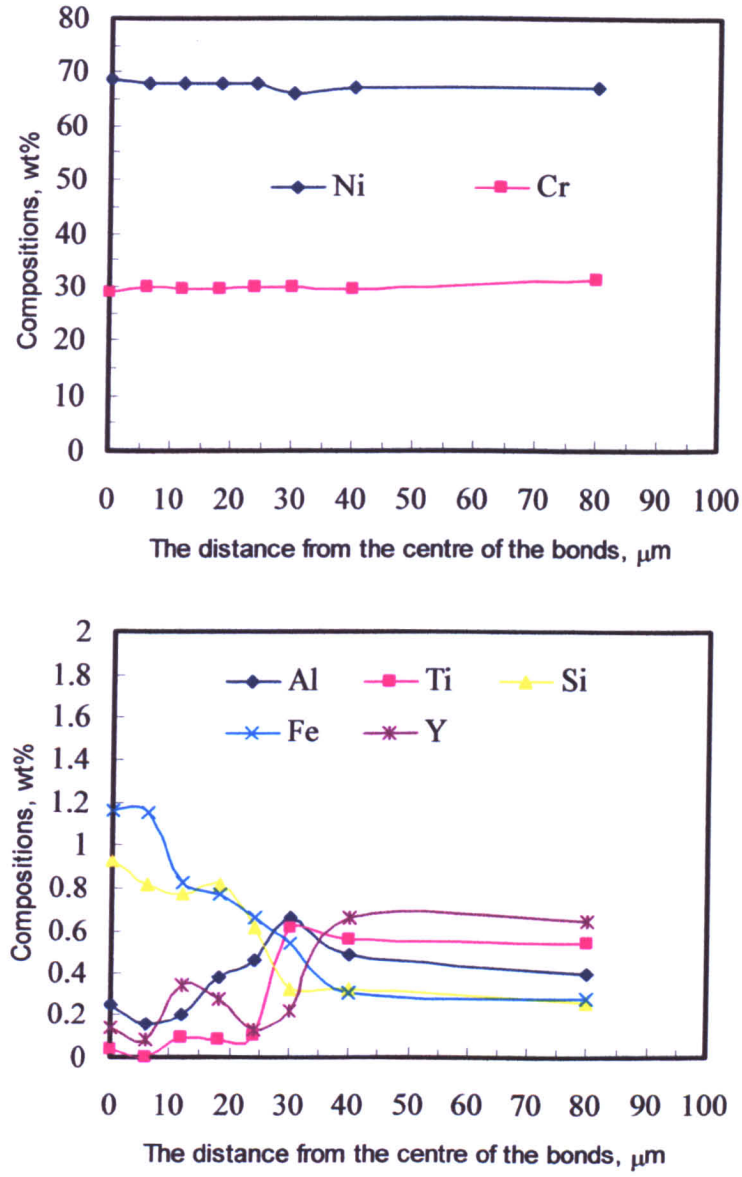

Figure 4-9 Composition profiles of the bonds made with the parent alloy in the fine-grained state at 1100 °C with a hold time of 30 minutes.

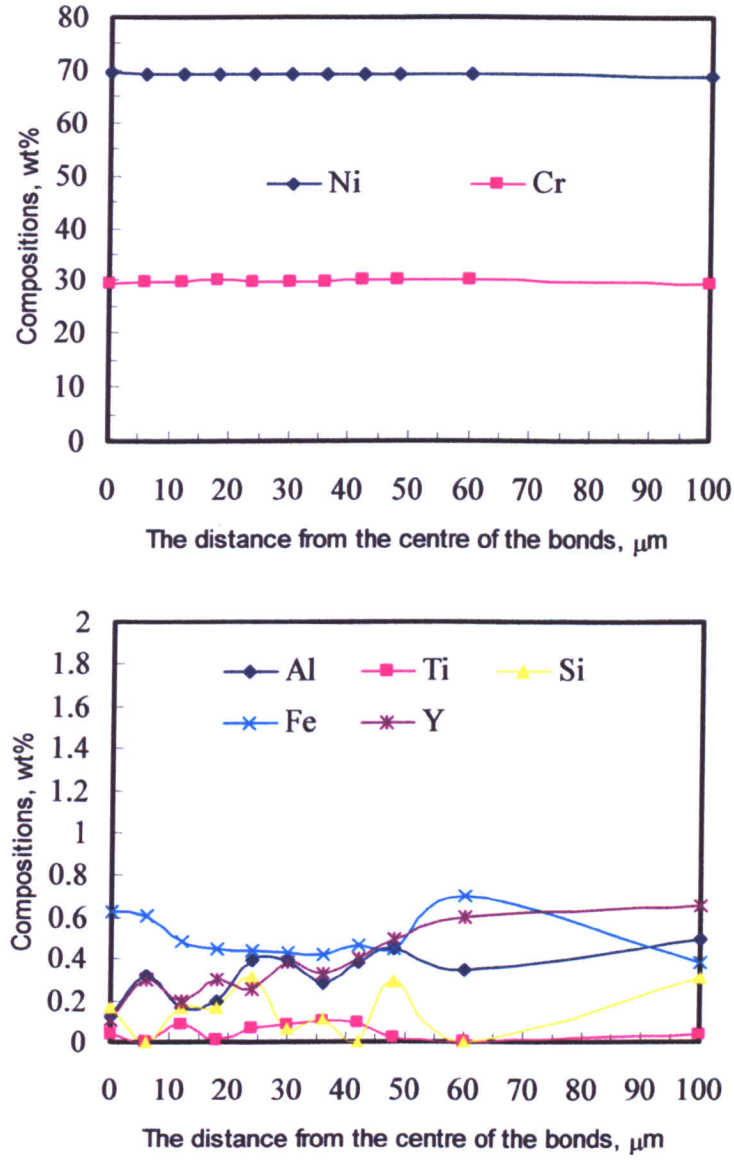

Figure 4-10 Composition profiles of the bonds made with the parent alloy in the fine-grained state at 1100 °C with a hold time of 30 minutes and subjected to a post-bond heat treatment.

4.2.2 TLP bonding with the ODS alloy in the recrystallized state.

4.2.2.1 Bond microstructure.

In order to study the effect of parent alloy grain size on the TLP bonding behaviour, bonds were made with the parent alloy in the elongated, recrystallized coarse-grained state, at 1100 °C for 5, 15, 30 and 60 minutes. A post bond heat treatment at 1360 °C for 120 minutes was also applied.

Figure 4-11 shows some eutectic phases along the bond joint interface within the joints made with a hold time of 5 minutes. When compared with the joint made under the same conditions but with the fine-grained parent alloy (as shown in Figure 4-1), there was a greater quantity of eutectic phase. However, when the bond was then subjected to a post bond heat treatment (Figure 4-13), the eutectic phase was removed. This implied that the phase was rich in nickel borides and silicides because the eutectic temperature of these phases is below that of the heat treatment temperature. Less eutectic phase was observed in the joint made for 15 minutes. These phases were not found in the joint with hold time of 30 and 60 minutes, as shown in Figure 4-12. This suggested that when the parent alloy was bonded in the recrystallized coarse grain condition, a hold time of 15 minutes is too short to allow complete isothermal solidification of the liquid interlayer. However, in the bonds made with fine-grained alloy, isothermal solidification was achieved with a hold time of less than 15 minutes. The time to complete isothermal solidification during TLP bonding is longer when joining the parent alloy in the coarser grained state. This difference was attributed to a decrease in grain boundary area and hence, the lower diffusion rate of B in the coarse-grain structure, an observation which was reported by Saida *et al.* [88]. TLP bonding is a diffusion-controlled process and the diffusion rate of B, in the solid parent alloy will be a key factor in determining isothermal solidification. It is known that the diffusion rate of solutes within the grain boundaries is much higher than that in the bulk material. With a higher volume fraction of grain boundaries within the fine-grained parent alloy, fast diffusion of B can be expected. As a result, a shorter hold time is required to complete isothermal solidification. However, at higher bonding temperatures, e.g. $T > 0.75\ T_m$ (where T_m

is the equilibrium melting temperature of the materials in Kelvin), the difference between the diffusion rate along grain boundaries and in the bulk material is much less than that at lower temperatures [105]. In this study, the bonding temperature was 1100 °C, which is higher than $0.75T_m$. As a result, there is relatively small contribution resulting from grain boundary diffusion. This was confirmed by the fact that there is not much difference during TLP bonding with the parent alloy of different grain sizes regarding dissolution and melt-back distance. However, it must be pointed out that bonding the alloy in the recrystallized, elongated grain state required a longer hold time to complete isothermal solidification.

No recrystallized grains along the bond interface were detected. This was attributed to the recrystallized grains having a low stored energy, which was insufficient for further grain growth. As discussed in section 4.2.1.1, the stored energy was generated during the mechanical alloying where a fine-grained material was produced. During the heat treatment applied to produce the elongated coarse-grained structure, alloy lost stored energy during recrystallization. Due to a lack of activated energy, no recrystallized grains were produced during the bonding process. In the meantime, with coarser grained structure, a low diffusion rate of B into the parent alloy could also make the flow of B insufficiently strong to trigger the recrystallization.

Post-bond heat treatment at 1360 °C for 120 minutes failed to produce a continuous microstructure across the joints, as shown in Figure 4-13 and Figure 4-14. The grains within the joint centre-line did not grow into the parent alloy, as seen for heat treated bonds made with the alloy in the fine-grained state. This is because there were no recrystallized grains adjacent to the bonding centre-line, but coarse grains within the parent alloy, which were larger than the grains within the joint. This confirmed the mechanisms for recrystallization of grains within the joint centre during post-bond heat treatment, as proposed in section 4.2.1.1. Although the grain sizes of the parent alloy are 200-300 μm in size, no recrystallization across the joints was achieved. This was attributed to the yttria dispersoids, which act as obstacles to grain boundary migration during grain growth. As shown later in section 4.6, the dispersoids were distributed homogeneously within the joint centre-line. Therefore, these results suggest that isothermal annealing could not provide enough activation energy to the

grains within the parent alloy to overcome the drag force from the dispersoids in order to consume the grains at the joint centre-line. In this case, directional recrystallization would perhaps be better to achieve homogeneity across the joint due to the higher activation energy supplied.

In this study, the thickness of the joint interlayer is about 30 μm. Consequently, the width of the joint centre-line was about 20 μm. This did not change when joining under different conditions, e.g. the parent alloy with a different grain size or when joining for various hold times (after the isothermal solidification). It was thought that a smaller grain size within the joint region would be beneficial for developing a homogeneous microstructure on post-bond heat treatment because smaller grains within the joint would be easier to consume than larger grains. This suggested that thinner interlayer would be beneficial.

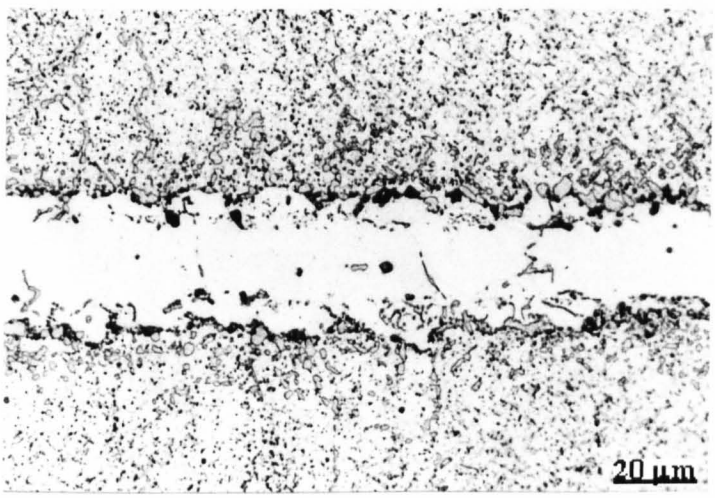

Figure 4-11 Microstructure of bond made at 1100 °C with the parent alloy in the recrystallized state with a hold time of 5 minutes (light micrograph).

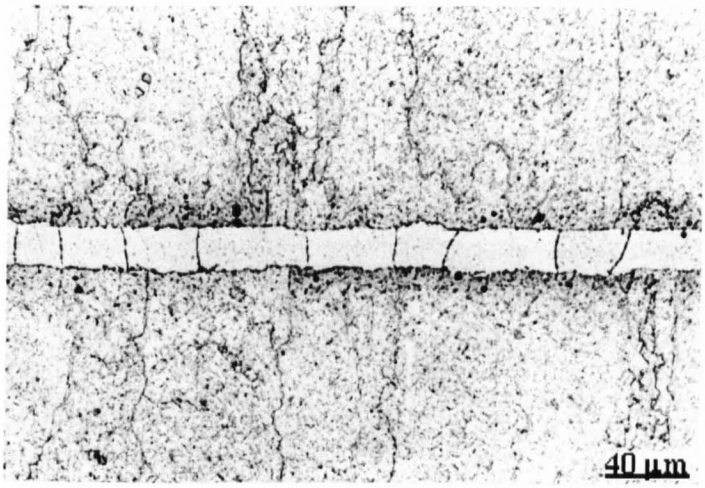

Figure 4-12 Microstructure of bond made at 1100 °C with the parent alloy in the recrystallized state with a hold time of 30 minutes (light micrograph).

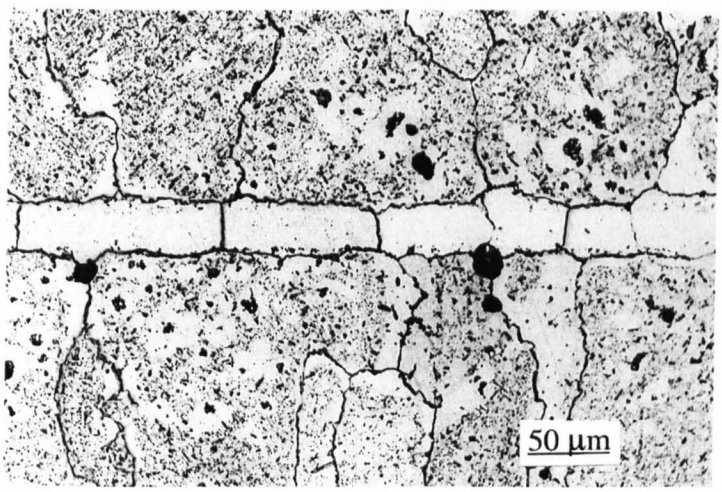

Figure 4-13 Microstructures of the joints made with the parent alloy in the recrystallized state at 1100 °C for hold time of 5 minutes and subjected to a post-bond heat treatment (light micrograph).

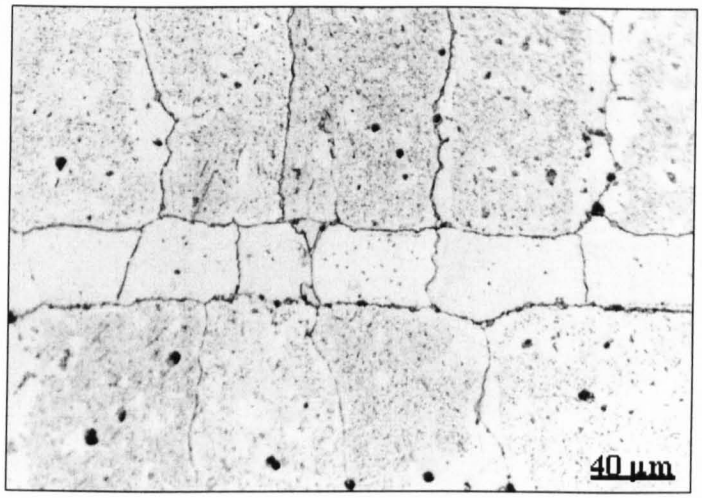

Figure 4-14 Microstructures of the joints made with the parent alloy in the recrystallized state at 1100 °C with a hold time of 30 minutes and subjected to a post-bond heat treatment (light micrograph).

4.2.2.2 Composition profiles.

Figure 4-15 shows the composition profiles of the bonds made at 1100 °C with a hold time of 30 minutes. The bond can be divided into three zones, namely, within the joint centre-line, a transition area, and the parent alloy. Within the joint centre-line, the concentration of Ni and Cr was homogeneous. The composition shows a higher Ni and a lower Cr content, compared with that of the parent alloy. In the transition area, the content of Ni decreased and at the same time, Cr increased gradually to a level similar to that of the parent alloy. The contents of Fe and Si decreased gradually with distance from the centre of the joints and became stable within the parent alloy. The concentration profile indicated a peak for Al at the joint interface.

The "transition area" with respect to compositional changes was wider for bonds made using the coarser-grained alloy compared to that for bonds made with the parent alloy in the fine-grained state. As discussed before, this transition area correlated to the melt-back distance. Therefore, these observations indicate that joining the parent alloy with a coarse grain size results in a wider melt-back distance. In addition, it must be pointed out that with a fine-grained structure, the composition profiles are more uniform across the joint. The concentration of Ni and Cr is similar to that of the parent alloys. Therefore, compositional analysis shows that bonds made with the parent alloy in the fine-grained state results in a more homogeneous joint region. This is attributed to the contribution of the grain boundaries to diffusion of solutes.

Figure 4-16 shows the composition profiles of the joint after post-bond heat treatment was applied. The content of Ni and Cr was homogenous across the joint region and the concentration of Fe and Si was evenly distributed across the joint area. The aluminium concentration was particularly high at the interfaces between the joint and parent alloy. There was no difference between the composition profiles of the bonds made with the parent alloy in the fine-grained state and that in the recrystallized state. Although the ideal bond with a continuous grain structure across

the joint was not achieved, isothermal annealing resulted in a homogeneous composition across the bond.

4.2.3 Summary.

MA758 ODS alloy was TLP bonded in the fine-grained and in the recrystallized states at 1100 °C for various hold times using a Ni-Cr-Fe-Si-B interlayer. Recrystallization of grains adjacent to the joint centre-line was observed in the bonds made with the parent alloy in the fine-grained state, but was not found in bonds made with the parent alloy in the coarser-grained state. This was attributed to the stored strain energy within the fine grain structure of the parent alloy during mechanical alloying. The time required to complete isothermal solidification is longer when bonding the parent alloy in the recrystallized state than when joining the parent alloy in the fine-grained state. This was attributed to the increase in grain boundary contribution to the diffusion of solutes. Post-bond heat treatments were successful in homogenizing compositions. Homogeneity of bonds was achieved by carefully controlling the bonding conditions, e.g. bonding at 1100 °C with a hold time of 30 minutes followed by a post bond heat treatment at 1360 °C for 120 minutes.

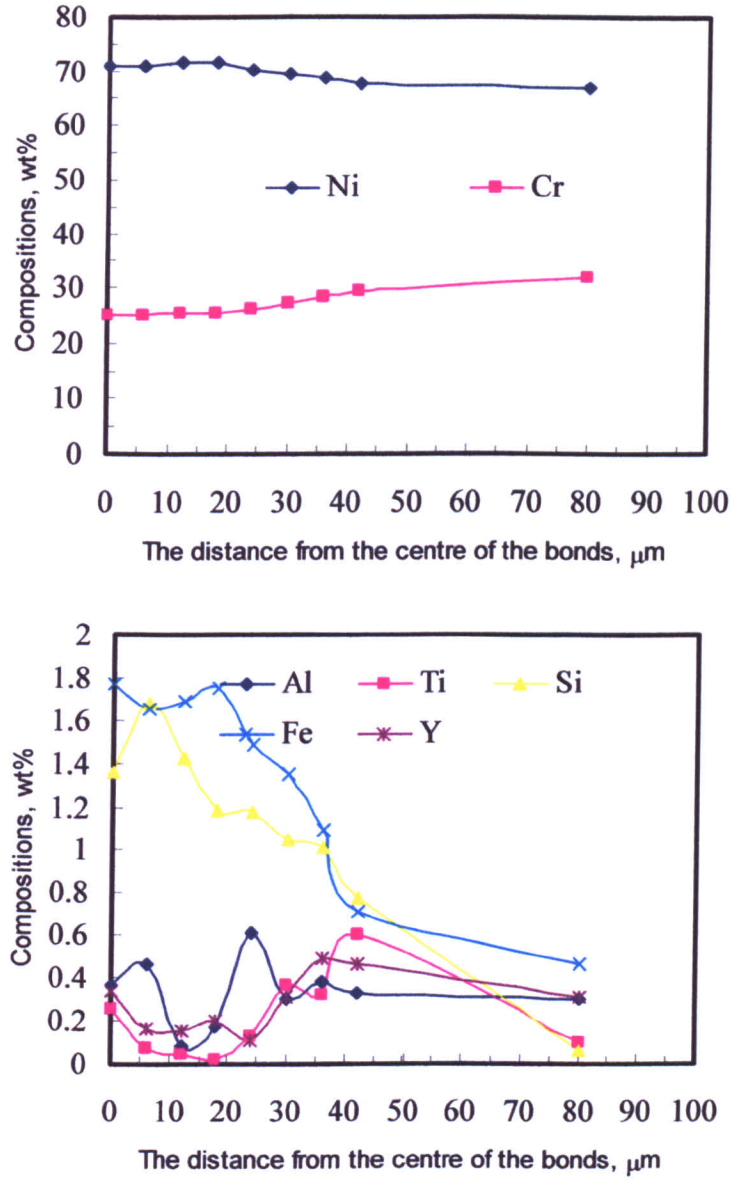

Figure 4-15 Composition profiles of the bonds made with the parent alloy in the recrystallized state at 1100 °C with a hold time of 30 minutes.

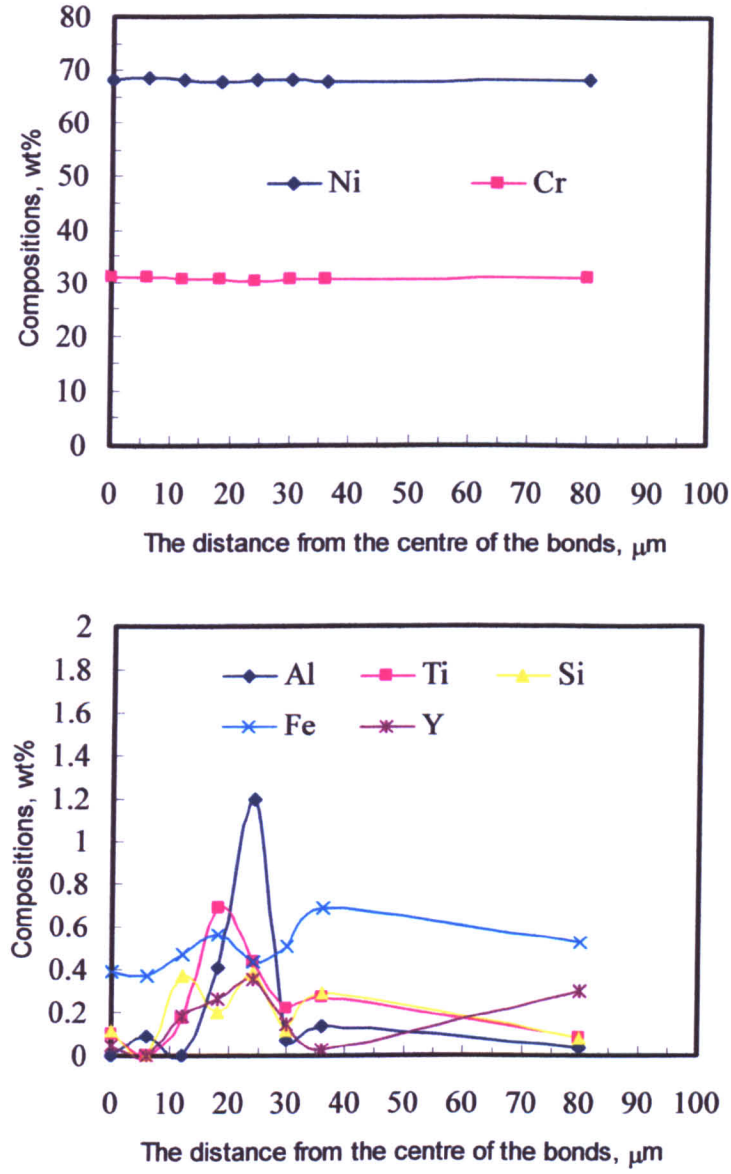

Figure 4-16 Composition profiles of the bonds made with the parent alloy in the recrystallized state at 1100 °C with a hold time of 30 minutes and subjected to a post-bond heat treatment.

4.3 The effect of the bonding temperature on TLP bonding.

The effect of bonding temperature on joint quality was investigated. The parent alloy with different grain sizes was joined at 1200 °C for hold times of 5, 15, and 30 minutes. A post-bond heat treatment was carried out to homogenize the bonds.

4.3.1 TLP bonding with the ODS alloy in the fine-grained state.

4.3.1.1 Bond microstructure.

Figure 4-17 shows the microstructures of bonds made with the parent alloy in the fine-grained state at 1200 °C for a 5 minutes hold time. A noticeable feature was the recrystallization of grains adjacent to the joint centre-line. No residual eutectic phase could be found in the bonds. This suggested that isothermal solidification of the TLP bond had been completed. It was also clear that the segregation of Y_2O_3 dispersoids was mainly along the joint interface. Figure 4-18 shows the joints made with the parent alloy in the fine-grained state for a longer hold time of 15 minutes. The microstructure indicated that the recrystallized grains along the interfaces grew into larger grains. In addition, no eutectic phases were present within the joint and segregation of Y_2O_3 was also clearly observed. Figure 4-19 shows the microstructure of joint made with longer hold time of 30 minutes. Similar microstructures were found, not only along the interfaces of the joints, the Y_2O_3 dispersoids were present along the grain boundaries of the recrystallized grains. EDX spectrum shows clearly the dispersoids were rich in Y and Al as shown in Figure 4-20. The reason why a large amount of Ni and Cr was detected in the EDX analysis from the agglomerates was the volume effect of the spot analysis (spectrum presents signals collected from an area of 1 μm in diameter).

In comparison to TLP bonding process at 1100 °C, bonding at a higher temperature of 1200 °C requires a shorter time for isothermal solidification to complete. This was attributed to the faster diffusion rate of B at the higher bonding temperature. Bonding at 1200 °C indicated that recrystallization was more severe than that seen at 1100 °C. The isothermal annealing of the parent alloy at 1200 °C does not produce such recrystallization. The recrystallization "zone 1" (which was described in section 4.2)

was not observed within the joint with a hold time longer than 5 minutes. As discussed before, the recrystallization during bonding at 1100 °C was attributed to two factors: flow of B into the parent alloy and stored energy within the fine-grained microstructure. During bonding at 1200 °C, faster diffusion of B can be expected and accordingly more severe recrystallization was shown.

The microstructure of the joints made with the parent alloy in the fine-grained state at 1200 °C with a hold time of 5 minutes followed by a post-bond heat treatment at 1360 °C for 120 minutes are shown in Figure 4-21. Grains within the joint centre-line recrystallized and grew into the parent alloy by consuming the grains close to the joint interface. However, continuity of the joints microstructure was not achieved. By heat-treating joints made for longer hold time of 15 minutes, similar microstructures were present, but with less grain growth of the grains within the joint centre-line, as shown in Figure 4-22. Nevertheless, in the joints made with an even longer hold time of 30 minutes followed by a post-bond heat treatment, different microstructures were observed. Grain growth within the joint as a result of consuming adjacent grains within the parent alloy was not seen, as shown in the Figure 4-23. The recrystallized grains located initially along the joint interface recrystallized and grew into larger grains, which were much larger than the recrystallized grains within the parent alloy. As a result, these recrystallized grains were too large for grains within the joint centre-line to consume during the post-bond heat treatment, which was seen for the bonds made at 1100 °C. Precipitates along the grain boundaries was formed after the post-bond heat-treatment.. EDX analysis shows that these precipitates were rich in Cr, as shown in Figure 4-24. These precipitates were not only detected within the joints but also within the parent alloy, which was thought to be Cr(Ni) borides.

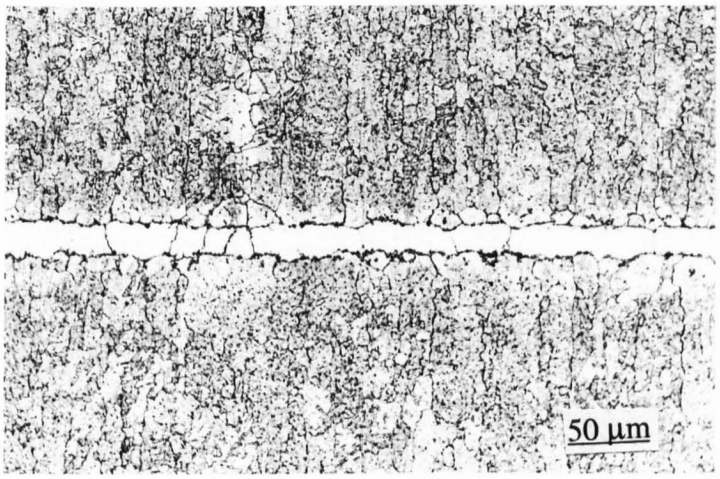

Figure 4-17 Joints made with the parent alloy in the fine-grained state at 1200 °C with a hold time of 5 minutes (light micrograph).

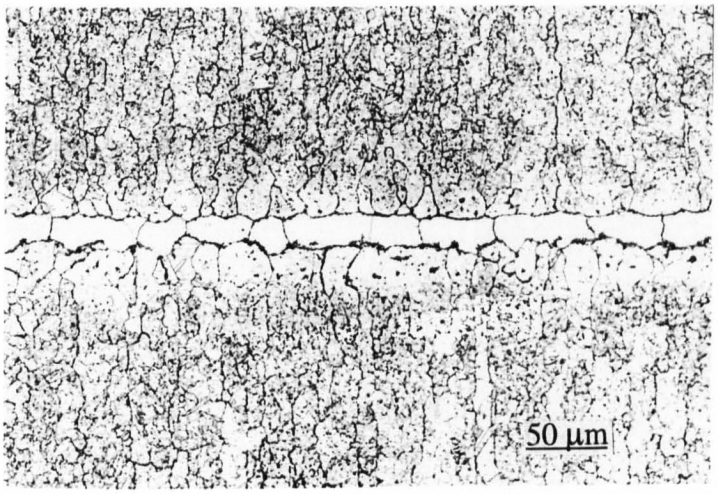

Figure 4-18 Joints made with the parent alloy in the fine-grained state at 1200 °C with a hold time of 15 minutes (light micrograph).

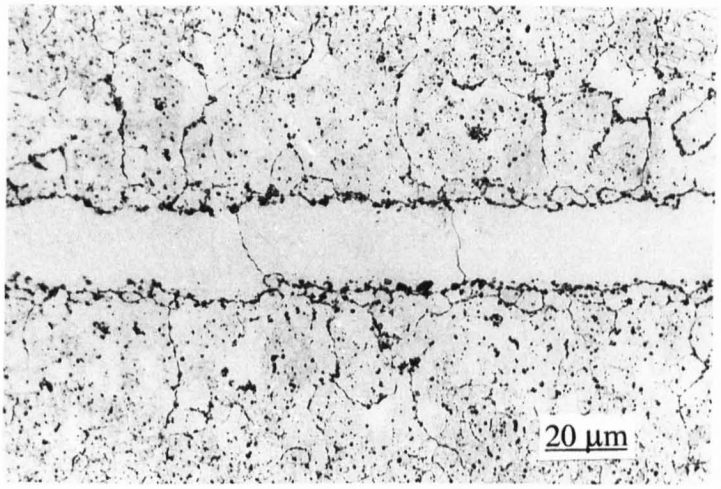

Figure 4-19 Microstructure of the bonds made with the parent alloy in the fine-grained state at 1200 °C with a hold time of 30 minutes (light micrograph).

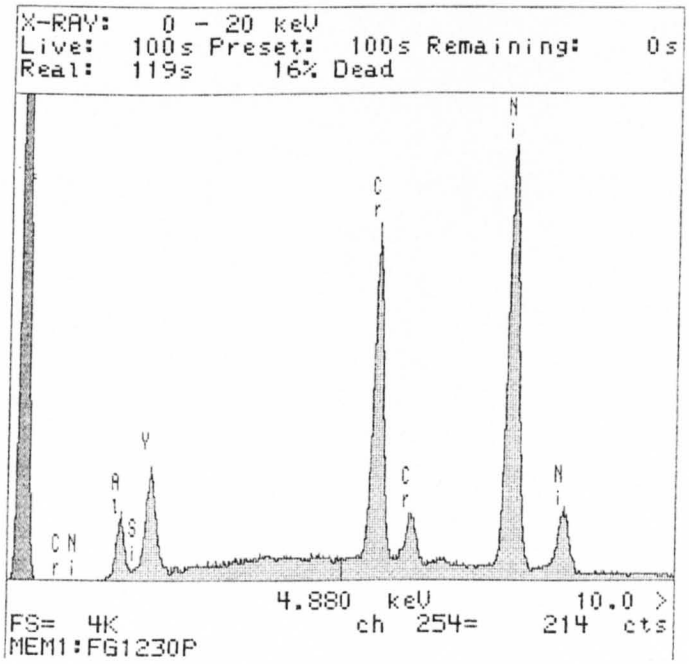

Figure 4-20 EDX of the agglomerates along the joint interface of the bond made with the parent alloy in the fine-grained state at 1200 °C with a hold time of 30 minutes.

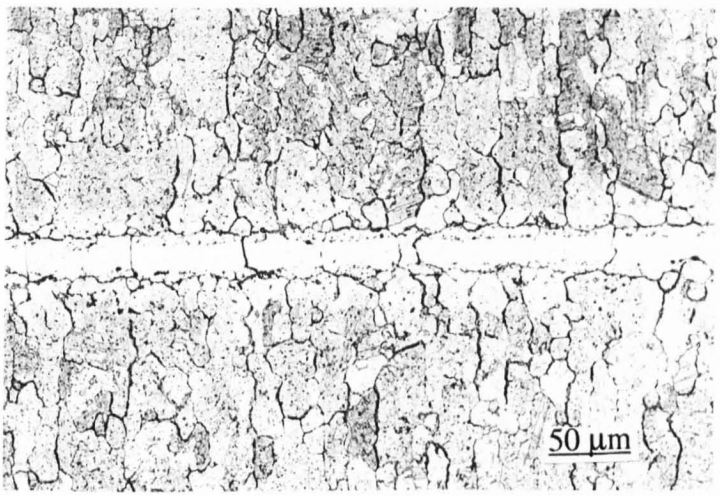

Figure 4-21 Joints made with the parent alloy in the fine-grained state at 1200 °C with a hold time of 5 minutes subjected to a post-bond heat treatment at 1360 °C for 120 minutes (light micrograph).

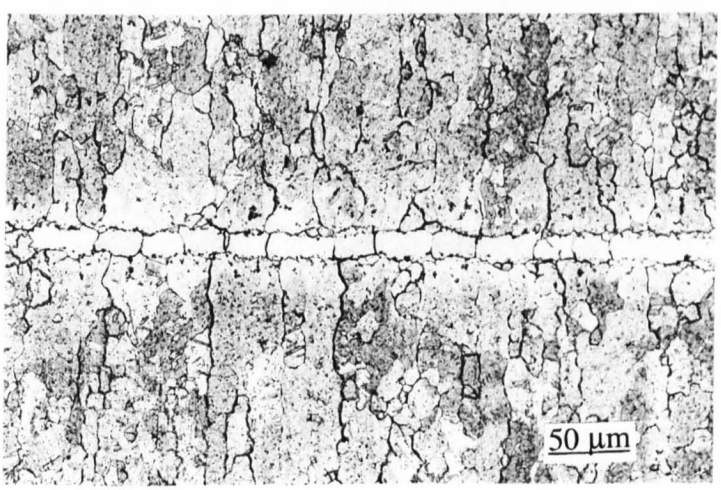

Figure 4-22 Joints made with the parent alloy in the fine-grained state at 1200 °C with a hold time of 15 minutes followed by a post-bond heat treatment at 1360 °C for 120 minutes (light micrograph).

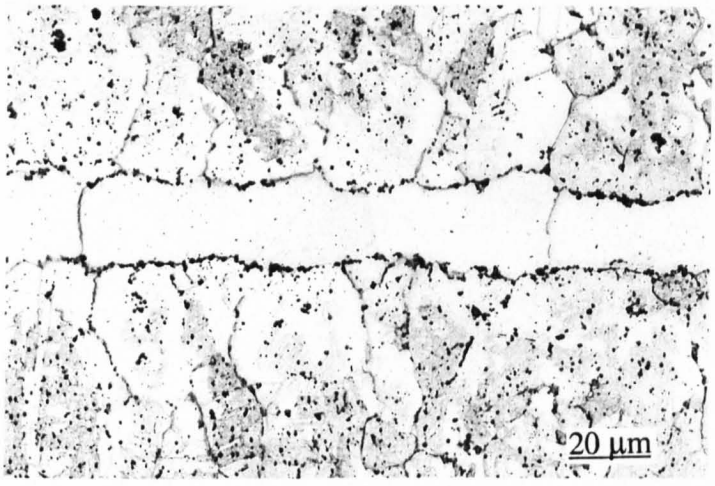

Figure 4-23 Joints made with the parent alloy in the fine-grained state at 1200 °C for 30 minutes followed by a post-bond heat treatment at 1360 °C for 120 minutes (light micrograph).

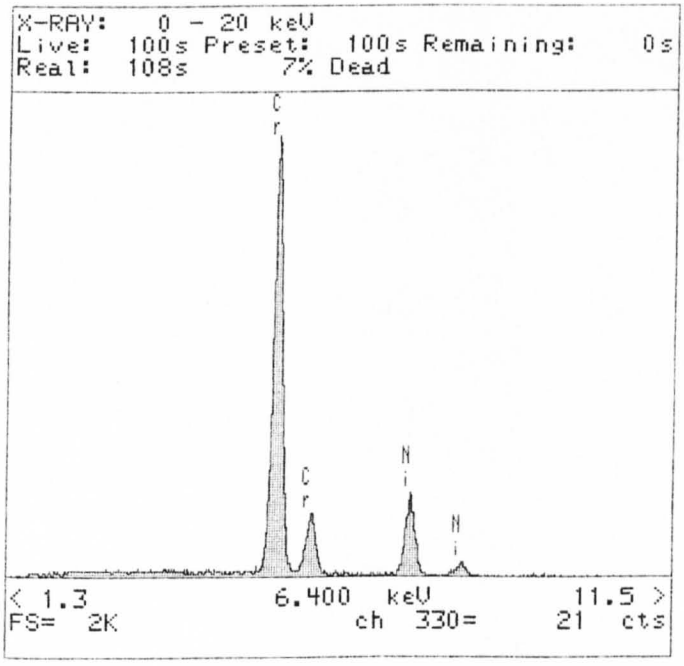

Figure 4-24 EDX of the precipitates along the grain boundaries in the joints made at 1200 °C with a hold time of 30 minutes followed by a the post-bond heat treatment.

4.3.1.2 Composition profiles.

Composition profiles were monitored as a function of the distance from the centre of bonds. Figure 4-25 shows the composition profiles of the bonds made with a hold time of 30 minutes. The graph indicates that the concentration of Ni across the joint was uniform. The content of Cr in the centre of the bond was ~29 wt%, which was close to that in the parent alloy, (30wt%). Bearing in mind that the original interlayer only contained about 14wt%Cr, this high value of Cr content indicated that the dissolution of the parent alloy occurred to a significant extent during TLP bonding. This was attributed to the higher bonding temperature, at which there is a lower B content in the equilibrium composition, as shown in the Ni-B phase diagram [106]. The distance from the centre of the bonds, within which the compositions of Ni and Cr were slightly different from that of the parent alloy, was about 40 μm. This could be taken as half of the maximum width of the liquid interlayer. If so, the dissolution of TLP at 1200 °C is more severe than that at 1100 °C, as shown in Figure 4-9. The content of Fe decreased gradually with distance away from the centre of the bonds and became stable within the parent alloy. The diffusion of Si at 1200 °C was rapid and the content of Si changed from ~5 wt% to less than 1 wt% in the joints made with a hold time of 30 minutes (as seen in Figure 4-25). Compared with the bonds made at 1100 °C, the content of Si and Fe were more uniformly distributed. The composition of Al and Ti was homogeneous throughout the joints. But as discussed above, TiO_2 and Al_2O_3, together with Y_2O_3 was shown to segregate at the joint interface and along the grain boundaries. The results presented here were gained by applying EDX spot analysis only on the area free of TiO_2, Al_2O_3, Y_2O_3 particles, so that it did not include the information of either aggregations or precipitates. The effect of the post-bond heat treatment on composition changes across the bonds is shown in Figure 4-26. The profiles clearly show that the post-bond heat treatment increases composition homogeneity.

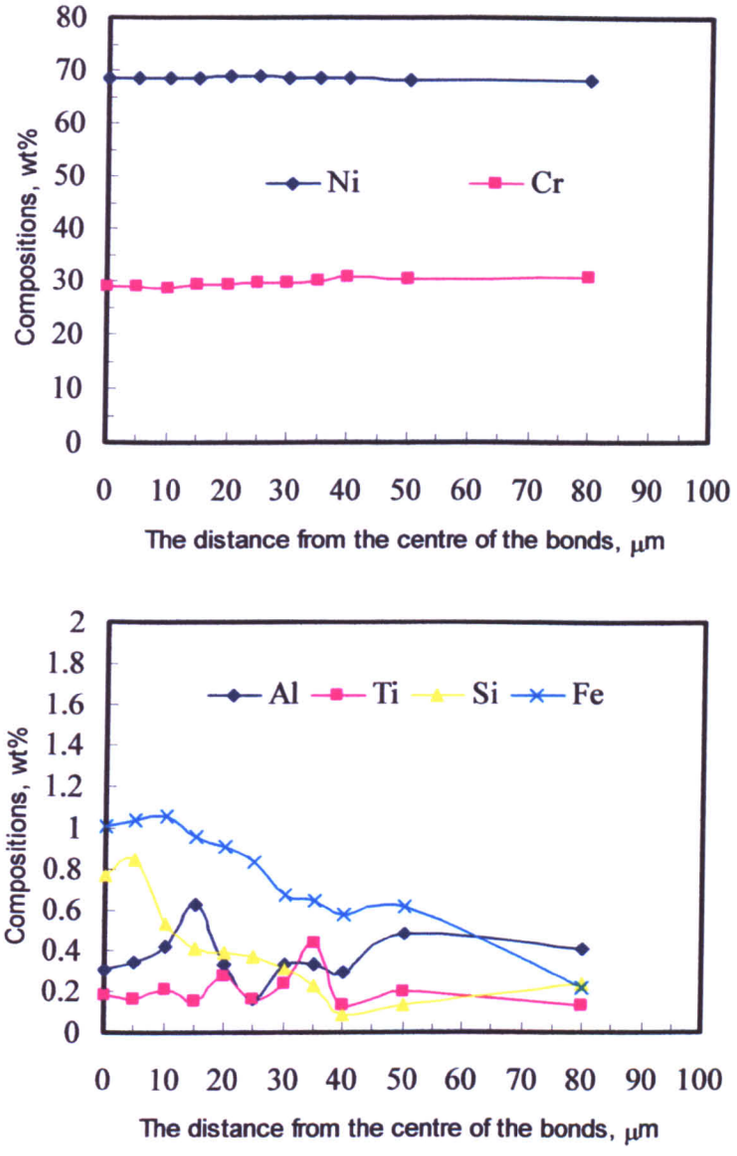

Figure 4-25 Composition profiles of the bonds made with the parent alloy in the fine-grained state at 1200 °C with a hold time of 30 minutes.

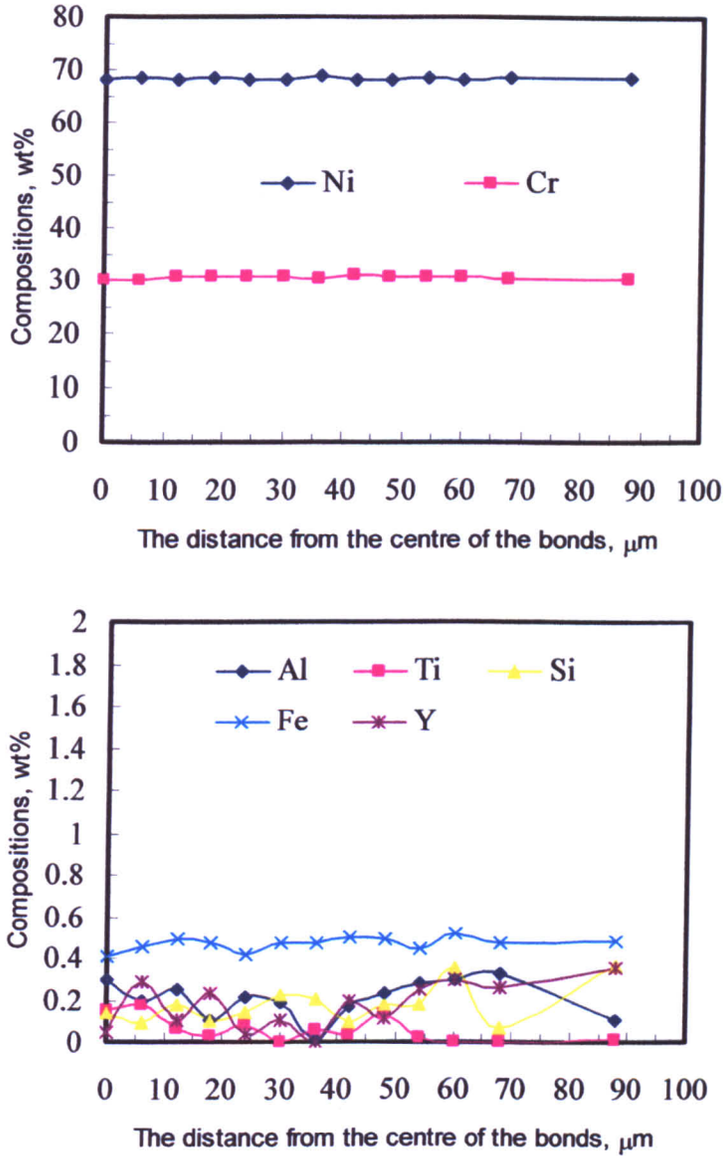

Figure 4-26 Composition profiles of the bonds made with the parent alloy in the fine-grained state at 1200 °C with a hold time of 30 minutes and subjected to a post-bond heat treatment.

4.3.2 TLP bonding with the ODS alloy in the recrystallized state.

4.3.2.1 Bond microstructure.

Microstructures of bonds made with the alloy in the recrystallized state at 1200 °C with a hold time of 60 minutes are shown in Figure 4-27. Segregation of Y_2O_3 dispersoids was found along the joint interface. No recrystallization was observed adjacent to the joint centre-line. However, in the bonds made with the parent alloy in the fine-grained state at 1200 °C, strong recrystallization was observed. This was attributed to a lack of activation energy, (i.e. stored energy during processing), although a strong flow of B into the parent alloy during TLP was expected. Pores were seen along grain boundaries following by a post-bond heat treatment, a homogenized microstructure across the joints was not produced, as illustrated in Figure 4-28. In addition, porosity was found along the bond interface. When the bonds isothermally solidified, segregation of Y_2O_3 dispersoids and Al_2O_3 particles along the interfaces produced micro-pores. The growth mechanism responsible for expanding the initial cavities is not yet totally clear [107]. It was observed that pores were also located along the grain boundaries of the elongated recrystallized grains. These have been attributed to stringers of inclusions, consisting of carbon nitride and oxide particles originating from the original powder surfaces or from incompletely alloyed regions [26, 108]. When the parent alloy is annealed, porosities are generated at these inclusions along the extrusion direction.

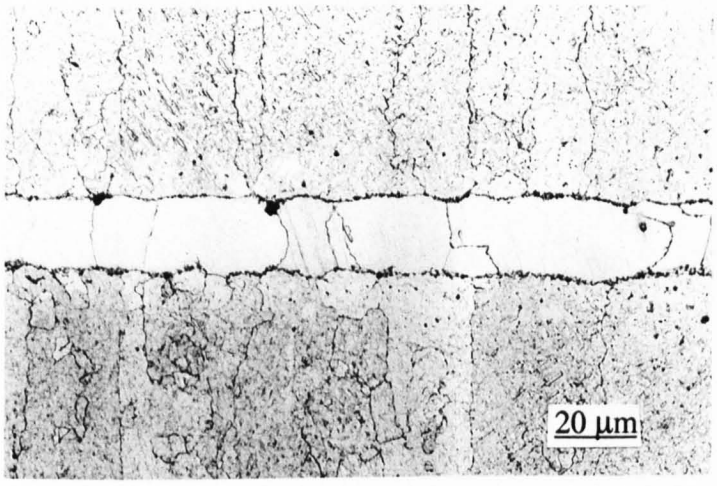

Figure 4-27 Microstructures of the bonds made with the parent alloy in the recrystallized state at 1200 °C with a hold time of 60 minutes (light micrograph).

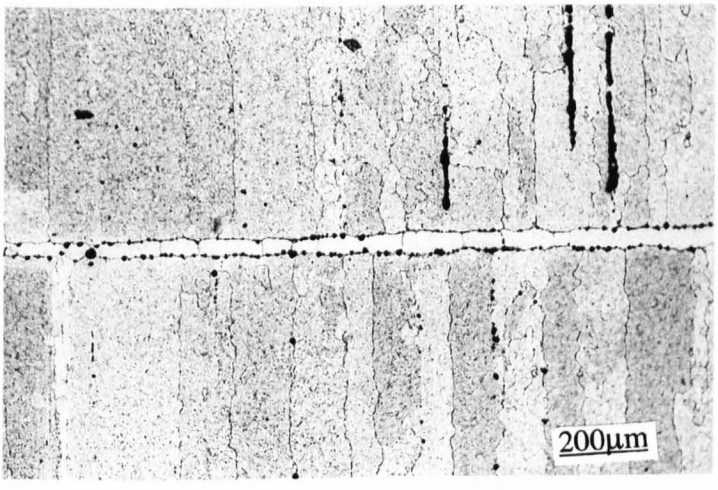

Figure 4-28 Microstructures of the bonds made with the parent alloy in the recrystallized state at 1200 °C with a hold time of 60 minutes followed by post-bond heat treatment at 1360 °C for 120 minutes (light micrograph).

4.3.3 Summary.

TLP bonding of an ODS alloy at a higher temperature of 1200 °C results in a shorter time to complete isothermal solidification, which in turn was attributed to the faster diffusion of B and Si in nickel. Strong recrystallization was observed adjacent to the joint centre-line in the bonds made with the parent alloy in the fine-grained state. This was attributed to the stored energy within the fine grained structure, and due to the strong flux of B into the parent alloy. No recrystallization was found in the bonds made with the parent alloy in the recrystallized state due to the grains having lost the driving energy for grain growth. Post-bond heat treatment failed to homogenize the microstructures across the joint interface although homogeneous composition profiles were produced.

4.4 The effects of pressure on bonding.

4.4.1 TLP bonding with the ODS alloy in the fine-grained state.

4.4.1.1 Bond microstructure.

The MA758 ODS alloy was joined at 1100 °C with a hold time of 30 minutes under pressures of 1.2 and 2.2 MPa in order to investigate the effects of pressure on the bonding process. The microstructures of the joints made with the alloy in the fine-grained state under a pressure of 1.2 MPa is shown in the Figure 4-29. Planar bond interfaces were produced. Less recrystallized grains were detected along the joint interface compared to bonds made at 1100 °C for 30 minutes without pressure. A planar interface was also seen in the bonds made under a pressure of 2.2 MPa, as shown in Figure 4-30. However, no visible recrystallization of the parent alloy was detected at the joint, and this suggested that applying a pressure during bonding could impede recrystallization, which also explains the presence of a planar joint interface.

Figure 4-31and Figure 4-32 show the microstructure of bonds subjected to a post-bond heat treatment at 1360 °C for 120 minutes. Secondary recrystallization was observed where grains within the joint centre-line grew into the parent alloy. Pores were present within the area close to the bond centre. No pores were detected within the parent alloy away from the joints. Also these pores were not detected within the bonds made under the same conditions but without pressure applied. It was discovered by Paulonis and Owczarski [109] that rapid diffusion of boron into fine-grained P/M alloy can cause joint porosity. This could explain the formation of the pores within the bonds made under pressure.

In joints made with a higher pressure, the grains within the joint centre-line grew more. However, a homogeneous microstructure across the joint was not achieved. It was thought that recrystallization was impeded by the applied pressure during bonding; therefore less stored energy was released during the bonding process compared to joints made without pressure. As a result, the grains within the area close to the joint centre-line would have more activation energy to recrystallize. This

was confirmed by the fact that grains close to the joint centre-line were larger than those in the case where no pressure was applied. However, further investigations and modelling work is necessary to substantiate this hypothesis.

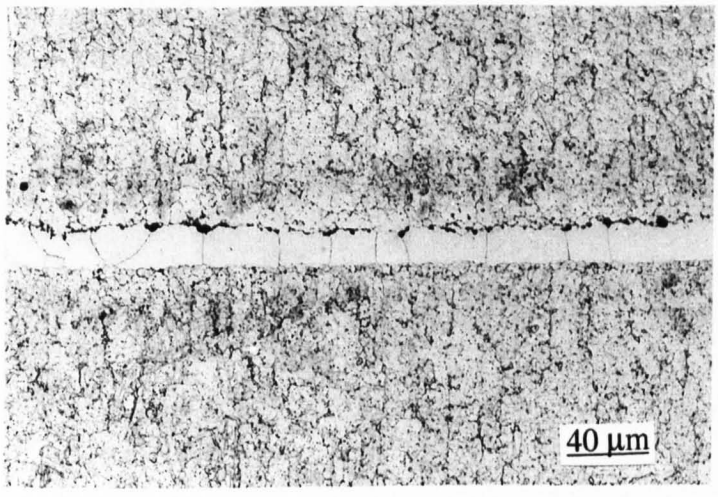

Figure 4-29 Microstructures of the bond made with the parent alloy in the fine-grained state at 1100 °C with a hold time of 30 minutes with 1.2 MPa pressure applied (light micrograph).

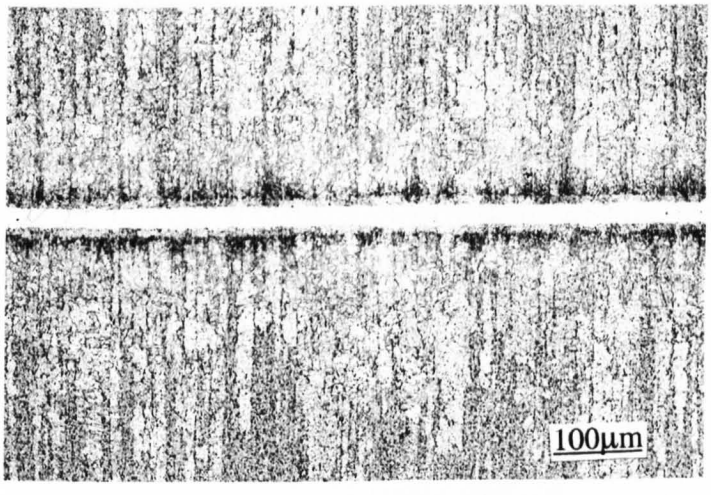

Figure 4-30 Microstructures of the bond made with the parent alloy in the fine-grained state at 1100 °C with a hold time of 30 minutes with 2.2 MPa pressure applied (light micrograph).

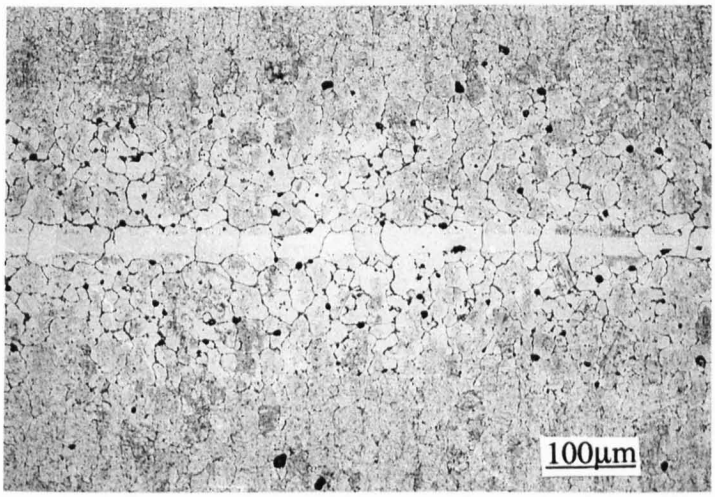

Figure 4-31 Microstructures of the bond made with the parent alloy in the fine-grained state at 1100 °C with a hold time of 30 minutes with1.2 MPa pressure applied and subjected to a post-bond heat treatment at 1360 °C with a hold time of 120 minutes (light micrograph).

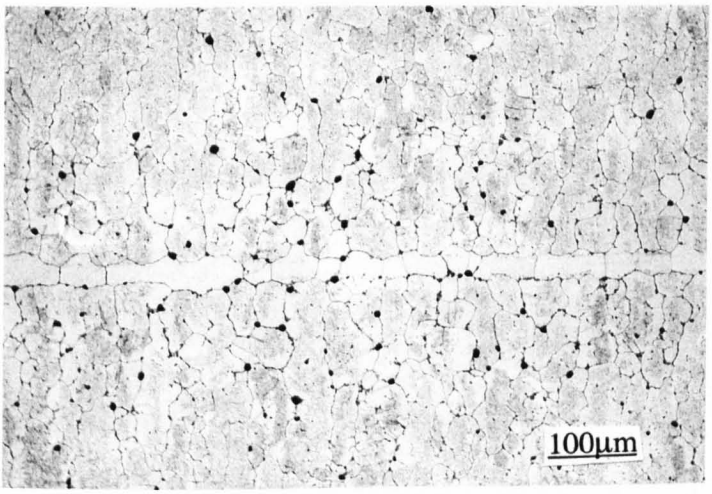

Figure 4-32 Microstructures of the bond made with the parent alloy in the fine-grained state at 1100 °C with a hold time of 30 minutes with 2.2 MPa pressure applied and subjected to a post-bond heat treatment at 1360 °C with a hold time of 120 minutes (light micrograph).

4.4.1.2 Composition profiles.

The effects of applied pressure on composition profiles across bonds made at 1100°C with a hold time of 30 minutes are shown in Figure 4-33. The Ni content decreased with distance from the centre of the bonds and became constant within the parent alloy. The Cr content increased with distance from the centre of the bonds and became stable within the parent alloy. The Fe content within the joint centre-line was much higher than that within the parent alloy and it decreased rapidly with distance from the centre of the bonds and became uniformly distributed within the parent alloy. The changes in Si concentration with the distance from the centre of the bonds had a similar pattern. The concentration of Al and Ti was homogeneous throughout the joint. In comparison with bonds made without pressure, the Ni content was higher and the concentration of Cr was lower in the middle of joint centre-line. A higher content of Fe and Si was observed within the joint centre-line and the concentration of these elements dropped more rapidly than that in the bonds made without pressure. These implied that more differences in compositions were observed between the joint centre-line and the parent alloy. This was not observed in the bonds made under a pressure of 1.2 MPa. It was thought that the ejection of B-rich liquid phase out from the liquid interlayer could be account for this. However, further investigation on the mechanisms of this effect of pressure on composition needs to be carried out.

Post-bond heat treatment homogenized the composition profiles across the joint centre-line, as shown in Figure 4-34.

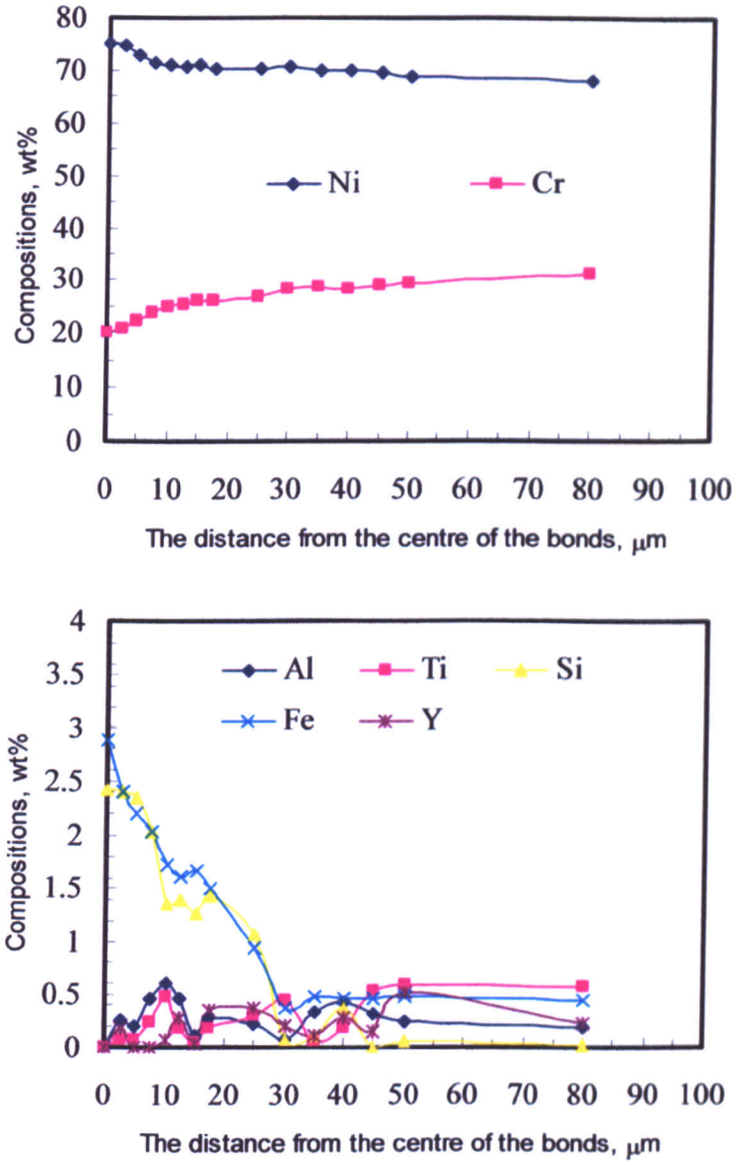

Figure 4-33 Composition profiles of the bonds made with the parent alloy in the fine-grained state at 1100 °C with a hold time of 30 minutes under pressure of 2.2 MPa.

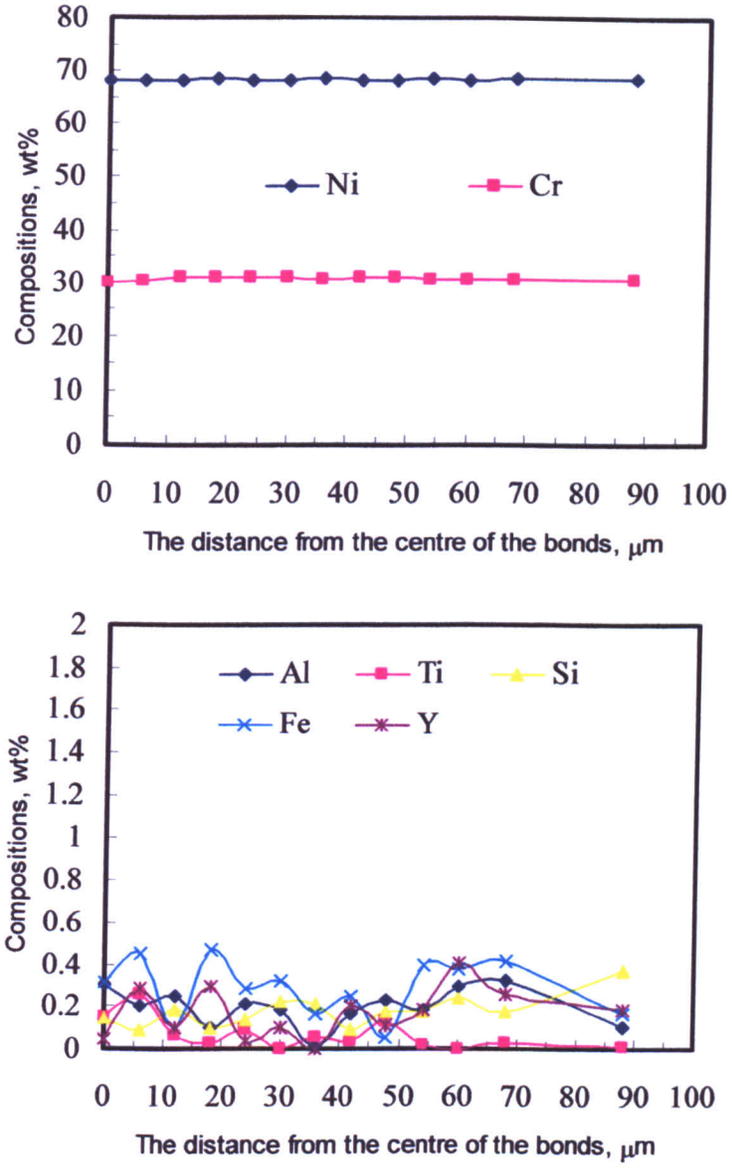

Figure 4-34 Composition profiles of the bonds made at 1100 °C with a hold time of 30 minutes under a pressure of 2.2 MPa and subjected to a post-bond heat treatment at 1360 °C for 120 minutes.

4.4.2 TLP bonding with the ODS alloy in the recrystallized state.

4.4.2.1 Bond microstructure.

The microstructures of the bonds made using the parent alloy in the recrystallized state under a pressure of 1.2 and 2.2 MPa were investigated. The microstructure of a bond made under a pressure of 1.2 MPa is shown in Figure 4-35. A similar joint microstructure was produced with respect to that without a pressure applied. A slightly narrower joint centre-line was made when increasing the pressure to 2.2 MPa, as shown in Figure 4-36. The joint interface between the centre-line and the parent alloy was distorted and a local curvature was observed. Compared with the planar interfaces in the bonds made with the parent alloy in the fine-grained state, this implied that more dissolution of the parent alloy during TLP bonding was observed as discussed in section 4.1. No recrystallization of the parent alloy was detected at the joint region.

All bonded specimens were post-bond heat treated at 1360 °C for 120 minutes. For the bonds made under a pressure of 1.2 MPa, a homogeneous microstructure across the bonds could not be achieved. However, it is worth noting that more grain growth was observed at the triple joints of grains, as shown in Figure 4-37. When increasing the pressure to 2.2 MPa, grains within the parent alloy grew across the joint centre-line and a homogeneous grain structure was achieved, as shown in Figure 4-38.

The effects of pressure on TLP were studied by Rabinkin and Pounds [77], Dammer [78], and Yeh and Chuang [79]. They claimed that the applied a pressure made better bonds by ejecting liquid phase enriched with the melting temperature depressant, e.g. P, out of the joint, which resulted in reducing brittle intermetallic phases. In this study, due to the high viscosity of the Ni-Cr-Fe-Si-B liquid interlayer at 1100 °C and the low pressure applied, the severe ejection of a B-rich phase was not observed. The driving energy for the grains within the parent alloy was sufficient to induce grain growth across the joint centre-line and this resulted in continuous microstructure.

4.4.3 Summary.

When joining the parent alloy in the fine-grained state, it was thought that an application of pressure hindered recrystallization of the grains within the parent alloy and produced flat joint interfaces. Joints made with an applied pressure produced large recrystallized grains within the joint region on post-bond heat treatment. Pores were produced in all the post-bond heat-treated specimens.

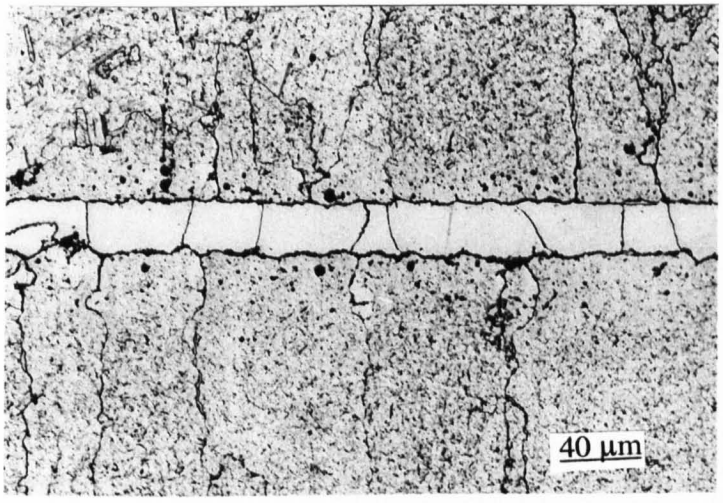

Figure 4-35 Microstructure of the bonds made with the parent alloy in the recrystallized state at 1100 °C with a hold time of 30 minutes under a pressure of 1.2MPa (light micrograph).

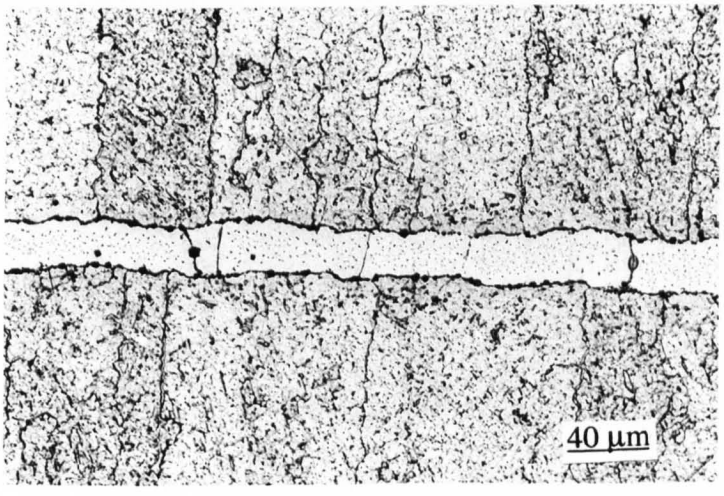

Figure 4-36 Microstructure of the bonds made with the parent alloy in the recrystallized state at 1100 °C with a hold time of 30 minutes under a pressure of 2.2 MPa (light micrograph).

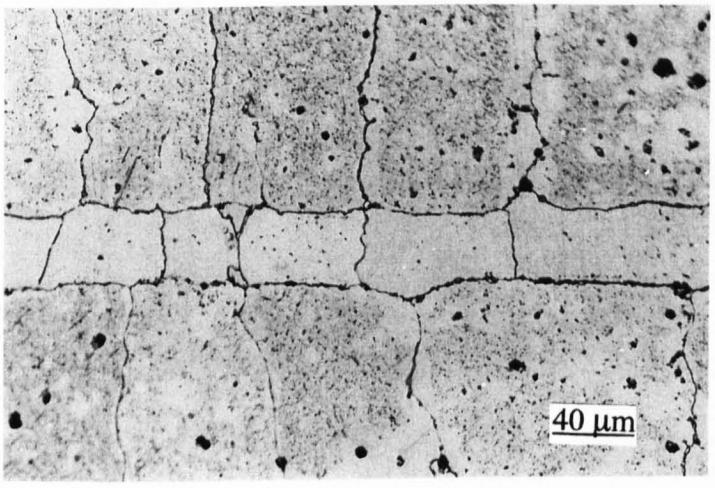

Figure 4-37 Microstructure of the bonds made with the parent alloy in the recrystallized state at 1100 °C with a hold time of 30 minutes under a pressure of 1.2 MPa followed by a post-bond heat treatment (light micrograph).

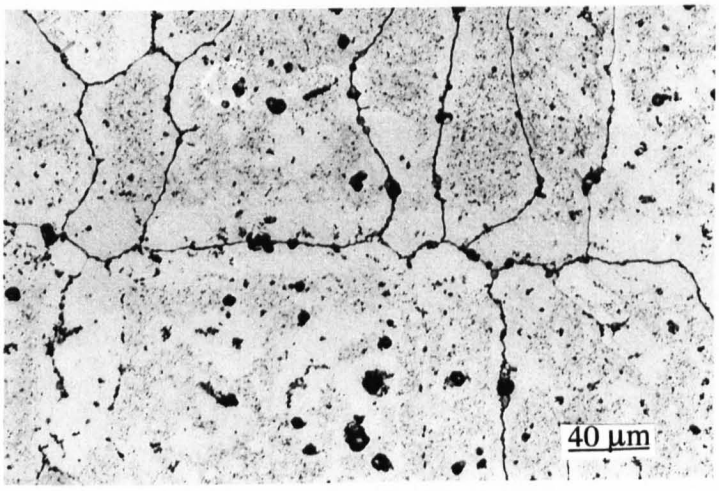

Figure 4-38 Microstructure of the bonds made with the parent alloy in the recrystallized state at 1100 °C with a hold time of 30 minutes under a pressure of 2.2 MPa followed by a post-bond heat treatment (light micrograph).

4.5 Mechanical properties.

4.5.1 Shear strength.

Initial metallurgical examinations show that the TLP bonds made using the Ni-Cr-Fe-Si-B interlayer under various bonding conditions produced different joint microstructures. It was necessary to assess the quality of these bonds by shear testing.

The shear test results from bonds made at 1100 °C are shown in Figure 4-39. Specimens made with the parent alloy in the fine-grained state with a hold time of 30 minutes had the highest shear strength (613 MP), which was ~96% that of the parent alloy. When joining for a longer hold time of 60 minutes, the bond shear strength reduced to 592 MPa. When joining the parent alloy in the recrystallized state with a hold time of 30 minutes, the shear strength (504 MPa) was lower than that of the bonds made with the parent alloy in the fine-grained state. With a longer hold time of 60 minutes, the shear strength of the bonds decreased slightly. Unlike the bonds made with the parent alloy in the fine-grained state, the bonds made with the parent alloy in the recrystallized state were affected less by bonding time.

After heat treatment at 1360 °C for 120 minutes were applied, the shear strength of the bonds decreased with respect to that of the as-bonded specimens. The bonds made at 1100 °C with a hold time of 30 minutes possessed a lower shear strength of 499 MPa, which was 81% that of the as-bonded specimens. Comparable shear strength (487 MPa) was produced in the heat-treated bonds made under the same conditions but with longer hold time of 60 minutes. The difference in the shear strength was reduced after a post-bond heat treatment was applied with a hold time of 30 and 60 minutes. The heat-treated bonds made with the parent alloy in the recrystallized state with a hold time of 30 minutes had the shear strength of 437 MPa, which was 86% that of the as-bonded specimens. A lower shear strength of 426 MPa was obtained for the bonds made under the same conditions but for a longer hold time of 60 minutes and subjected to post-bond heat treatment. When joining the parent alloy in the recrystallized state, the shear strength of the heat-treated bonds was not sensitive to the bonding time.

When TLP bonds were made at a higher temperature of 1200 °C, a lower bond shear strength was produced compared with that for bonds made at 1100 °C, as shown in Figure 4-40. The shear strength of the bond made with the parent alloy in the fine-grained state with a hold time of 30 minutes was 530 MPa, which was ~83% that of parent alloy and lower than that of the bonds made at 1100 °C. After applying a post-bond heat treatment, the shear strength of the bonds was reduced to 429 MPa, which was ~80% that of the as-bonded specimens. This shear strength was lower than that of bonds made at 1100 °C and subjected to the post-bond heat treatment. For the bonds made with the parent alloy in the recrystallized state at 1200 °C, the shear strength was 395 MPa. This value was the lowest among that for the as-bonded specimens. When a post-bond heat treatment was applied, the shear strength fell to 320 MPa, which was the lowest value recorded in the tests.

In order to interpret the differences in shear strength, fracture surfaces of the specimens made under different joining conditions were examined using SEM. Figure 4-41 shows the fractographs of the bond made with the parent alloy in the fine-grained state at 1100 °C with a hold time of 30 minutes. It is clear that the grains within the joint were severely stretched before breaking. Apparently, the joint was ductile under the shear forces. The deformation of the joint was also shown in the cross-sectional microstructures, as shown in Figure 4-42. The failure pattern of this bond was mainly within the joint centre-line. This implied that the interface between the parent alloy and the joint-centre line was strong and failure was shown to propagate through the joint centre-line. When joining the parent alloy in the fine-grained state at a higher temperature of 1200 °C, the joints failed in a different pattern during the shear tests, as illustrated in Figure 4-44. Two distinct features were observed, namely dimples and facets. These features corresponded to failure along the interface and through the joint centre-line. As illustrated in Figure 4-43, large recrystallized grains and the aggregation of the Y_2O_3 dispersoids will weaken the joint interface. This would explain why the fracture route changes from propagation within the joint centre-line to along the interface. After post-bond heat treatment was applied, the failure of the bonds made at 1100 °C changed from being mainly within the joint centre-line to that at the joint/parent alloy interface, as shown in Figure 4-45. However, this failure pattern was different from that of as-bonded specimens made at

1200 °C because of a visible residual braze on the fracture surface. A similar failure pattern was found in bonds made with the parent alloy in the fine-grained state at 1200 °C with a hold time of 30 minutes followed by a post-bond heat treatment, as shown in Figure 4-46.

The fractographs of the bonds made with the parent alloy in recrystallized state at 1100 °C, are shown in Figure 4-47. These implied that the failure of the bonds was in some places located along the joint interface and in other places within the parent alloy. When the failure propagated along the joint interface, it was seen as a ductile fracture, which was characterized by small dimples. Failure within the parent alloy was indicated by brittle fracture showing transgranular cleavage fracture. No visible deformation of the joint centre-line caused by a shear force was detected. When bonding the parent alloy in the recrystallized state at a higher temperature of 1200 °C, fracture was located mainly along the joint interface showing a smooth surface and many dimples, as shown in Figure 4-48. The smooth fracture surface corresponded to the area where Y_2O_3 dispersoids segregated during bonding. Fractographs of the bonds made with the parent alloy in the recrystallized state followed by a post-bond heat treatment are shown in Figure 4-49 and Figure 4-50, respectively. Smoother fracture surfaces were found compared with that of the as-bonded specimens. Large pores were visible all over the surface. As discussed before, origin of these pores was attributed to stringers of inclusions, consisting of carbonide, nitride and oxide particles originating from the original powder surfaces or from incompletely alloyed regions [26, 110]. When the parent alloy is annealed, pores are generated at these inclusions along the extrusion direction. For the bonds made at 1200 °C, pores were also caused by the segregation of the Y_2O_3 dispersoids. It is thought that these surface pores provide a route for the penetration of oxygen into the ODS alloy [111].

When the strength of joint is investigated, three features of the bonds should be considered: the interfaces, the joint centre-line and the parent alloy. Failure will start from the weakest area within the joint region within which it propagates, if possible. For bonds made under different conditions, the grain size and compositions within the joint centre-line were similar to each other. Therefore, it is reasonable to assume that the strength of the joint centre-line would be similar. It is well known that parent

alloy in the fine-grained state is stronger than that in the recrystallized state because of the fine-grained structure. The strength of the joint interface needs to be clarified and considered as a key factor for the changing of mechanisms for failure.

It is worth noting that bonds made with the parent alloy in the fine-grained state were stronger than those bonds made with the parent alloy in the coarser-grained state. In this study, the strongest bonds were produced with the parent alloy in the fine-grained state at 1100 °C, in which failure occurred only through the joint centre-line. This shows that a very strong joint interface was achieved in these bonds. The shear strength of TLP bonds in this condition was ~96% that of the parent alloy, showing that the interface strength is similar to that of the parent alloy. However, the joint centre-line within bonds made with the parent alloy in the recrystallized state at 1200 °C is stronger than the interfaces because the cracks propagate only along the interfaces. In this case, the strength of the interfaces was the key factor in determining the strength of the bonds. As discussed before, in section 4.1, with a finer-grained structure in the parent alloy, the corresponding diffusion rate of B into the parent alloy was rapid. As a result, the dissolution of the parent alloy was less, and the time to complete isothermal solidification was shorter. This would be beneficial because it minimises disruption to the parent alloy microstructure, e.g. smaller recrystallized grains along the joint interface, and less segregation of Y_2O_3 dispersoids. It is suggested that these observations could explain the high bond strengths achieved.

The bonds made at 1100 °C were stronger than those made at a higher temperature of 1200 °C. This is because stronger interfaces were achieved in the bonds made at 1100 °C than that at 1200 °C. For instance, when joining the parent alloy in the fine-grained state, the failure occurs along the joint centre-line/parent alloy interface when the bonding temperature is raised from 1100 to 1200°C. Joints made at 1200 °C had bond interfaces which were weaker than the joint centre-line, and this was caused by aggregates of Y_2O_3 dispersoids and formation of larger recrystallized grains along the interfaces.

Post-bond heat treatment will reduce the strength of the bonds. When joining the parent alloy in the fine-grained state, the decrease in bond strength was attributed to

the recrystallization of grains within the parent alloy. With larger recrystallized grains along the bond interface, the strength of the joint interface decreased and therefore, failure was observed to propagate through the joint centre-line and parent alloy interface. However, the reduction in the shear strength of the bonds made with the parent alloy in the recrystallized state was not only attributed to the recrystallized grains, but also to the formation of pores, which can act as nucleation sites for cracks.

Although only shear testing of the bonds at room temperature was carried out, it did suggest the type of high-temperature properties that could be expected. The strongest bonds at room temperature would not be a candidate for high temperature applications due to the presence of a fine grain size and intermetallic precipitates along the joint interface. The bonds made at 1200 °C with the parent alloy in either fine-grained state or recrystallized state suffered from the segregation of Y_2O_3 dispersoids along the joint interface and hence, could not be considered for high temperature applications. Therefore, it suggested that the best route to produce bonds for high temperature applications is to TLP bond the ODS alloy at 1100 °C and then apply a post-bond heat treatment in a temperature gradient to homogenize the bonds in terms of microstructure and compositions.

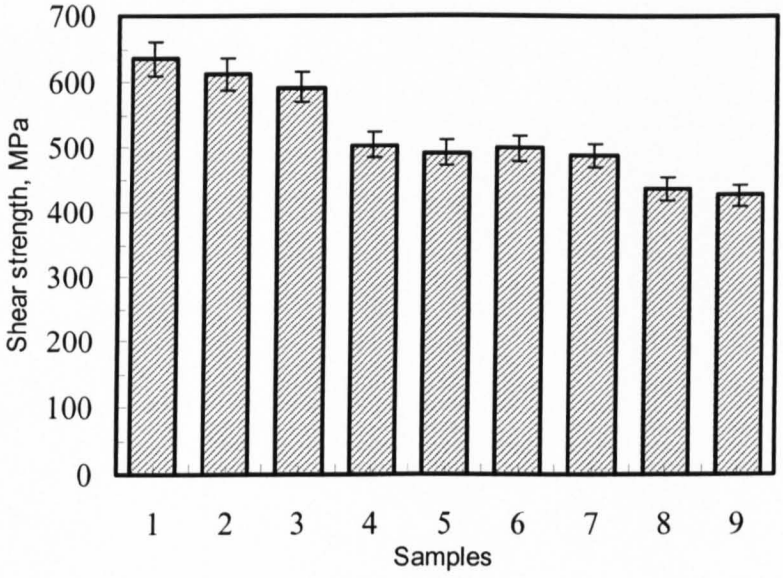

Figure 4-39 Shear strength of the bonds made at 1100 °C: 1- FG parent alloy; 2- FG 30 minutes; 3- FG 60 minutes; 4- RC 30 minutes; 5- RC 60 minutes; 6, 7 - FG 30, 60 minutes and heat treated; 8, 9 - RC 30, 60 minutes and heat treated. Note: FG: the parent alloy in the fine-grained state; RC: the parent alloy in the elongated recrystallized state.

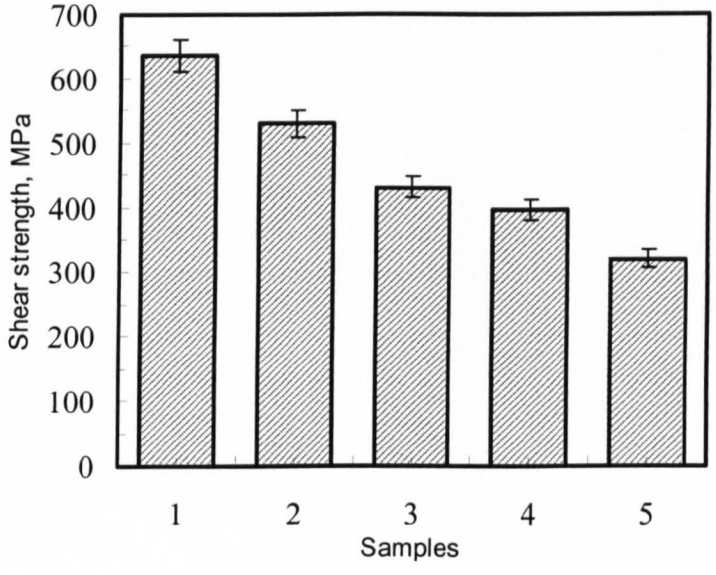

Figure 4-40 Shear strength of the bonds made at 1200 °C; 1- FG parent alloy; 2- FG 30 minutes; 3- RC 30 minutes; 4- FG 30 and heat treated; 5- RC 30 and heat treated.

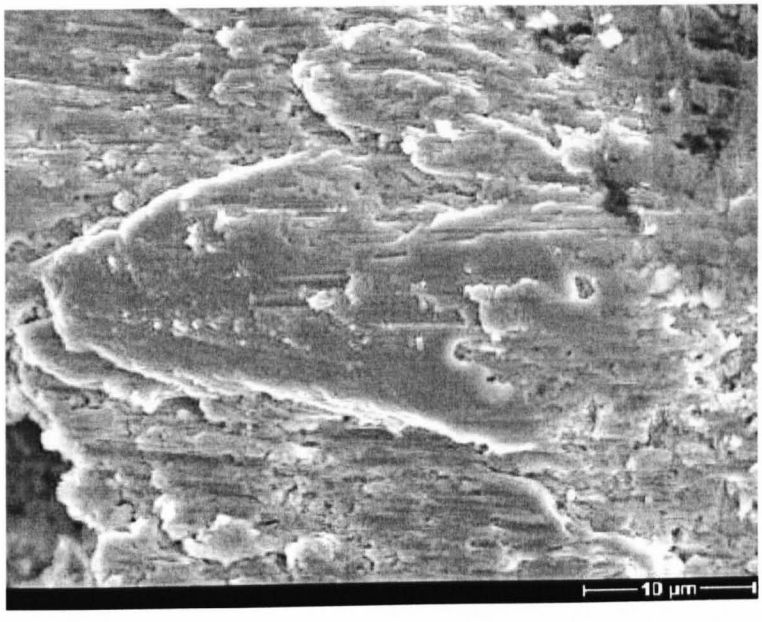

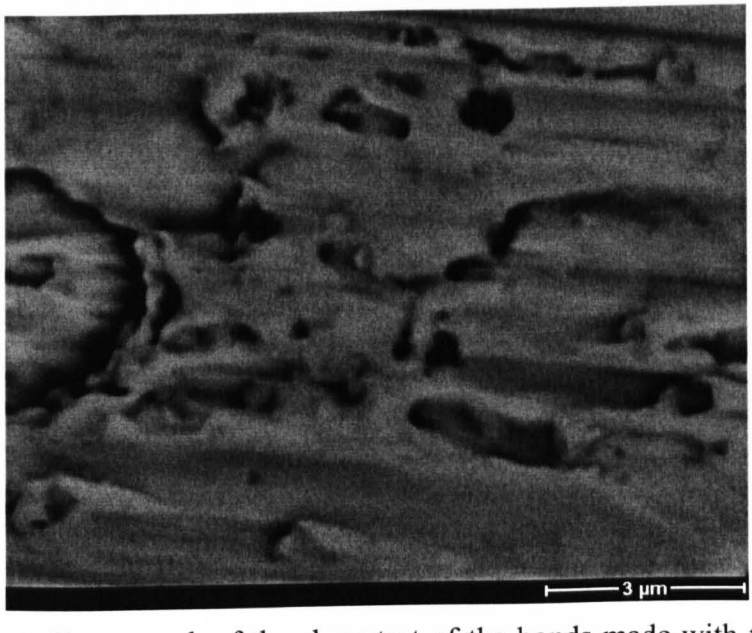

Figure 4-41 Fractograph of the shear test of the bonds made with the parent alloy in the fine-grained state at 1100 °C with a hold time of 30 minutes (J840 SEM image).

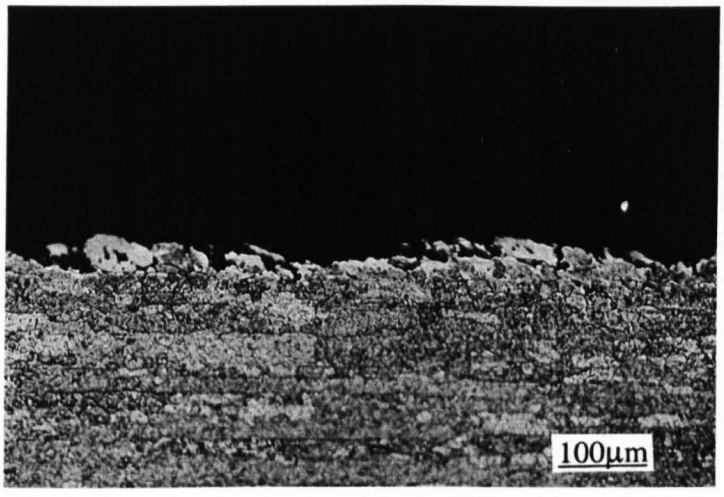

Figure 4-42 Microstructure of a cross-section of the specimen in Figure 4-41 (light micrograph).

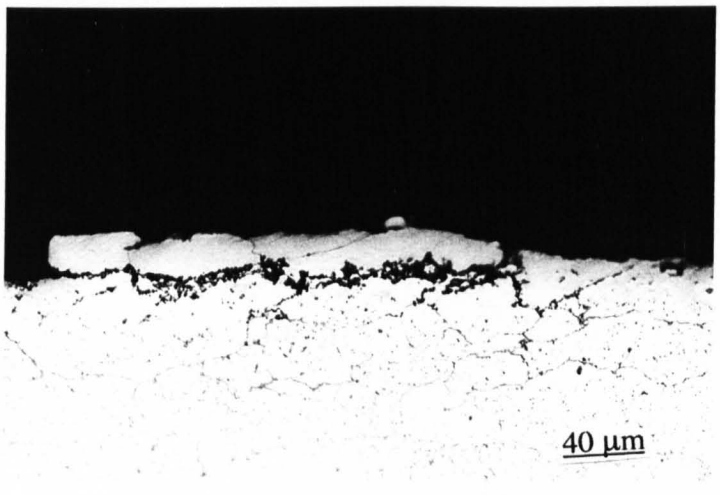

Figure 4-43 Microstructure of a cross-section of the specimen in Figure 4-44 (light micrograph).

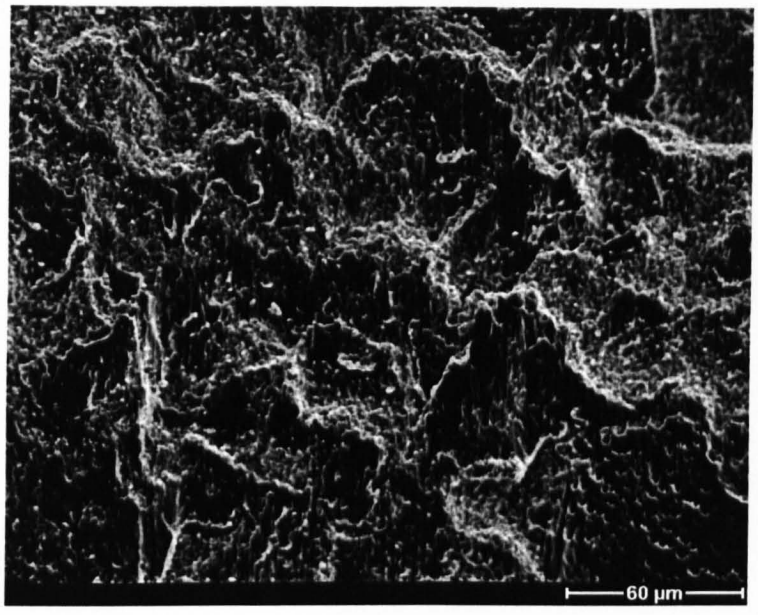

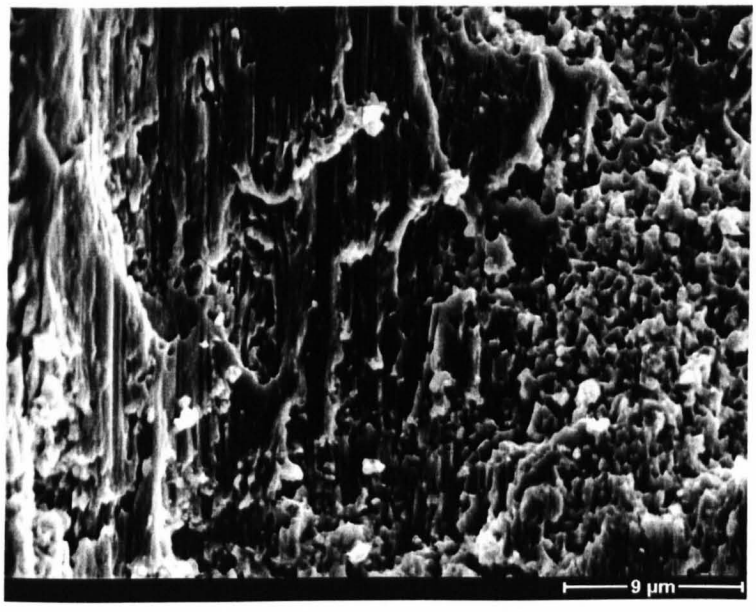

Figure 4-44 Fractograph of the shear test of the bonds made with the parent alloy in fine-grained state at 1200 °C with a hold time of 30 minutes.

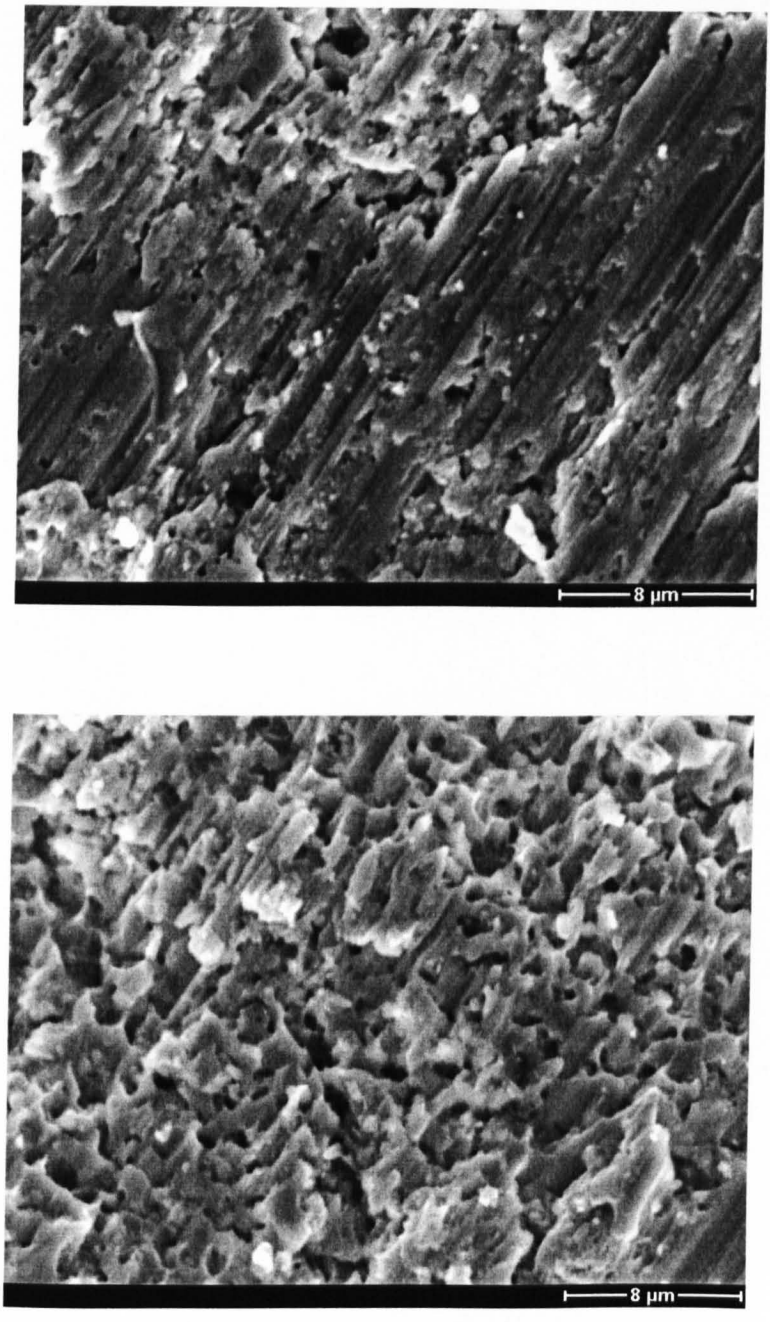

Figure 4-45 Fractograph of the shear test of the bonds made with the parent alloy in the fine-grained state at 1100 °C with a hold time of 30 minutes followed by a post-bond heat treatment.

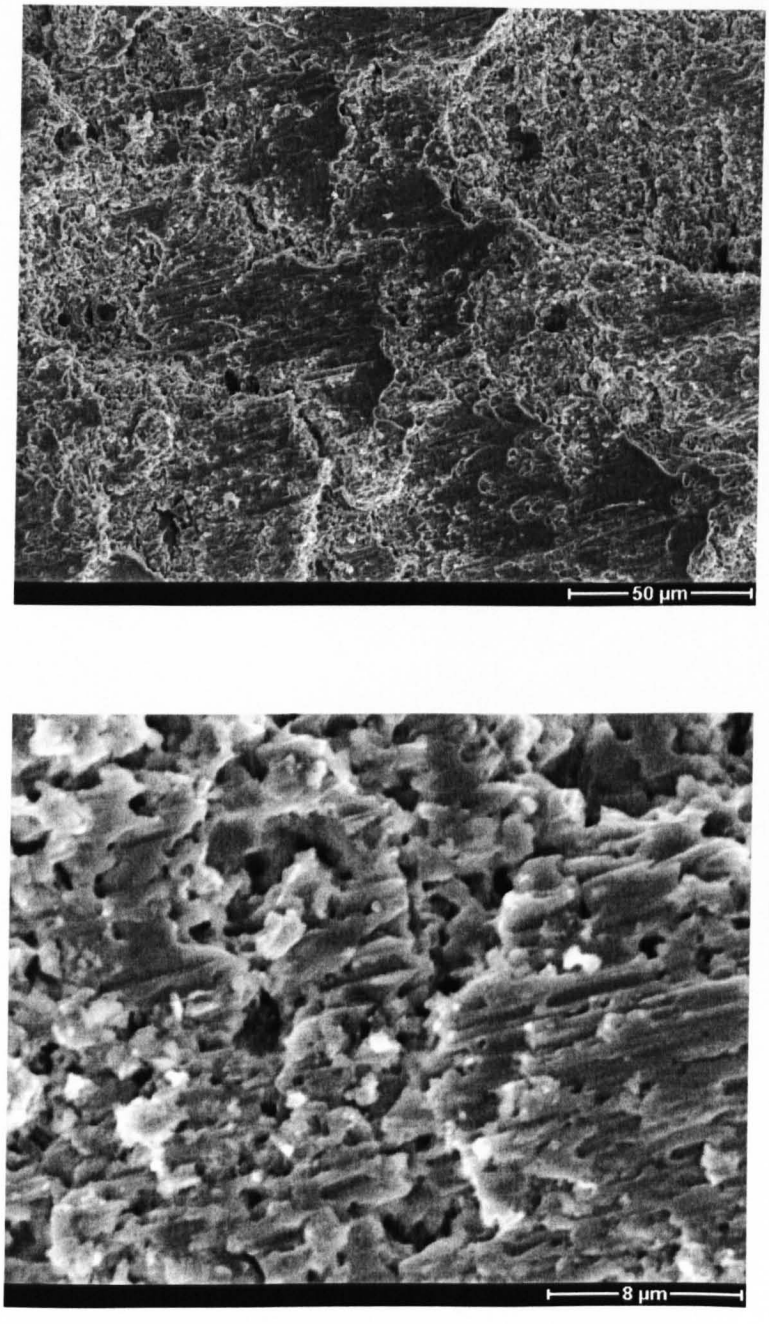

Figure 4-46 Fractograph of the shear test of the bonds made with the parent alloy in the fine-grained state 1200 °C with a hold time of 30 minutes and subjected to a post-bond heat treatment.

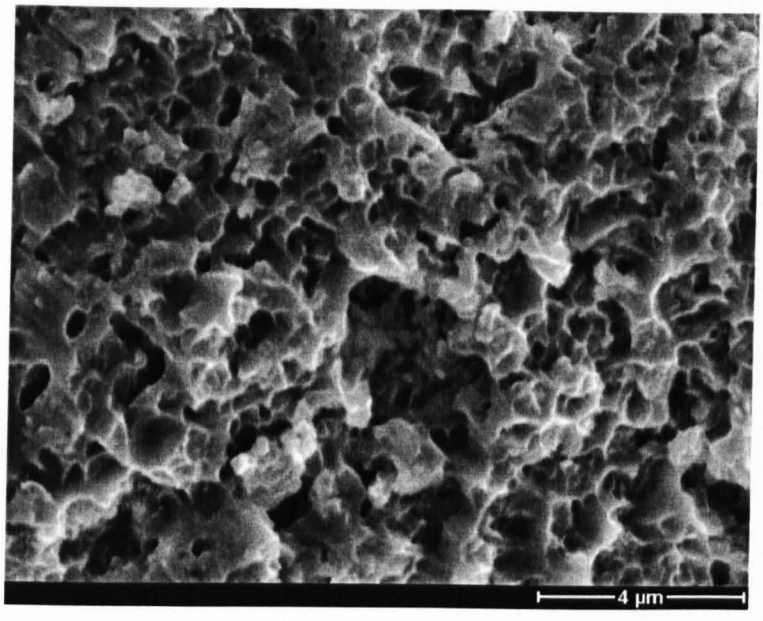

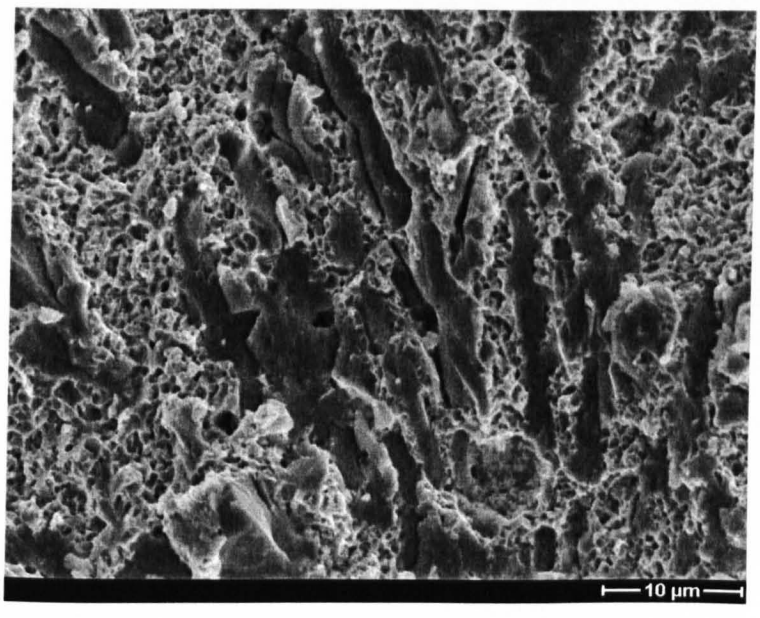

Figure 4-47 Fractograph of the shear test of the bonds made with the parent alloy in the recrystallized state at 1100 °C with a hold time of 30 minutes.

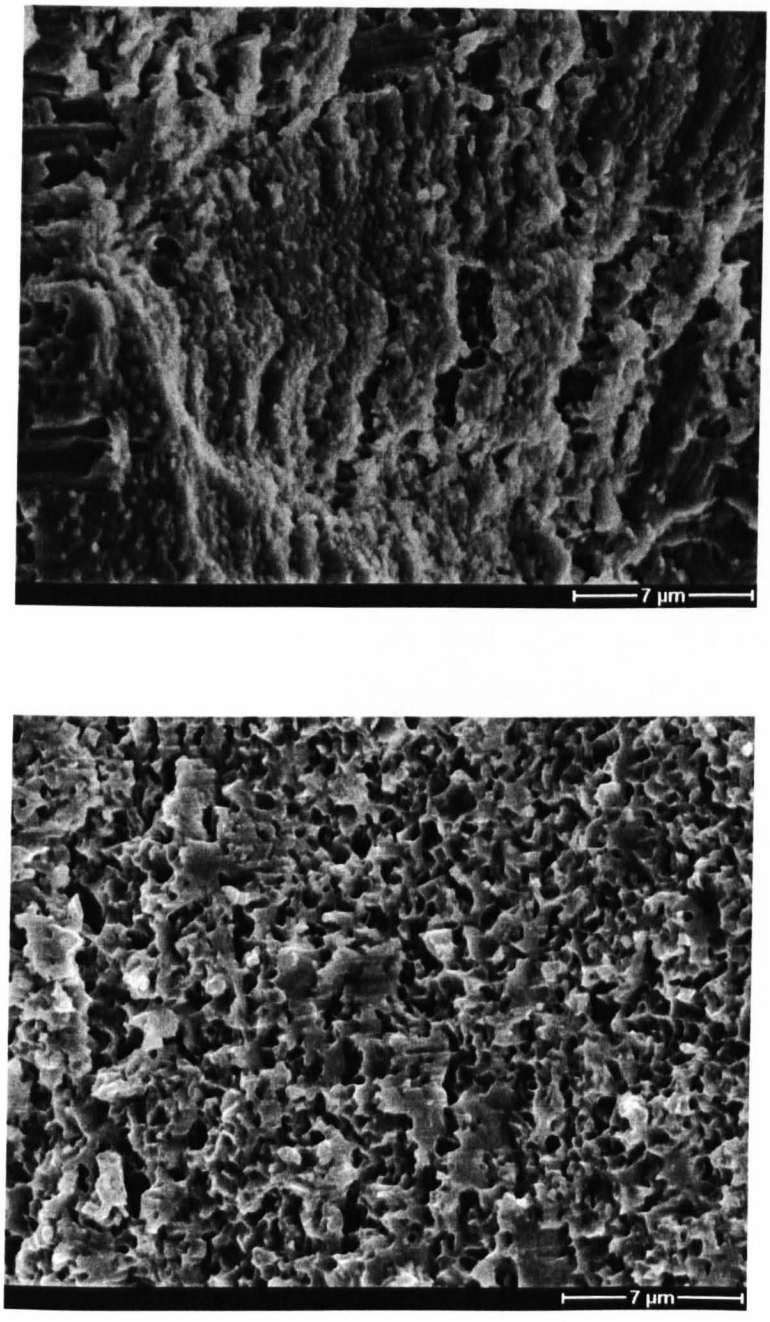

Figure 4-48 Fractograph of the shear test of the bonds made with the parent alloy in the recrystallized state at 1200 °C with a hold time of 30 minutes.

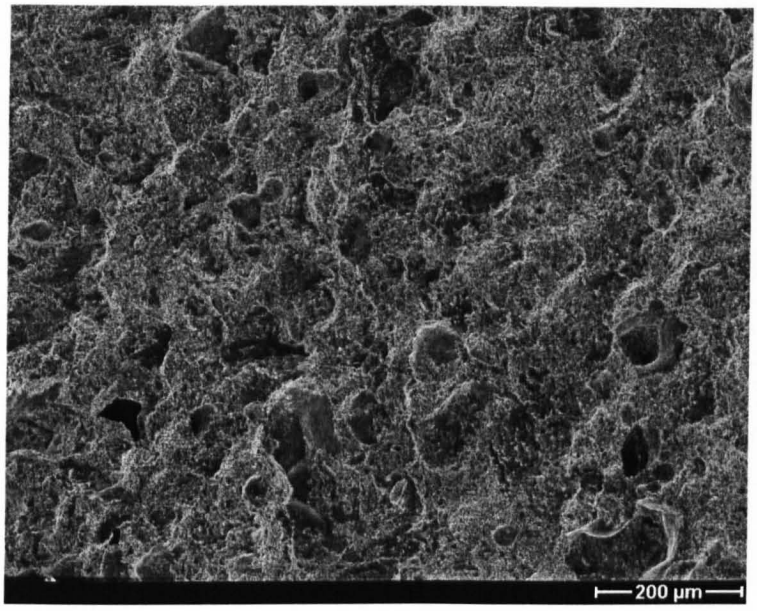

Figure 4-49 Fractograph of the shear test of the bonds made with the parent alloy in the recrystallized state at 1100 °C with a hold time of 30 minutes and subjected to a post-bond heat treatment

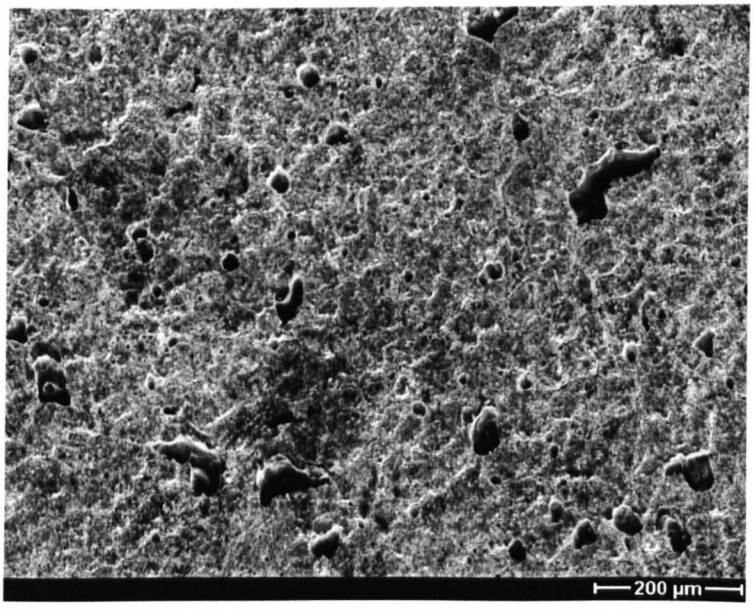

Figure 4-50 Fractograph of the shear test of the bonds made with the parent alloy in the recrystallized state at 1200 °C with a hold time of 30 minutes and subjected to a post-bond heat treatment.

4.5.2 Microhardness.

Microhardness profiles were measured from the centre of the bonds. When bonding the parent alloy in the fine-grained state, hardness increased with the distance from the joint centre-line, as shown in the Figure 4-51. When joining at 1100 °C with a hold time of 30 minutes, the hardness peaked at the interface. The hardness then became constant until a distance of 400 μm away from the joint centre-line, where the hardness has a highest value of HV 410. At a higher bonding temperature of 1200 °C with a hold time of 30 minutes, the hardness changes with the same pattern as the bonds made at 1100 °C but without a peak at the joining interface. However, the hardness was lower. After a post-bond heat treatment, the bonds made at 1100 °C show an increase in hardness with the distance from the centre of the bond, and became uniform within the parent alloy. Heat treatment made the joint interface softer.

The peak hardness in the area close to the joint interface was attributed to intermetallic precipitates within that area (as shown in Figure 4-58), which had higher microhardness than the nickel solid solution. Considering the fact that bonds made at 1100 °C with the parent alloy in the fine-grained state have the highest shear strength, as shown in section 4.5.1, the intermetallic precipitates within the area close to the joint interface might not be harmful, at least at room temperature. This result needs further investigation at elevated temperature, e.g. stress rupture tests. During post-bond heat treatment, the precipitates dissolved into the nickel solution at 1360 °C and this explain why the hardness peak disappeared after heat treatment.

As we know the hardness is the resistance to surface indentation and it is correlated with the grain size of the materials from the well known Hall-Petch relations [112, 113]. In other words, the hardness will be proportional to the square root of the diameter of grains. Therefore a recrystallized grain structure would be lower in hardness than a finer grain structure. As shown in Figure 4-19, due to the high bonding temperature of 1200 °C, recrystallized grains along the joint interface were observed, which were much bigger than that within the bond made at 1100 °C. Therefore, the interface had a lower hardness value compared with that of the bonds

made at 1100 °C. Although precipitates were found within the area close to the joint interface, the large recrystallized grain size made the hardening of the precipitates negligible. Therefore, no hardness peak was detected. In the heat-treated bonds, the parent alloy had the lowest hardness value indicting an increase in ductility due to an increase in grain size.

When the parent alloy in the recrystallized state was bonded at 1100 °C with a hold time of 30 minutes, hardness increased with distance away from the centre of the joint and the hardness values became uniform in the parent alloy, as shown in the Figure 4-52. The hardness profiles of the bonds made at different bonding temperatures, 1100 °C and 1200 °C, were identical. This implied that the effect on the hardness of the bonding temperature was negligible when joining the parent alloy in the recrystallized state due to the similar grain structure produced. Post-bond heat treatment made bonds much softer with respect to the as-bonded samples. The reduction in hardness was not only caused by an increase in grain size due to recrystallization, but also caused by the precipitation of a Cr-rich phase along the grain boundaries, as shown in Figure 4-13, which reduced the solid-solution hardening effect of Cr.

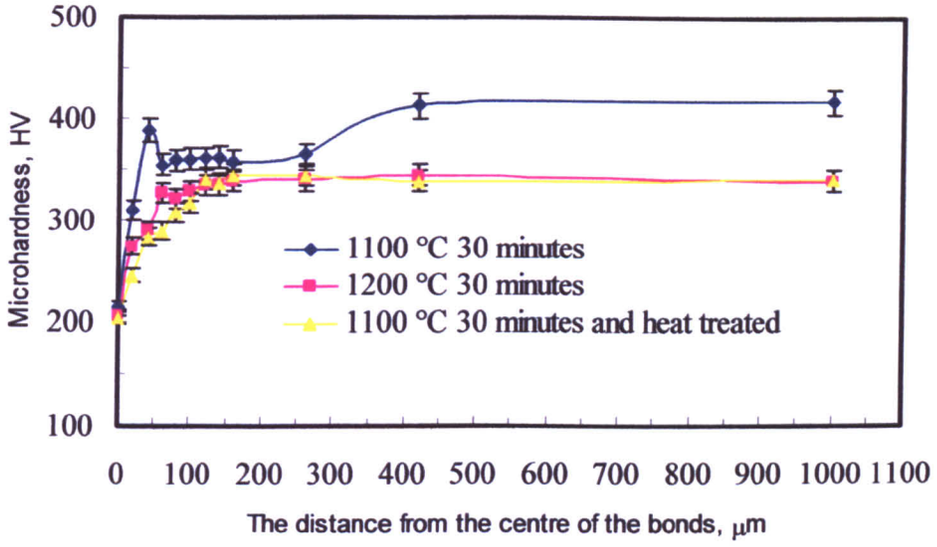

Figure 4-51 Hardness profiles for bonds made with the parent alloy in the fine-grained state.

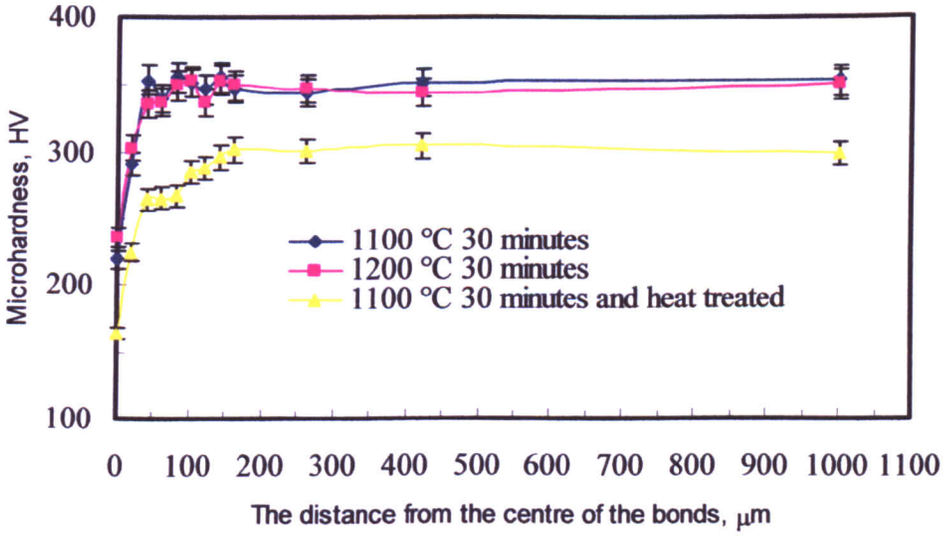

Figure 4-52 Hardness profiles for bonds made with the parent alloy in the recrystallized state.

4.5.3 Summary.

The bonding of MA758 ODS alloy at 1100 °C with a hold time of 30 minutes produces the strongest bonds. Bonding at 1200 °C results in weak interfaces due to segregation of Y_2O_3 dispersoids and disruption in the microstructure of the parent alloy and therefore makes weaker bonds. Microhardness measurements confirmed the formation of intermetallic precipitates during bonding, which contribute to the hardness of the joint interface. Recrystallization at the joint results in a low hardness value. The results suggest that the best route for joining the ODS alloy for high temperature applications is to TLP bond the parent alloy in the fine-grained state at 1100 °C with a hold time of 30 minutes followed by a post bond heat treatment at 1360 °C for 120 minutes.

4.6 Counteraction of Y_2O_3 dispersoids segregation.

4.6.1 Results and discussions.

TLP bonding comprises a number of distinct stages – parent alloy dissolution following melting of the filler metal, isothermal solidification and homogenisation. Particulate segregation has been observed during the bonding of yttria-bearing oxide dispersion strengthened (ODS) alloy such as MA956 [114], and also in the bonding of aluminium-based metal matrix composites [115, 116, 117]. This was attributed to the particles experiencing a "pushing effect" from the moving solid/liquid interface during solidification. As discussed earlier (in section 4.3), the region of weakness produced by the segregation of Y_2O_3 dispersoids at the joint interface region promotes preferential failure of joints because a fine dispersoid size and a small inter-particle spacing is necessary for good mechanical properties [26].

As discussed earlier in section 2.4.1, Stefanescu *et al.* [72] and Shanguan *et al.* [71] developed an analytical model to explain pushing or engulfment of insoluble particles by the advancing solid/liquid interface. In that model, if particles were pushed rather than being engulfed, segregation of particles would occur. They indicated that the particulate materials would be pushed when the rate of movement of the solid/liquid interface was less than a critical value. The critical velocity is given by equation 2.1, according to which, for a given rate of movement of the solid/liquid interface, particles having radii larger than Rc would be engulfed and the particles with radii less than Rc would be pushed.

This model had been successfully applied in the interpretation of segregation behaviour in TLP bonding of Al composites [115, 116, 117]. However, Rc would be expected to be much larger in TLP bonding process than that in the directional solidification due to lower velocity of solid/liquid interface. This implied that the particles were prone to segregation during slow isothermal solidification. For example, in this study, the ODS alloy has Y_2O_3 dispersoids with radii as small as 15-50 nm. According to equation 2.1, all the dispersoids should be pushed rather than engulfed during the isothermal solidification stage. As a result, we would expect all dispersoids would finally segregate along the joint interface resulting in a weak

bond. Theory suggests that it will not be possible to TLP bond the ODS alloy without significant segregation considering the fine Y_2O_3 particle sizes. However, results from this study show that if the joining condition is monitored carefully, a good quality joint which is free of segregation can be fabricated.

Figure 4-53 shows a homogenous distribution of particles within the grains of the joint centre-line. It is clear that nano-metre-sized particles were engulfed during isothermal solidification. EDX analysis shows peaks for yttrium, indicating that Y_2O_3 particles were present within the joint, as illustrated in Figure 4-54. Not only did the Y_2O_3 particles distribute homogeneously within the joint grains, but also no segregation of particles was observed across the grain boundaries, and at interface between the parent alloy and joint centre-line, as shown in Figure 4-55 and Figure 4-56, respectively. However, the density of dispersoids within joint centre-line and along the interfaces is lower than that within the parent alloy (as shown in Figure 4-57).

As discussed earlier, during the bonding of the ODS alloy using a Ni-Cr-Fe-Si-B interlayer, precipitates formed within the area adjacent to the joint. As illustrated in Figure 4-58, precipitates were much larger than yttria dispersoids and were clearly not agglomerates of yttria particles. EDX analysis, in Figure 4-59, implies that these precipitates are Cr rich. These precipitates were produced during bonding because no such precipitates were found in the parent alloy before bonding, as shown in Figure 4-60. Another type of particle which was identified within the parent alloy was shown to be TiO_2, see Figure 4-57 and the EDX spectrum from those particles is shown in Figure 4-61. In summary, there were three types of particle within the joints, namely, nano-metre sized Y_2O_3 dispersoids, Cr-rich precipitates, and TiO_2 particles. No segregations of any of these three types of particles had been found during bonding. This is in contrast with the predictions of Stefanescu *et al.* [69] and Shanguan *et al.* [71], who predicted at least the segregation of nano-metre-sized dispersoids within the joint region.

When equation 2.1 was applied to predict the segregation behaviour of particles during solidification, the viscosity of liquid was presumed to be unchanged throughout. Normally, the viscosity of molten metal and alloy, which has a low value,

e.g. 1.3×10^{-3} Pa·s for molten Al and 4.9×10^{-3} for molten Ni, was used. However, in this study, a semi-solid solution must be considered, which has much higher apparent viscosity [118] (as illustrated in Figure 4-62). This was thought to be attributed to the low bonding temperature and multiple elements involved in bonding. Figure 3-5 and Figure 3-6 show DTA and DSC traces of Ni-Cr-Fe-Si-B interlayer. Upon heating, the interlayer recrystallized and three phases were produced during recrystallization from amorphous alloy. The first phase started to melt at 960 °C and the second phase started to melt at 980 °C, and then finally the third phase was seen to melt at 1020 °C. The interlayer fully melted at 1095 °C. After cooling to room temperature and repeating the DTA test two times, identical DTA traces were recorded. This confirmed the 3-stage melting behaviour of Ni-Cr-Fe-Si-B interlayer.

When bonding is performed at a temperature close to the temperature of the third stage melting, i.e. at 1100 °C, the molten liquid is in the semi-solid-state. Accordingly, the viscosity of the liquid would increase dramatically depending on the amount of volume fraction of the solid within the liquid interlayer [118]. Therefore, the drag force on the particles increases due to the increase in viscosity of liquid [71, 76]. As a result, the particles in the liquid would be much more stable when interacting with the moving solid/liquid interface. It is suggested that instead of being pushed, the yttria particles were engulfed and therefore homogeneously distributed.

During the heat-up stage, some solid-state diffusion of B from filler metal into parent alloy can be expected even though a fast heating rate was applied (e.g. of $10°Cs^{-1}$ in this study). This will have some effects on raising the melting temperature of the interlayer, which is thought to contribute to obtaining a semi-solid interlayer. As Nakagawa *et al.* [119] indicated in their work, a slow heating rate can promote solidification when the specimen temperature increases from the filler metal melting point to the bonding temperature. This implies that a slow heating rate would increase the viscosity of the molten liquid by increasing the volume fraction of the solid within the liquid interface.

Secondly, the interface morphology plays a significant role in the engulfment or pushing of particles. For example, Stefanescu and co-worker [69] found that particles, which were not engulfed, could be entrapped in the intercellular spacing in a directional solidified Al-Mg-SiC system. In the present study, isothermal solidification of the liquid interlayer could have two distinct mechanisms. Initially, joint formation followed the isothermal solidification where the solid/liquid interface moved from the parent alloy into the interlayer from both sides of the bond. In theory, the solidification continues until the two solidification fronts meet each other upon full solidification. However, in this study, the solidification fronts stopped short resulting in two visible interfaces between the parent alloy and the joint, as seen in Figure 4-4. These observations implied that another solidification process involving the nucleation of the solid phase within the molten interlayer must be occurring. Therefore, the solidification fronts changes from a flat interface to inter-granular morphology. Particles were pushed not only by one interface moving in one direction but also by several interfaces moving in different directions. This change in solidification interface morphology will influence the pushing or entrapment of particulates on solidification.

When the parent alloy was joined at a higher temperature of 1200 °C, different results were observed. Severe segregation of yttria particles along the joint interface was detected, especially those located at the triple joints of grains, as illustrated in Figure 4-19. Increasing the bonding temperature had a two-fold effect on the segregation of the particles during bonding. Firstly, when the bonding temperature was much higher than the melting temperature of the interlayer, the semisolid slurry could not be formed and therefore the molten liquid interlayer has a low viscosity. According to equation 2.2, yttria particles would be pushed when in contact with the moving front of the solid/liquid interface. Secondly, when joining at higher temperature, the diffusion rate of B into the parent alloy increased. As a result, the rate of the moving solid/liquid interface increased. As Li *et al.* [114] claimed increasing the bonding temperature will decrease the time required for the isothermal solidification and therefore increase the velocity of the solid/liquid interface. The movement of the solid/liquid interface during bonding is very slow compared to that achieved in directional solidification. Stefanescu *et al.* [69] found that when the

solidification rate was increased from 16 μms^{-1} to 40 μms^{-1}, was there significant change from particle pushing to engulfment for particles with a size of 80-100 μm. When considering the nano-metre-sized particles and the slower movement of the solid/liquid interface (compared with that in directional-solidification, as in Stefanescu *et al.* [69]), it is unlikely that increasing the bonding temperature will counteract the segregation of particles by changing the solid/liquid interface velocity.

Another possible factor which is known to influence the solidification rate during bonding is the parent alloy grain size. For example, Kokawa *et al.* [76] observed that the rate constant increased when a fine grain size parent alloy was employed during TLP bonding of Nickel 200 alloy. It was found that the rate constant increased from 0.046 $\mu ms^{-1/2}$ to 0.076 $\mu ms^{-1/2}$ when the parent alloy grain size decreased from 4 mm to 40 μm. Nevertheless, as discussed before, the average rate of solid/liquid interface movement will still be low even when a fine-grained alloy was used. Therefore, changing the grain size of the ODS alloy does not affect the segregation of Y_2O_3 particles. This is confirmed by the fact that a homogenous distribution of yttria particles was found in bonds made with the alloy in both the fine-grained and the recrystallized states at 1100 °C. In the mean time, the segregation of particles was found at the joint interface for bonds made at 1200 °C with the alloy in both the fine-grained and in recrystallized states.

4.6.2 Summary.

The Ni-Cr-Fe-Si-B interlayer has three melting stages and joining the MA758 ODS alloy at low temperature can produce segregation-free joints. This is mainly attributed to a dramatic increase in viscosities of the liquid interlayer as a result of the formation of a semi-solid solution. Bonding ODS alloy at a higher temperature results in segregation of Y_2O_3 particles. Grain size variations within the parent alloy do not affect the degree of dispersoids segregation within the TLP bond region.

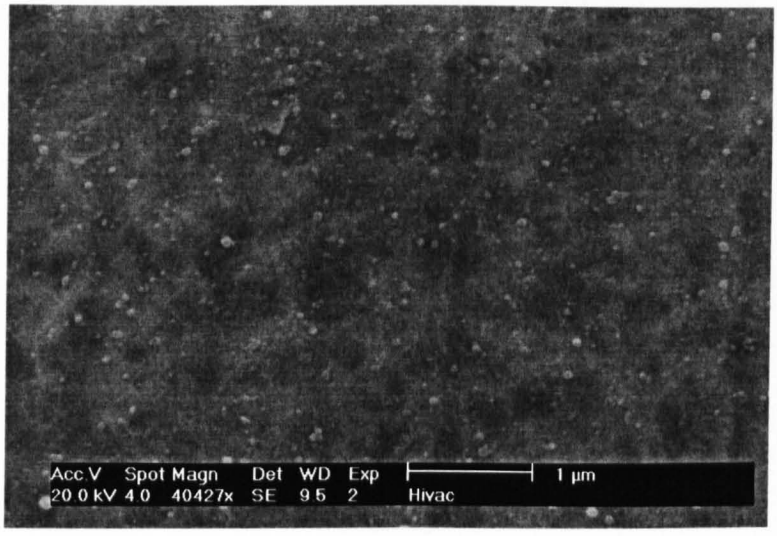

Figure 4-53 Distribution of Y_2O_3 particles inside the grains within the joint centre-line of the bond made with the parent alloy in the fine-grained state at 1100 °C with a hold time of 30 minutes.

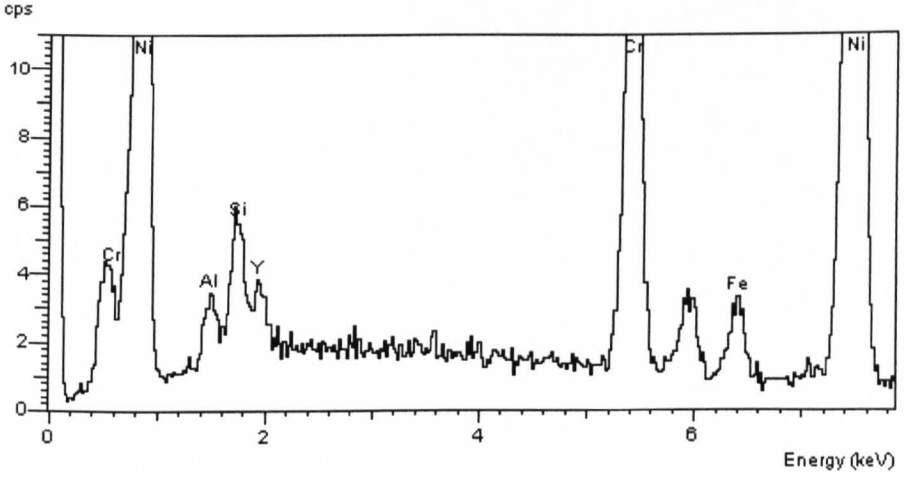

Figure 4-54 EDX spectrum on a particle inside the grains within the joint centre-line.

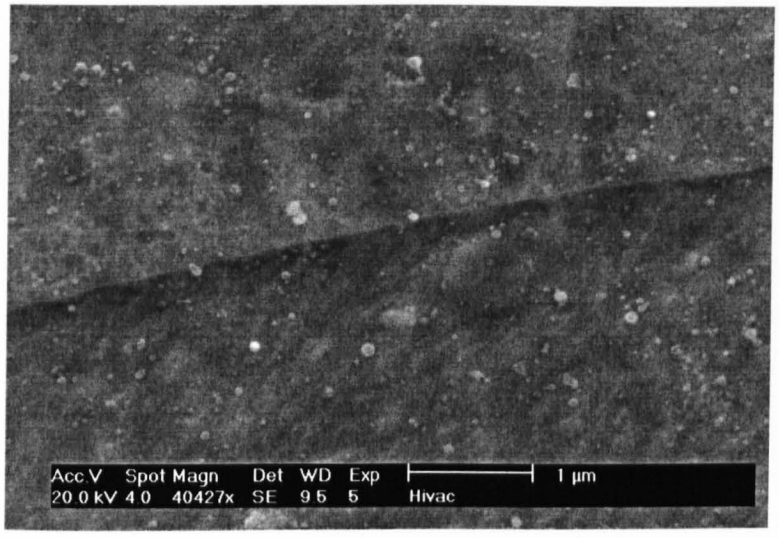

Figure 4-55 Distribution of Y_2O_3 particles across a grain boundary within the joint centre-line of the bond made with the parent alloy in the fine-grained state at 1100 °C with a hold time of 30 minutes.

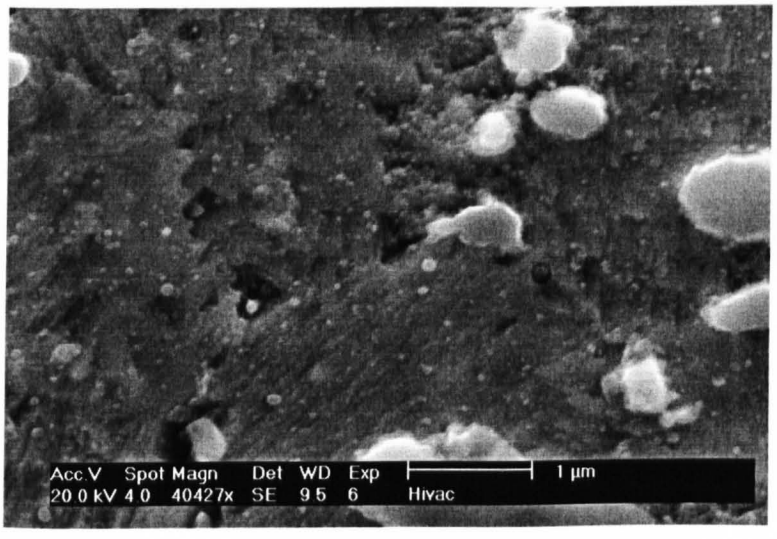

Figure 4-56 Distribution of Y_2O_3 particles across joint interface in the bond made with the parent alloy in the fine-grained state at 1100 °C with a hold time of 30 minutes.

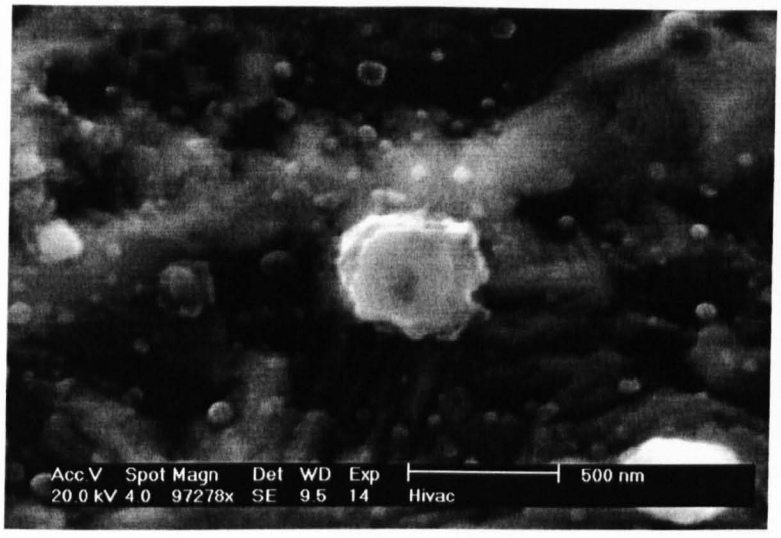

Figure 4-57 Distribution of Y_2O_3 particles and the existence of TiO_2 within the parent alloy in the fine-grained state.

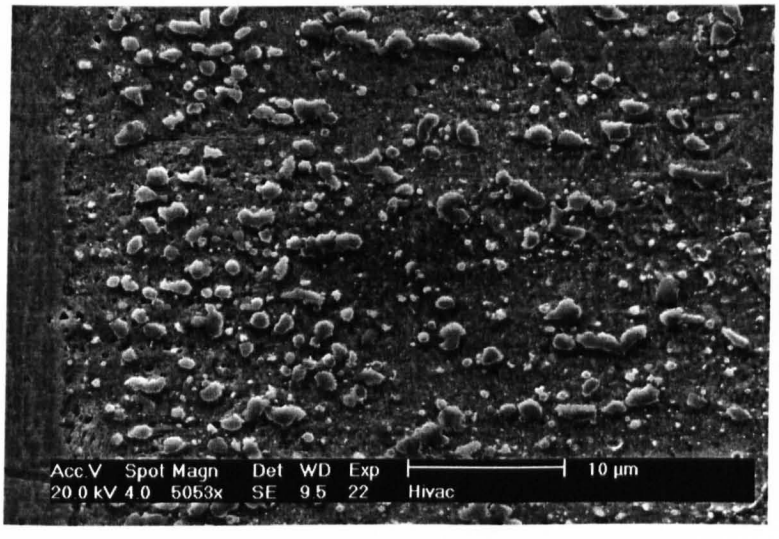

Figure 4-58 Precipitates adjacent to the joint interface.

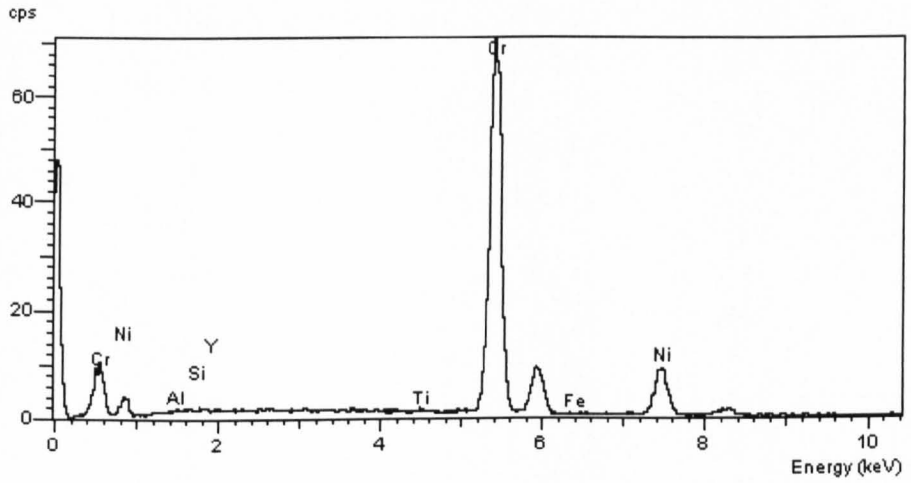

Figure 4-59 EDX spectrum of the precipitates adjacent to the interfaces.

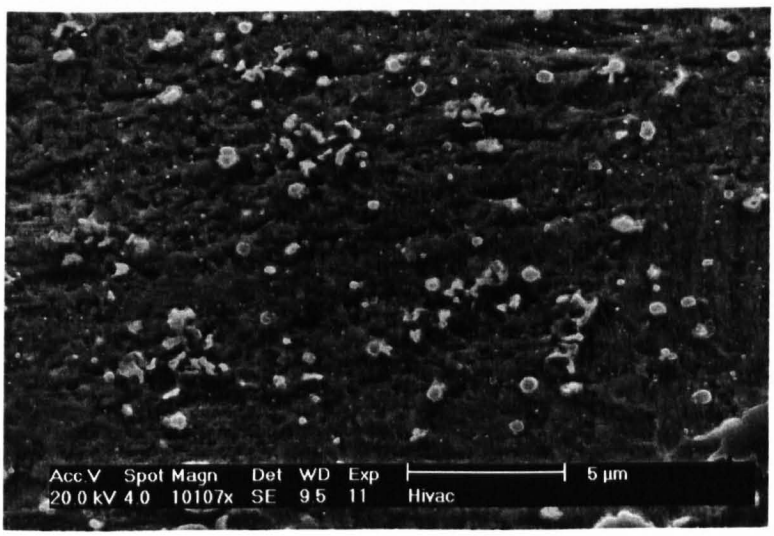

Figure 4-60 Precipitates within the parent alloy in the fine-grained state.

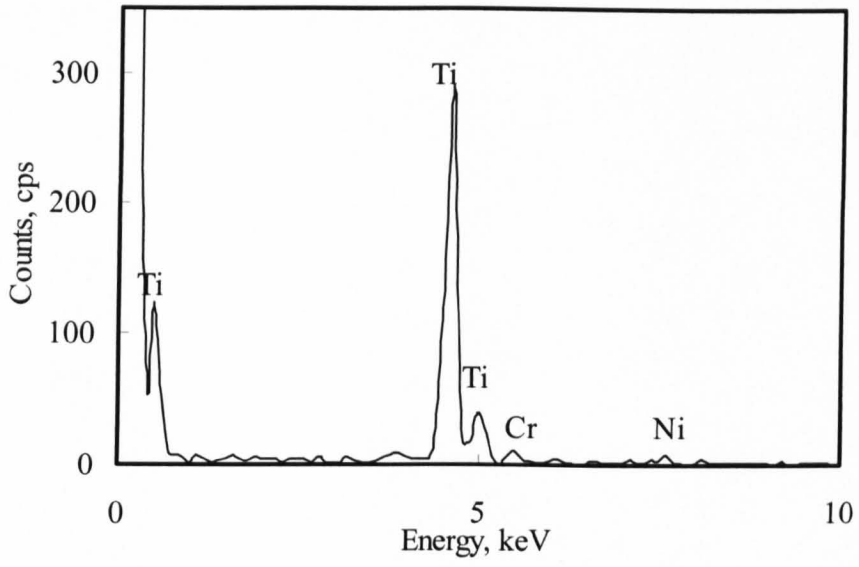

Figure 4-61 EDX spectrum on TiO_2 particles.

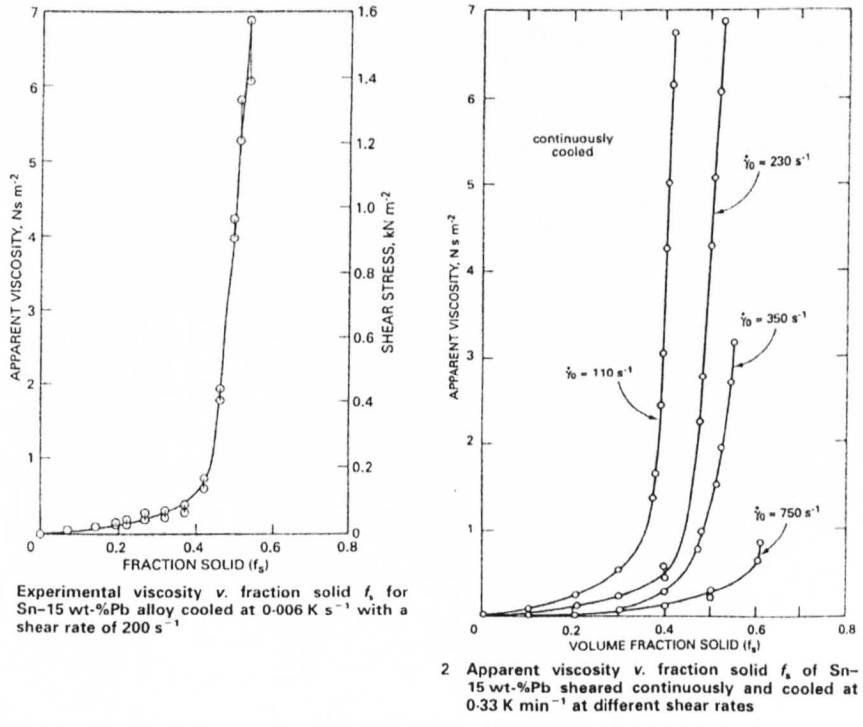

1 Experimental viscosity *v.* fraction solid f_s for Sn–15 wt-%Pb alloy cooled at 0·006 K s^{-1} with a shear rate of 200 s^{-1}

2 Apparent viscosity *v.* fraction solid f_s of Sn–15 wt-%Pb sheared continuously and cooled at 0·33 K min^{-1} at different shear rates

Figure 4-62 Experimental viscosity v fraction solid for Sn-15 wt%Pb alloy (after Ref.118)

4.7 Summary.

The effects of the grain structures on the TLP bonding of MA758 ODS alloy using a Ni-Cr-Fe-Si-B interlayer have been investigated. The stored energy during processing of the fine-grained alloy, combined with the strong diffusion of B from interlayer into the parent alloy caused recrystallization during bonding the parent alloy in the fine-grained state.

Bonding at a higher bonding temperature shortens the time for completion of isothermal solidification. However, joining at a high temperature of 1200 °C caused segregation of the Y_2O_3 particles and disruption to the microstructures of the parent alloy.

Preliminary results on the effects of a pressure on the TLP process show that a pressure applied could impede recrystallization of the parent alloy in the fine-grained state during bonding and results in bigger recrystallized grains during post-bond heat treatment.

Segregation of ultra-fine particles during bonding of ODS alloy can be avoided by using a semi-solid interlayer, together with multiple element reactions. A low bonding temperature, a slow heating rate and a thin interlayer would be preferred.

Post-bond heat treatment could homogenize the microstructure and compositions across the joints.

Chapter 5 TLP bonding using a Ni-P interlayer.

5.1 Introduction.

As a comparison to the Ni-Cr-Fe-Si-B system, the MA758 alloy was also TLP bonded using a Ni-P interlayer. The Ni-P interlayer has a lower bonding temperature than that for the Ni-Cr-Fe-Si-B system and a low bonding temperature is important in reducing disruption to the microstructure of the parent alloy. The effect of grain size, pressure, and the diffusion of alloying elements, on the TLP bonding process was studied. The quality of the joints was assessed by studying the composition profile and degree of microstructure homogeneity across the joint region. The effect of bonding conditions on the segregation of particles across the joint region was investigated. Furthermore, the effect of chromium on the TLP bonding process and a formation of phosphides in raising the solidus temperature of the liquid interlayer was studied.

5.2 The effect of grain size on bonding behaviour.

As discussed in chapter 4, TLP bonding is a diffusion controlled process. As a result, grain size, which affects the diffusion behaviour of solutes, could alter the bonding process.

5.2.1 TLP bonding with the ODS alloy in the fine-grained state.

5.2.1.1 Bond microstructure.

Figure 5-1 shows the microstructure of the bonds made at 1000 °C with a hold time of 5 minutes. A wide melt-back distance was observed and the presence of residual eutectic phases indicated that isothermal solidification had not been completed. An isothermal solidification resulted in the development of a very fine microstructure along the joint interface.

Bonds made for a longer hold time of 15 minutes (as shown in Figure 5-2) produced the isothermally solidified joints due to the diffusion away of P from the liquid interlayer. A thin bond-line with negligible disruption to the microstructure of the

parent alloy was produced. As illustrated in Figure 5-3, the microstructure of the joints was not altered with a longer hold time of 30 minutes. These results confirmed observations that isothermal solidification was complete with a hold time of 15 minutes. Studies show that holding at 1000 °C does not alter the microstructure of the joint region or that of the parent alloy after a hold time of 15 minutes.

In order to homogenize the microstructure and composition across the joints, a post-bond heat treatment at 1360 °C for 120 minutes was applied to the bonds. Figure 5-4 shows the microstructure of the heat-treated bond made at 1000 °C with a hold time of 5 minutes. Although the parent alloy recrystallized, the recrystallized grains failed to grow across the joint region. The ultra-fine-grained structure along the joint interface still remained, and no further grain growth was observed. This implied that the fine structure was stable. A loss in driving force for grain growth and a pinning force exerted by Y_2O_3 particles could account for this stability. Figure 5-5 shows the microstructure of the bonds made at 1000 °C with a hold time of 15 minutes followed by a post-bond heat treatment. A continuous microstructure across the joint region was produced. The grains within the joint grew into the parent alloy by consuming the grains adjacent to the joint centre-line. For the bonds made with a hold time of 30 minutes followed by a post-bond heat treatment, a similar homogenized microstructure across the joint was produced, as shown in Figure 5-6. This implied that when the joints isothermally solidified, the post-bond heat treatment produces a continuous microstructure across the joint region regardless of the bonding time.

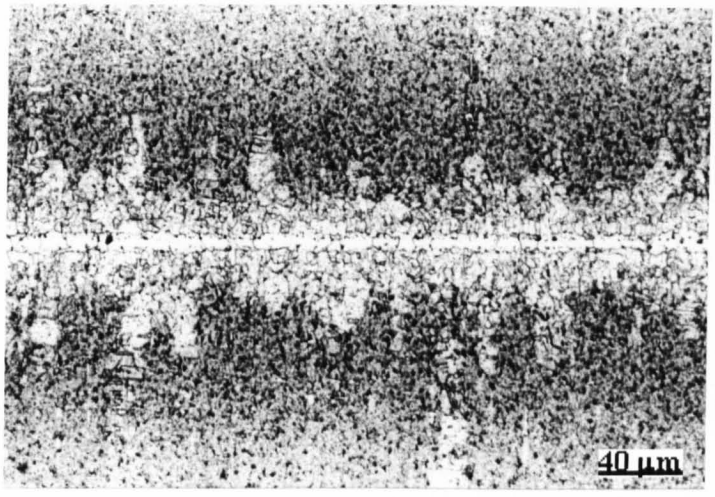

Figure 5-1 Microstructure of the bonds made with the parent alloy in the fine-grained state at 1000 °C with a hold time of 5 minutes (light micrograph).

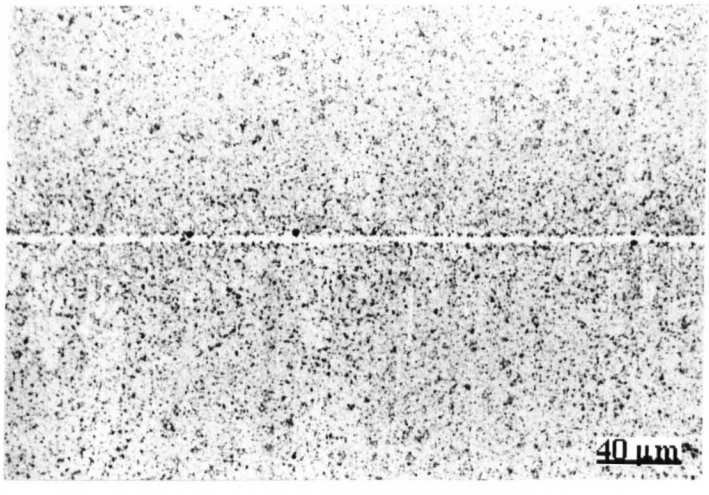

Figure 5-2 Microstructure of the bonds made with the parent alloy in the fine-grained state at 1000 °C with a hold time of 15 minutes (light micrograph).

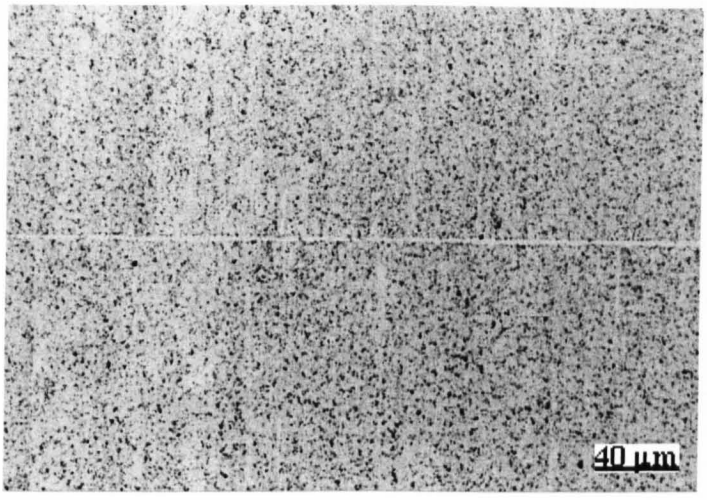

Figure 5-3 Microstructure of the bonds made with the parent alloy in the fine-grained state at 1000 °C with a hold time of 30 minutes (light micrograph).

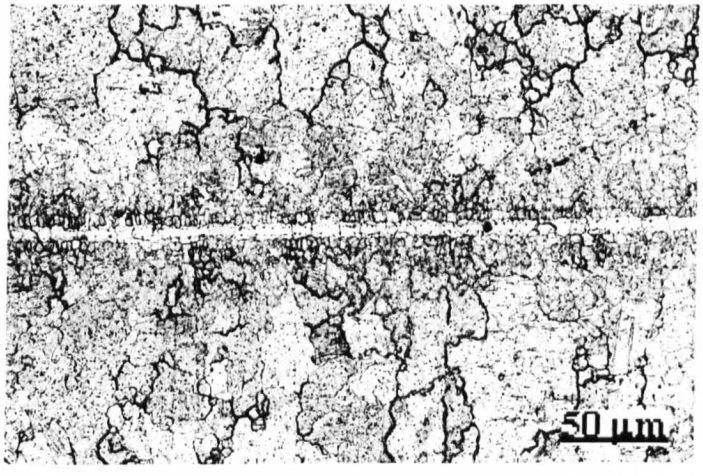

Figure 5-4 Microstructure of the bonds made with the parent alloy in the fine-grained state at 1000 °C with a hold time of 5 minutes followed by a post-bond heat treatment at 1360 °C for 120 minutes (light micrograph).

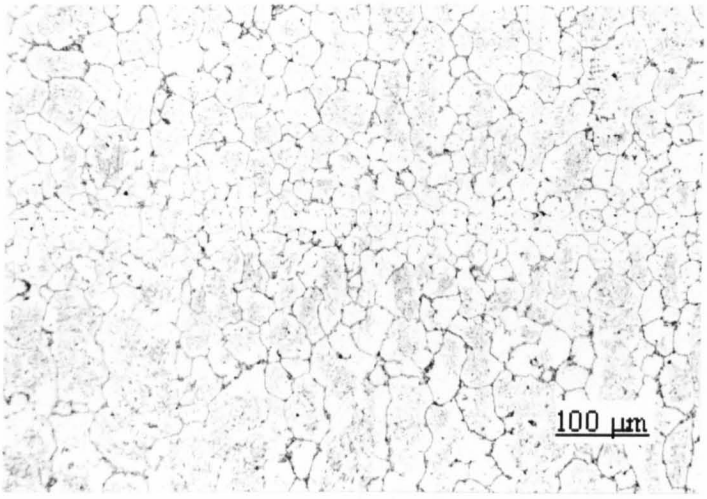

Figure 5-5 Microstructure of the bonds made with the parent alloy in the fine-grained state at 1000 °C with a hold time of 15 minutes followed by a post-bond heat treatment at 1360 °C for 120 minutes (light micrograph).

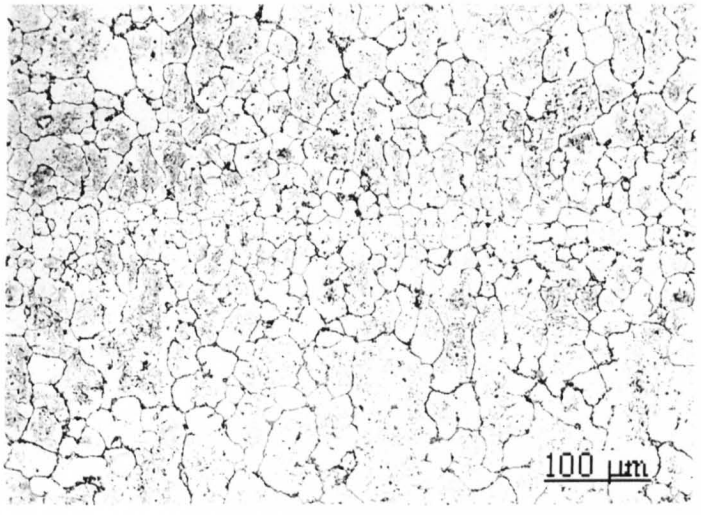

Figure 5-6 Microstructure of the bonds made with the parent alloy in the fine-grained state at 1000 °C with a hold time of 30 minutes followed by a post-bond heat treatment at 1360 °C for 120 minutes (light micrograph).

5.2.1.2 Composition profiles.

The composition profile of elements as a function of distance from the centre of the bond was investigated. Figure 5-7 shows the composition profile of the bond made at 1000 °C with a hold time of 5 minutes. The distribution of Ni and Cr was not homogeneous within the joint. Firstly, in the joint centre there was a high concentration of Ni (~ 73.5wt%) and a low concentration of Cr (~25wt%) within this thin bond region (6μm in width). This corresponded to the centre-line of the bonds, as shown in Figure 5-1. Secondly, a lower concentration of Ni (~71.5wt%) and a higher concentration of Cr (~26.7wt%) was observed in the area next to the joint (12 μm in width). This zone corresponded to the melt-back region. Within these two areas, the distribution of Ni and Cr was homogeneous. Thirdly, the content of Ni decreased (content of Cr increased) gradually with distance away from the centre of the joint and finally it became constant within the parent alloy. Compositional analysis also shows that the high concentration of P (~8wt%) in the Ni-P interlayer reduced to very low value of ~0.6wt%. This decrease in P concentration was attributed to the pushing out of the liquid interlayer during TLP bonding, an observation confirmed by Yeh and Chuang [79], and also due to the high diffusivity of P in the Ni-base alloy. There was a high localized concentration of Al and Ti along the grain boundaries within the joint. This could be attributed to segregation of Al_2O_3 and TiO_2. Figure 5-8 shows the composition profile of the bond made at 1000 °C with a longer hold time of 30 minutes. A lower concentration of Ni (~71.8wt%) and higher concentration of Cr (~27wt%) was observed within the centre of joint when compared with that of the bond made with a hold time of 5 minutes. This implies that the isothermal solidification process was completed. The content of Ni decreased (the content of Cr increased) with distance away from the centre of the joint and it became constant within the parent alloy. A longer hold time of 60 minutes did not alter the composition profile of elements.

A post-bond heat treatment homogenized the composition profiles of the joints, as illustrated in Figure 5-9. The Ni and Cr contents were homogenously distributed across the joint region. The heat treatment had reduced the concentrations of Fe, Al, and Ti present within the joint producing a homogenized bond.

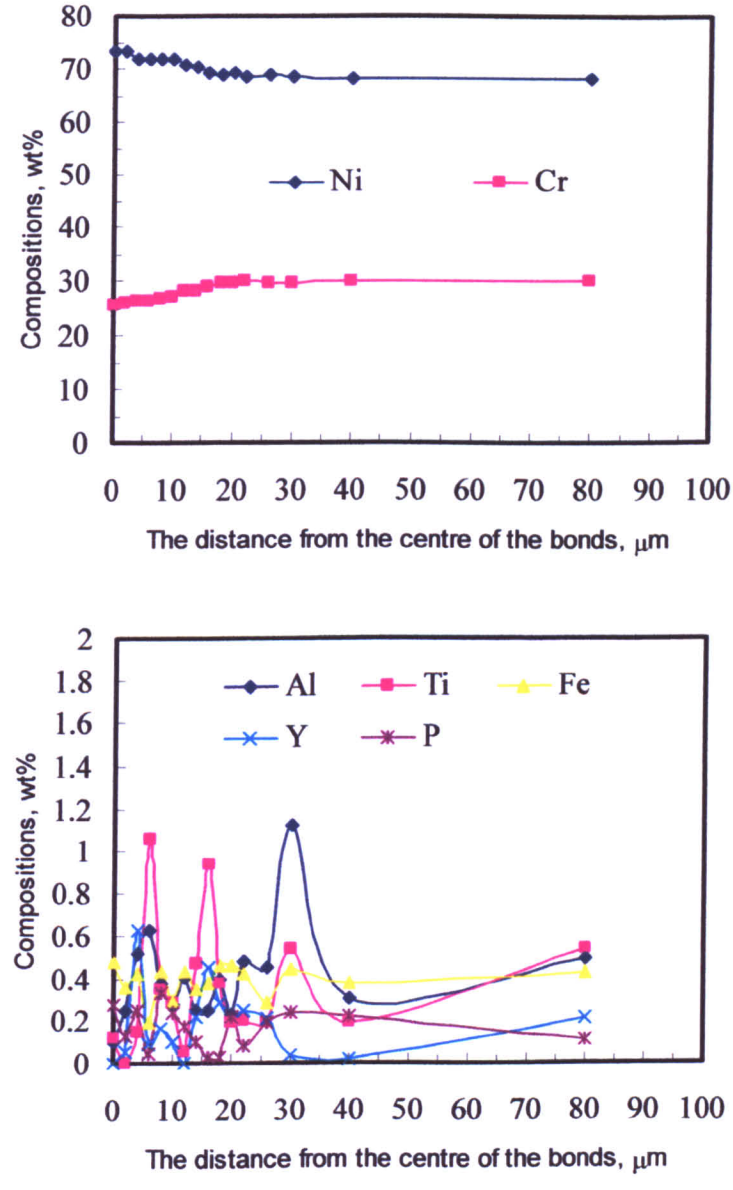

Figure 5-7 Composition profiles of the bond made at 1000 °C with a hold time of 5 minutes.

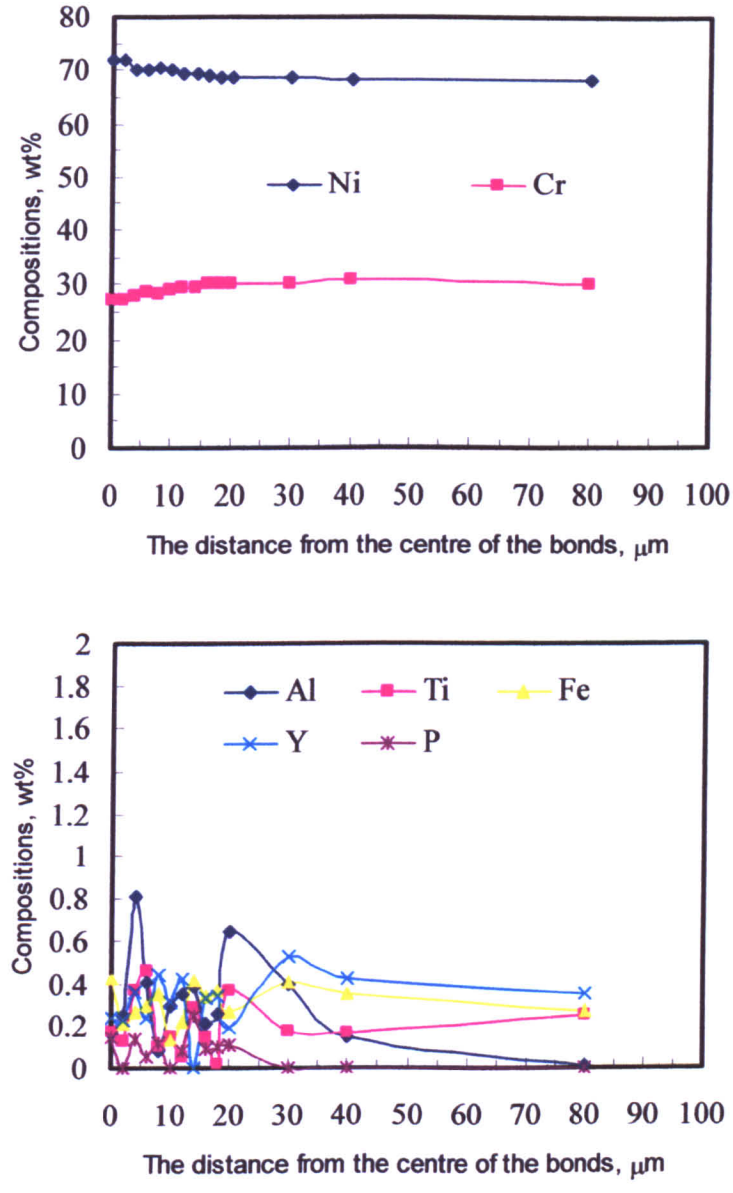

Figure 5-8 Composition profiles of the bond made at 1000 °C with a hold time of 30 minutes.

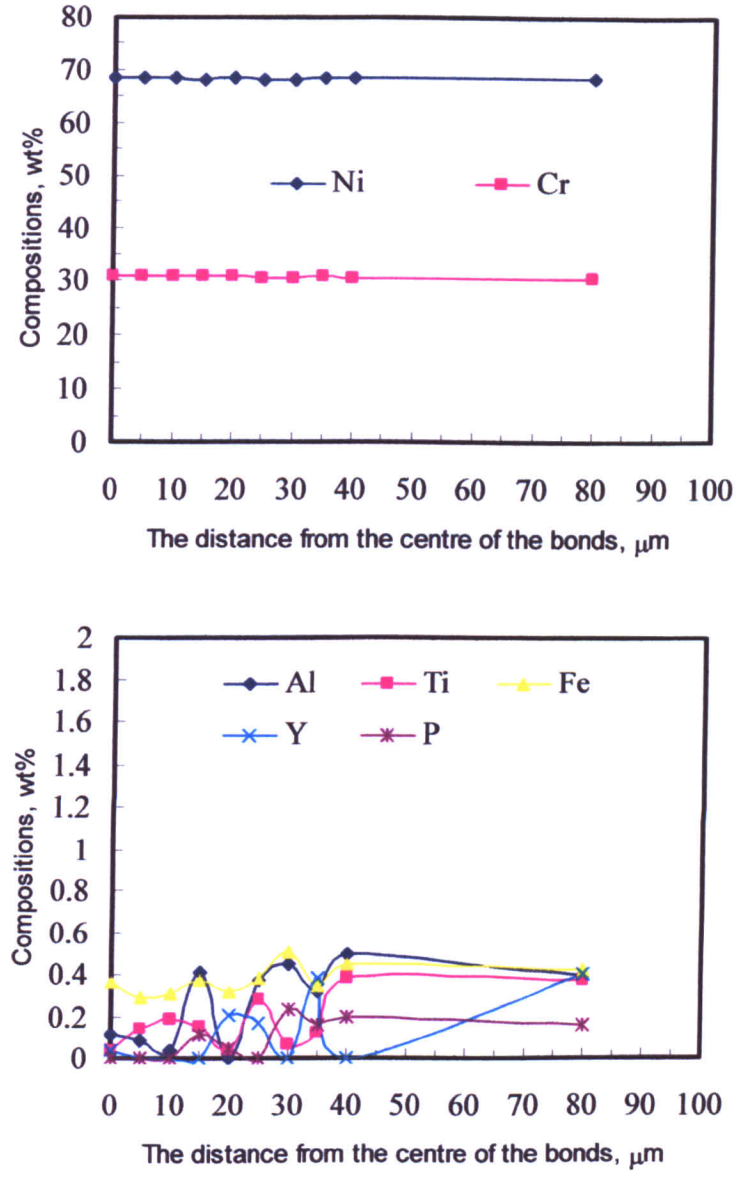

Figure 5-9 Composition profiles of the bond made at 1000 °C with a hold time of 30 minutes followed by a post-bond heat treatment at 1360 °C for 120 minutes.

5.2.2 TLP bonding with the ODS alloy in the recrystallized state.

5.2.2.1 Bond microstructure.

The micrograph in Figure 5-10 shows the microstructure of a bond made using a Ni-P interlayer at 1000 °C with a hold time of 5 minutes with the parent alloy in the recrystallized state. Some liquid penetration along grain boundaries adjacent to the joint was seen. This was attributed to the high rate of grain boundary diffusion compared to that of bulk diffusion. Tuah-Poku *et al.* suggested that liquid penetration into grain boundary regions increased the effective solid/liquid interfacial area and the amount of phosphorus diffusion into the parent alloy [64]. As a result, this penetration accelerated the isothermal solidification of the liquid interlayer. A cluster of small grains was present on either side of the bond interface. With a longer hold time of 30 minutes, as shown in Figure 5-11, these small grains could not be homogenized. Figure 5-12 shows that a hold time of 60 minutes could not alter the microstructure of the joint. The width of the joint did not change with hold time after a bonding time of 30 minutes, which implied that the isothermal solidification was complete and the clusters of grains was the product of isothermal solidification. This will be discussed later in chapter 5, section 4.

The microstructure of a joint made with a hold time of 30 minutes followed by a heat treatment at 1360 °C for 120 minutes is shown in Figure 5-13. The micrograph shows a microstructure with an elongated grain structure across the joint region. The grains within the parent alloy grow across the joint and meet in the centre of the joint. This continuity of microstructure across the joint region is important for these alloys in order to maintain some of their high temperature properties, such as creep resistance. However, also noticeable at the centre of bond was a string of precipitates, which were found to be rich in Cr and P.

The grain size effect on microstructural development of the joints made using Ni-P interlayers was clearly noticed. Firstly, bonds made with the parent alloy in the fine-grained state produced a much thinner dissolution width than that produced when using the alloy in coarser-grained state, as shown in Figure 5-2 and Figure 5-11. Secondly, the isothermal solidification rate for TLP bonds made with the parent alloy

in the fine-grained state was faster than that observed when bonding the alloy in the coarser grained state, although liquid penetration along grain boundaries can accelerate isothermal solidification. These observations were consistent with the results by Kokawa *et al.* [76]. They found that when TLP bonding Ni at 1200 °C using a Ni-11 wt% P interlayer, the rate of isothermal solidification was greater when fine-grained parent alloy was employed. Thirdly, the diffusion of the melting point depressants (e.g. P) alters not only isothermal solidification, but also the extent of parent alloy dissolution. When the parent alloy was bonded in the fine-grained state, faster diffusion of P into the base alloy caused a narrower melting-back distance and hence, a shorter time for dissolution to complete compared with the bonds made with the parent alloy in recrystallized state. However, in the case when Ni-Cr-Fe-Si-B interlayers were used, less difference in melt-back distances was observed when the parent alloy in the different grain state were used. This can be attributed to an insignificant difference in the diffusion rate of B in bulk Ni and along grain boundaries. Earlier research discovered that [120], at high temperatures, e.g. $T \geq 0.75$ T_m, D_{gb}/D_l ratio is 10^3 or less, and consequently, the contribution resulting from grain boundary diffusion will be much less (T_m is the melting temperature; D_{gb} and D_l are the diffusion rate along grain boundaries and in the lattice). The TLP bonding of the ODS alloy using Ni-Cr-Fe-Si-B was consistent with this claim but bonding using a Ni-P interlayer deviated from this observation.

Nakagawa *et al.* [119] found that the presence of Cr in the interlayer or in the parent alloy would prolong the time required for complete dissolution by considering the diffusion of solute in the liquid layer. The time to complete the bonding process is in order of a few hours. However, in this study, the results showed the presence of Cr within the parent alloy shortened the time to complete the bonding process rather than prolong it. For example, when bonding the alloy in the fine-grained state, the dissolution time was less than 5 minutes and the time for complete isothermal solidification was estimated to be less than 30 minutes, even when the parent alloy was bonded in the coarse-grained state.

Firstly, the Cr content of MA758 alloy before joining is ~30 wt%, which is high enough to raise the solidus temperature of the liquid interlayer, which in turn accelerates the bonding process. After dissolution was complete, the Cr content of

the bond would increase due to the Cr dissolved from the parent alloy. With an interlayer composition of Ni-30wt%Cr-8.8wt%P content, the solidus temperature of the liquid could be expected to increase up to 980 °C. In other words, the transport of Cr from the parent alloy into the liquid interlayer would have the effect of raising the solidus temperature of the interlayer by about 100 °C. Diffusion of P from the interlayer to the parent alloy would lower the content of P in the interlayer, which in turn will also raise the solidus temperature of the liquid interlayer. Such a change would make the dissolution and solidification processes much faster than otherwise observed during the TLP bonding processes.

Furthermore, when Nakagawa *et al.* [119] predicted the prolonged time for complete dissolution during TLP process, the grain-boundary penetration was not considered, which can accelerate decrease the time for completion of dissolution (this was observed when bonding the parent alloy in the recrystallized state). Also in their study, only the diffusion of solute was taken into account. But in the present work, an induction heating was used, which resulting stirring effect and accelerating the homogenization process. Meanwhile, the formation of phosphides and squeezing-out of the P-rich phase from the liquid interlayer could also reduce the time to complete TLP process.

Both the changes in bond composition (as discussed in section 5.2.2.2) and microstructural developments appear to support this new bonding mechanism. In previous research, when TLP bonding process was studied, more attention was given to the diffusion of elements within the interlayer, especially the melting point depressants, e.g. B, Si, and P. In this study, it shows the composition of the parent alloy, e.g. Cr content also has been shown to play a very important role in determining the TLP bonding process. For instance, the MA 758 ODS alloy has a high Cr content, Ni-P could be a good interlayer to choose not only because it has a low bonding temperature but also because it could form a Ni-Cr-P liquid interlayer, which would reduce dissolution and the time to complete isothermal solidification, resulting in less disruption to the microstructure of the parent alloy.

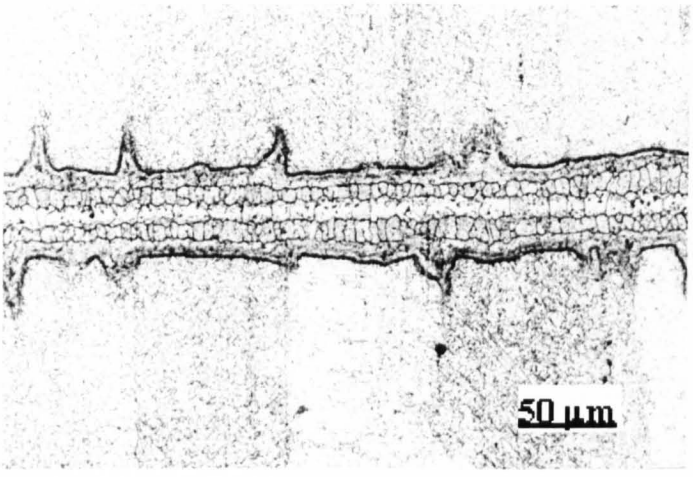

Figure 5-10 Microstructure of the bonds made with the parent alloy in the recrystallized state at 1000 °C with a hold time of 5 minutes (light micrograph).

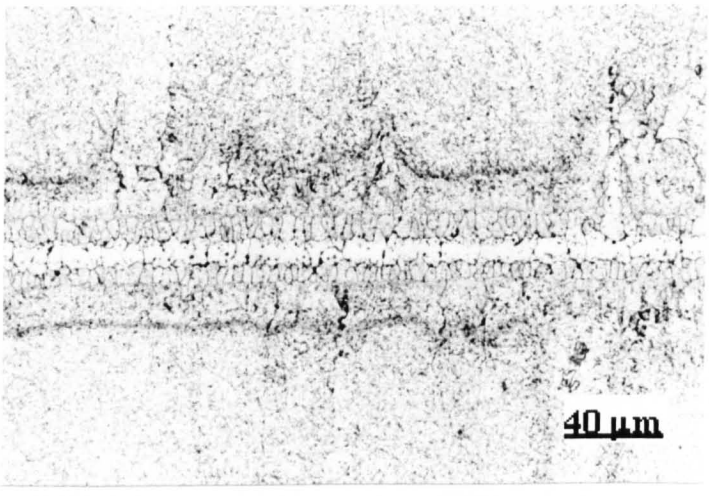

Figure 5-11 Microstructure of the bonds made with the parent alloy in the recrystallized state at 1000 °C with a hold time of 30 minutes (light micrograph).

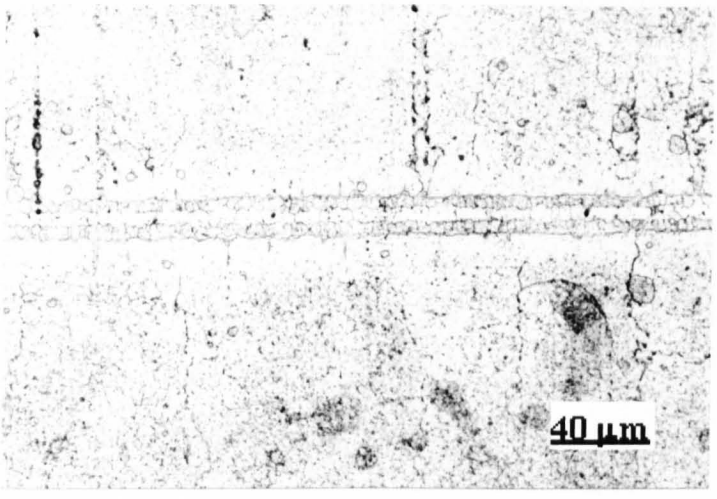

Figure 5-12 Microstructure of the bonds made with the parent alloy in the recrystallized state at 1000 °C with a hold time of 60 minutes (light micrograph).

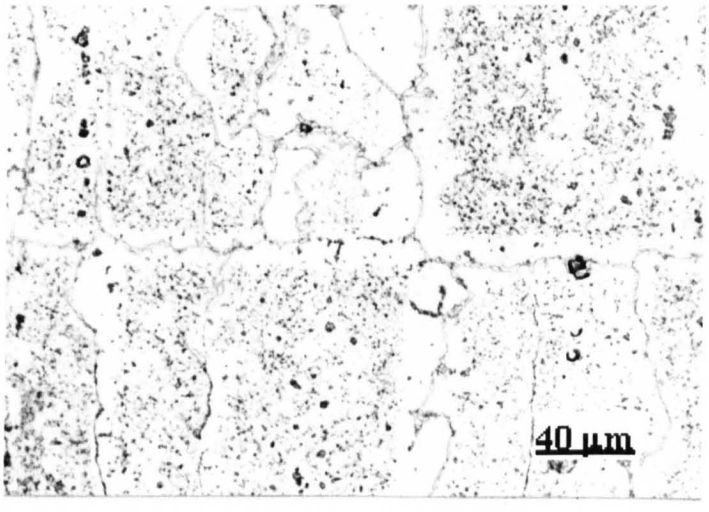

Figure 5-13 Microstructure of the bonds made with the parent alloy in the recrystallized state at 1000 °C with a hold time of 30 minutes followed by a post-bond heat treatment at 1360 °C for 120 minutes (light micrograph).

5.2.2.2 Composition profiles.

Figure 5-14 shows the composition profiles for a bond made using a Ni-P interlayer at 1000 °C with a hold time of 30 minutes with the parent alloy in the recrystallized state. A higher concentration of Ni (~71.2wt%) and a lower concentration of Cr (~27.2wt%) was detected within the bond region when compared with that of the parent alloy. The concentration profile for both elements was uniform across the joint region. However, there is a sudden change in the content of Ni and Cr at the joint interface. This sudden change in composition confirms the earlier discussion (see section 5.2.2.1) regarding an increase in Cr content in the Ni-P liquid interlayer. Concentration of P within the joint centre-line is higher compared with that of the parent alloy.

Figure 5-15 shows the composition profile of the bond made with the parent alloy in the recrystallized state followed by a post bond heat treatment at 1360 °C for 120 minutes. The concentration profiles for Ni and Cr were homogenous across the joint region, as were Fe and P. Only Al and Ti appear to accumulate at joint interface. When a post bond heat treatment was applied to the as-bonded specimens, there was no difference between the composition profiles of the bonds made with the parent alloy in the fine-grained state and that in the recrystallized state. The post-bond heat treatment homogenized the composition profiles across the bond.

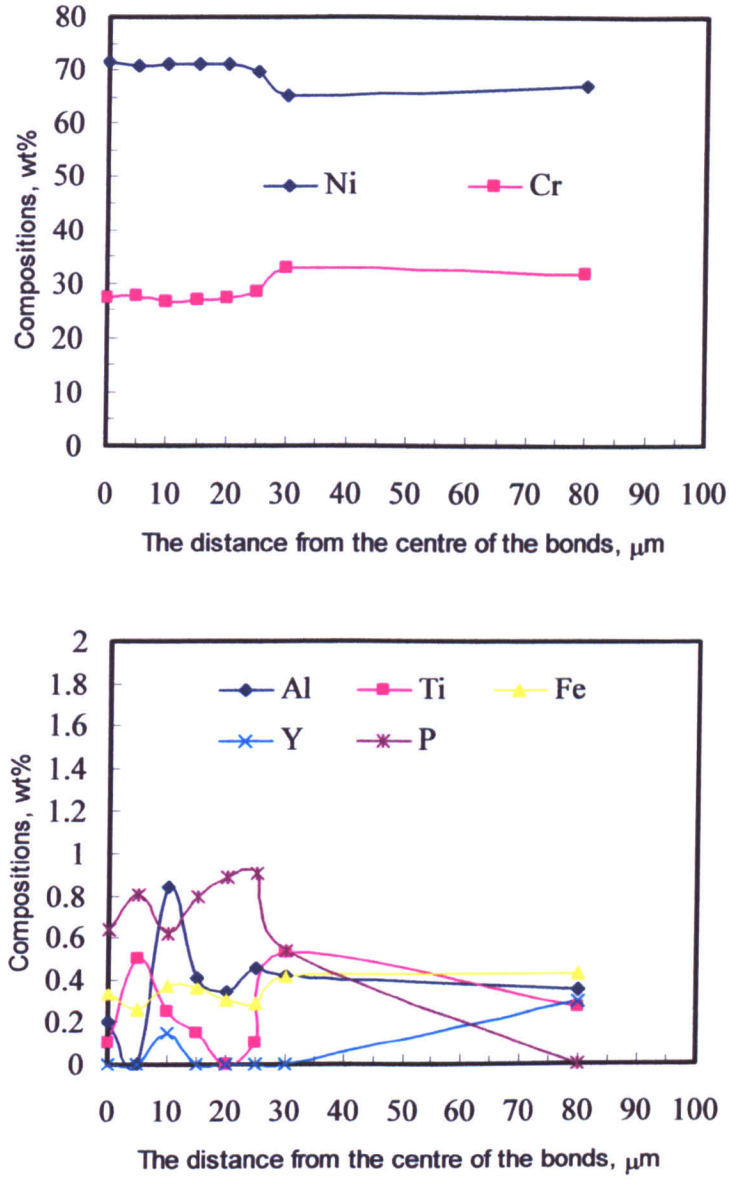

Figure 5-14 Composition profiles of the bond made with the parent alloy in the recrystallized state at 1000 °C with a hold time of 30 minutes.

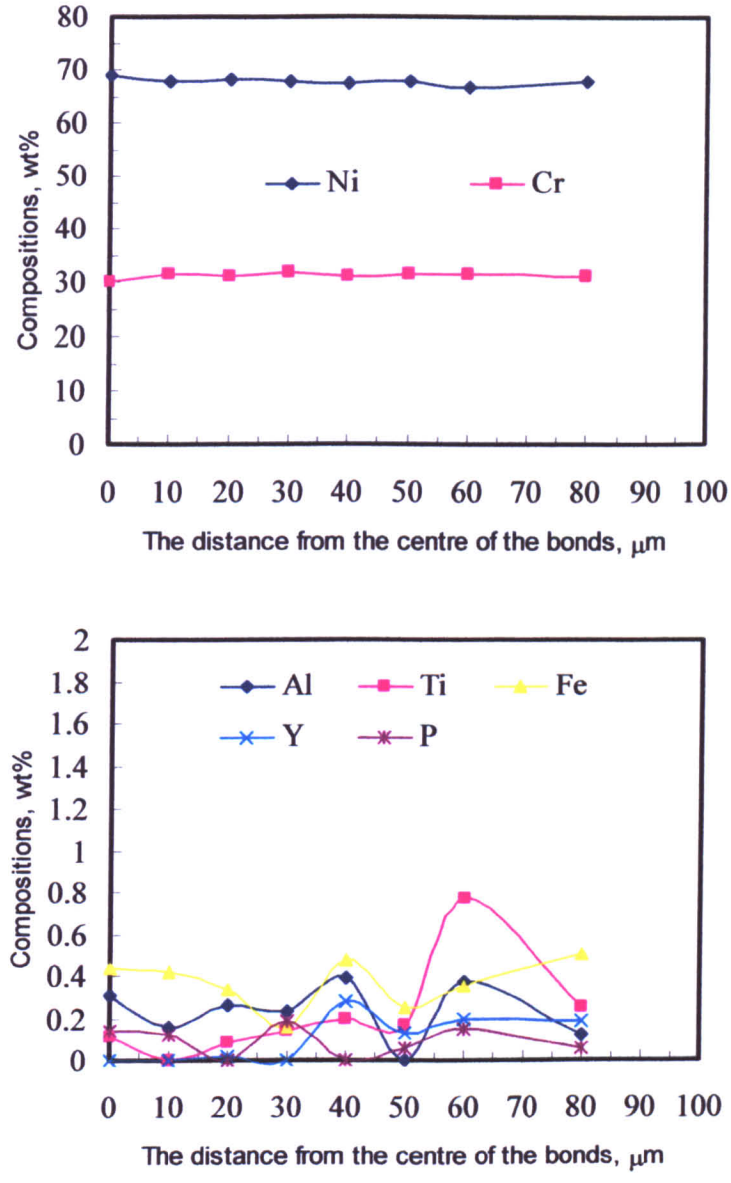

Figure 5-15 Composition profiles of the bond made with the parent alloy in the recrystallized state at 1000 °C with a hold time of 30 minutes followed by a post-bond heat treatment at 1360 °C for 120 minutes.

5.2.3 Summary.

MA 758 ODS alloy was bonded both in the fine-grained and recrystallized states at 1000 °C for various bonding times using a Ni-P interlayer. When bonds were made with the parent alloy in the fine-grained state, a very thin joint was produced with negligible disruption to the parent alloy microstructure. Bonds made with the parent alloy in the recrystallized state had a wider dissolution width and more disruption to the microstructure of the parent alloy. This was attributed to a difference in the diffusion rate for P within different grain structures. A faster time for isothermal solidification was observed and this reduced the degree of parent alloy dissolution. This change in bonding behaviour was attributed to the dissolution of Cr from the parent alloy into the liquid interlayer and therefore resulted in an increase in the solidus temperature for the Ni-P systems. Post-bond heat treatments were successful in homogenizing the composition and microstructure across the joint region when bonding the parent alloy both in the fine-grained and the recrystallized states.

5.3 The effect of external pressure on TLP bonding.

Figure 5-16 shows a bond made with the parent alloy in the recrystallized state at 1000 °C with a hold time of 30 minutes using a pressure of 196 kPa. In comparison, a bond made using the same conditions, but without using external pressure, is shown in Figure 5-11. The width of the solidified joint is found to be the same irrespective of pressure applied. When a higher pressure was applied during bonding, a noticeable decrease in the width of the joint was observed, see Figure 5-17 and Figure 5-18. This implied that when the external pressure was higher than 588 kPa, it resulted in the ejection of the liquid phase from the joint. The effect of bonding pressure has been reported in the literature. Rabinkin and Pounds [77] found that when joining copper with a Cu-P interlayer under a pressure of 9.8 MPa, the Charpy impact energy of the joints increased. The liquid phase which was enriched with melting temperature depressants was squeezed out from between the joining surfaces. This resulted in fewer intermetallic phases forming at the joint hence giving the joint enhanced toughness. Dammer [78] found a similar beneficial effect when applying pressure to the joining of an Al alloy. Yeh and Chuang [79] also came to the same conclusion when studying TLP bonding of INCONEL 718 alloy using a Ni-P interlayer under pressure.

In this study, applying a pressure on the liquid layer reduced the bond width by ejecting a P-rich phase from the joint. This in turn would reduce the concentration of P within the liquid interlayer, which in turn contribute to a reduction in the melt-back distance and time to complete isothermal solidification. As shown in Figure 5-18, a narrow melt-back distance would result in less disruption to the parent alloy than that for a bond made without the use of pressure. Figure 5-19 shows the microstructure of a bond made with the parent alloy in the recrystallized state at 1000 °C with a hold time of 30 minutes using a pressure of 1.58 MPa followed by a post-bond heat treatment at 1360 °C for 120 minutes. A homogeneous microstructure was produced with the recrystallized grains growing across the joint region. A post bond heat treatment also homogenized the composition profiles across the joint, as shown in Figure 5-20.

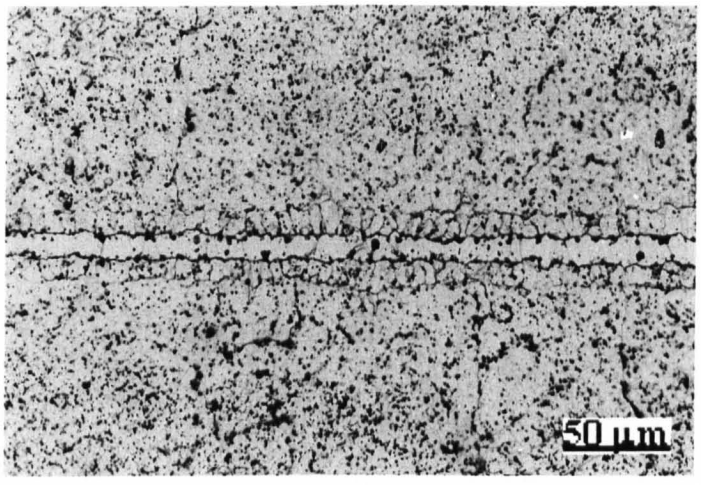

Figure 5-16 Microstructure of the bonds made with the parent alloy in the recrystallized state at 1000 °C with a hold time of 30 minutes using a bonding pressure of 196 kPa.

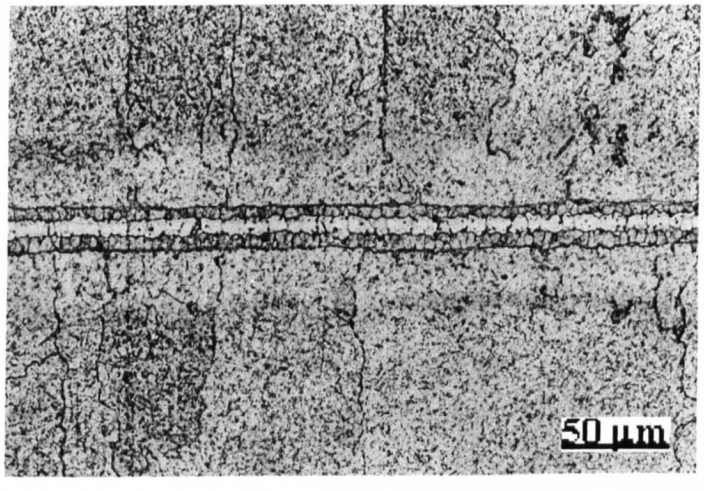

Figure 5-17 Microstructure of the bonds made with the parent alloy in the recrystallized state at 1000 °C with a hold time of 30 minutes using a bonding pressure of 784 kPa.

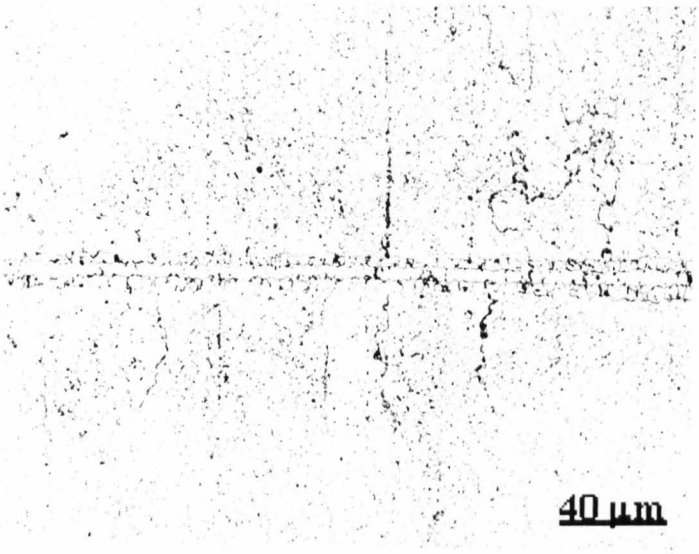

Figure 5-18 Microstructure of the bonds made with the parent alloy in the recrystallized state at 1000 °C with a hold time of 30 minutes using a bonding pressure of 1.58 MPa.

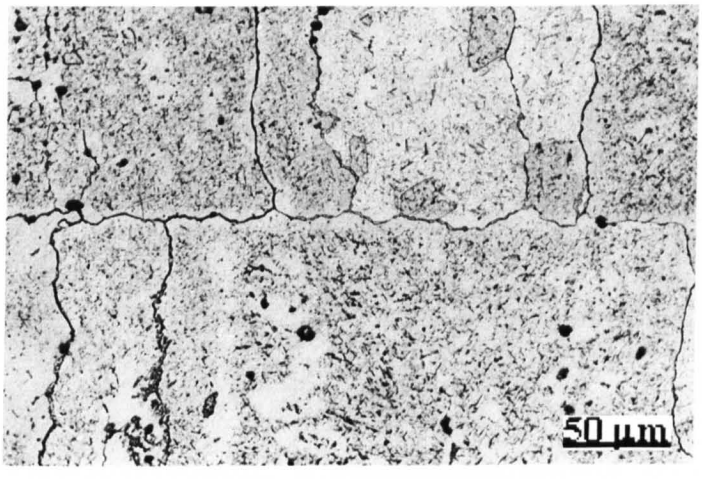

Figure 5-19 Microstructure of the bonds made with the parent alloy in the recrystallized state at 1000 °C with a hold time of 30 minutes using a bonding pressure of 1.58 MPa followed by a post-bond heat treatment at 1360 °C for 120 minutes.

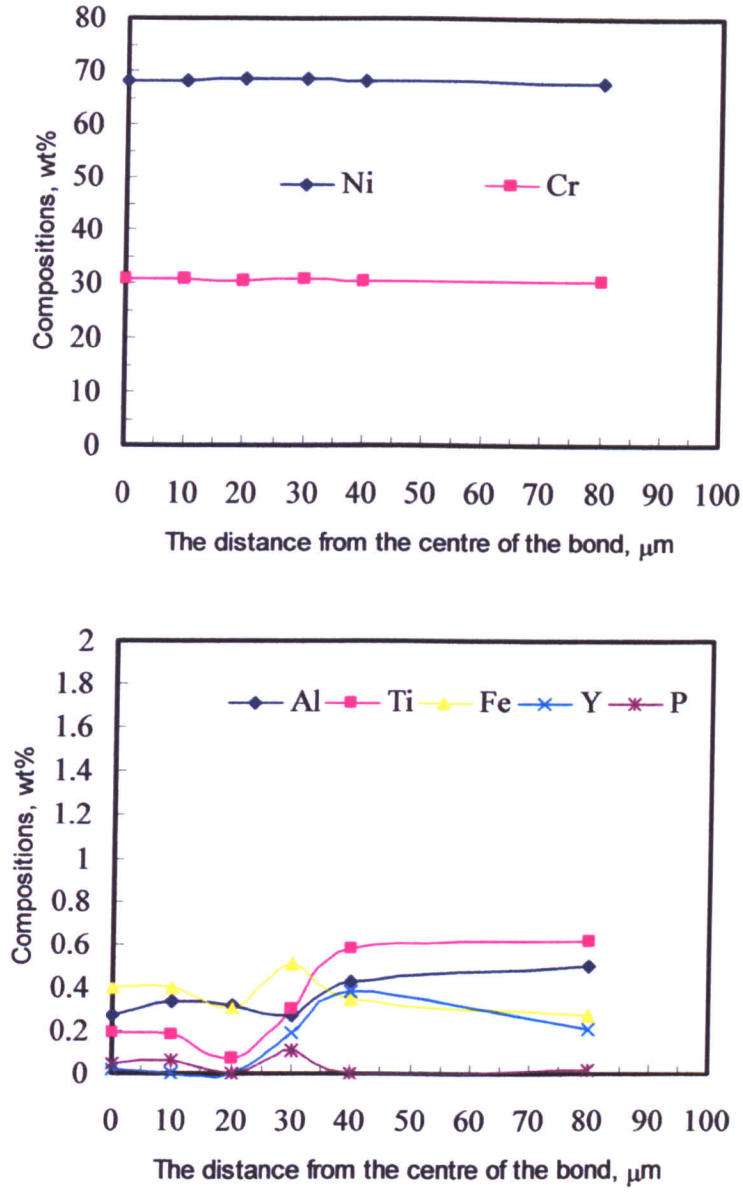

Figure 5-20 Composition profiles of the bond made with the parent alloy in the recrystallized state at 1000 °C with a hold time of 30 minutes using a bonding pressure of 1.58 MPa followed by a post-bond heat treatment at 1360 °C for 120 minutes.

5.4 The effect of Cr on the TLP bonding process.

The TLP bonding process involves the isothermal solidification of the liquid at a rate determined primarily by solid-state diffusion of melting point depressants from the liquid interlayer. In the simplest case, the parent alloy is a pure component, and forms an eutectic when in contact with the interlayer. However, in practice, the parent alloy and the interlayer will be made up of more than two components. For the most part, the literature makes only passing reference to the possible effects of a third component on the process of isothermal solidification [63, 121]. The experimental situation is reviewed, along with the analysis of the binary problem in an article by Kokawa *et al.* [76]. The process is considered as a sequence of distinct stages: heating to the bonding temperature, melting of the interlayer and dissolution of the parent alloy (melt-back), isothermal solidification, and homogenization. The usual treatment of the isothermal solidification stage is relatively simple for the case of bonding a pure element using an interlayer containing a solute, which lowers the melting point of the solvent. However, it is more complicated when dealing with a multi-component system. Microstructural developments in a multi-component system have been studied by Gale and Wallach [89]. Direct experimental evidence for the formation of an intermediate phase at the bonding temperature has been presented when bonding a nickel base alloy using a Ni-Si-B interlayer. Orel *et al.* [90] also observed boride formation in NiAl/Ni-Si-B/Ni joints. In previous studies, attention was given to the formation of intermediate phases and their effect on bonding behaviour. In the present study, the formation of phosphides is discussed, and the effect of high Cr content on the bonding process was studied.

Figure 5-21 shows a SEM micrographs of bond microstructures made at 1000 °C with a hold time of 30 minutes with the parent alloy in the recrystallized state. In the joint region, there are two distinct regions: the joint centre-line and a cluster of small grains on either side of the bond interface. There are precipitates present along the grain boundaries. This was made clearer at higher magnifications, as shown in Figure 5-22. EDX analysis shows that these precipitates were rich in P. It also shows that there was a higher Cr content and a lower Ni content when compared with the EDX data taken from the parent alloy, as seen in Chapter 4. As shown in Figure 5-24, the

elemental mapping of Figure 5-22 confirmed that the precipitates along the grain boundaries were Cr (Ni) phosphides. The formation of phosphides was found to occur during the dissolution and isothermal solidification stages because precipitates formed not only along the grain boundaries, but also within the parent alloy. Although the solubility of P in Cr is very limited (about 0 wt% at 1000 °C), the solubility of P in Ni-Cr is much higher (≥14 wt% P at 1000 °C). Kokawa *et al.* [76] did not discover phosphide when studying the TLP bonding of this Ni/Ni-4wt%Cr-10wt%P/Ni system. This suggested that a high Cr content (e.g. ~30 wt% as in this study) was necessary for the formation of phosphides. In order for such a high Cr content to build up within the liquid interlayer, a rapid diffusion of Cr from the parent alloy into the liquid interlayer is required. It is suggested that local equilibrium was not established across the solid/liquid interface, and Cr was free to diffuse from the parent alloy into the liquid interlayer immediately during melting of the parent alloy. The continuous Cr diffusion results in a P concentration in excess of the P solubility in Ni-Cr, which would then result in the formation of phosphides. The formation of phosphides reduces the concentration of P in the liquid interlayer and as a result accelerates isothermal solidification of the joint. This is consistent with the results by Blanc and Mevrel [122], who found that boron consumption as a result of boride formation accelerated the isothermal solidification process in TLP bonding of the Ni/Ni-Si-B/Ni system.

Figure 5-25 and Figure 5-26 show the difference between the microstructure of the joint centre-line and within the clustered grains. There was an absence of Y_2O_3 dispersoids within the joint centre-line. The even distribution of Y_2O_3 particles in the clustered grains is the same as that seen within the parent alloy, as shown in Figure 4-58. However, dissolution of the parent alloy was clearly observed, as shown in Figure 5-21. This suggested that during dissolution, the melted parent alloy retained an even distribution of Y_2O_3 dispersoids. This confirmed that the Y_2O_3 dispersoids within the ODS alloy have a very good stability when heating the alloy up to 1000 °C.

In this study, the nickel alloy contains a high Cr content and was bonded using a binary Ni-P system. This system allows us to observe the effects of P and Cr (from

the parent alloy, which raises the solidus temperature of the liquid interlayer) on the TLP bonding process.

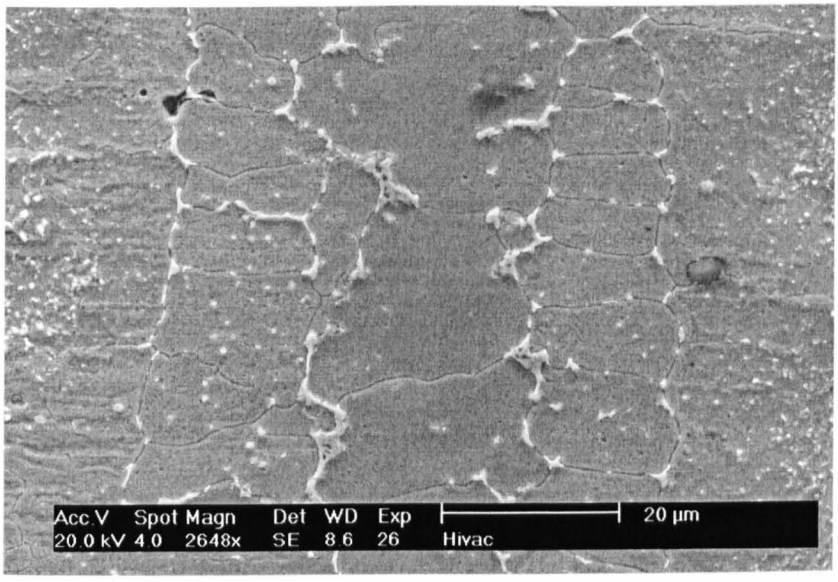

Figure 5-21 The microstructure of the bond made at 1000 °C with a hold time of 30 minutes with the parent alloy in the recrystallized state.

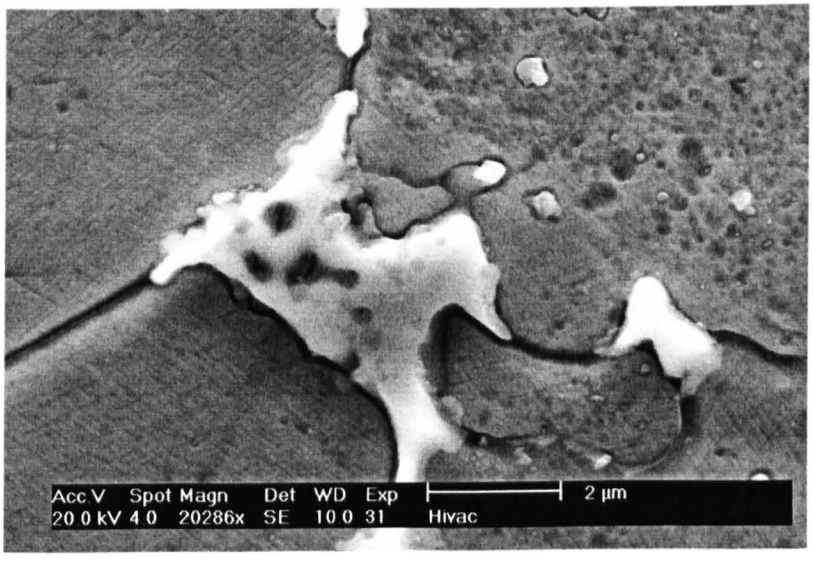

Figure 5-22 Participates along the grain boundaries.

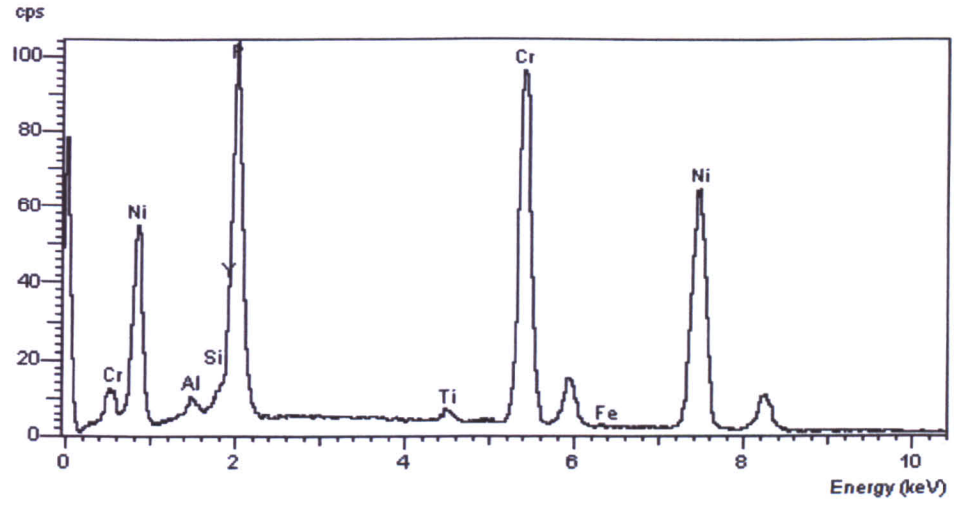

Figure 5-23 EDX spectrum on the precipitates along grain boundaries.

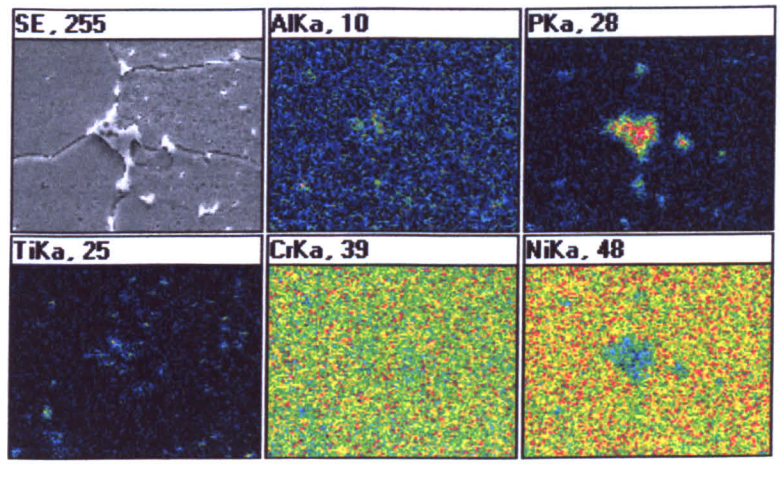

Figure 5-24 Elemental mapping of Al, P, Ti, Cr and Ni in Figure 5-22.

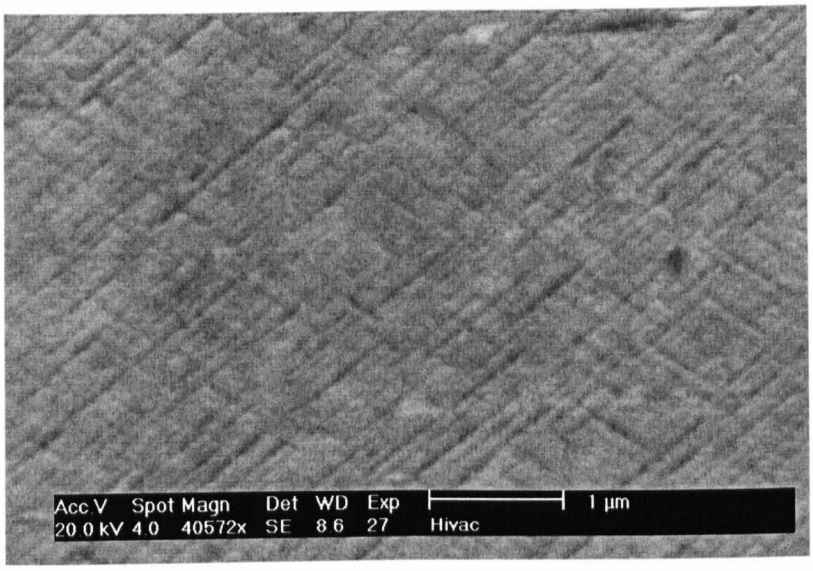

Figure 5-25 The grains within the joint centre-line.

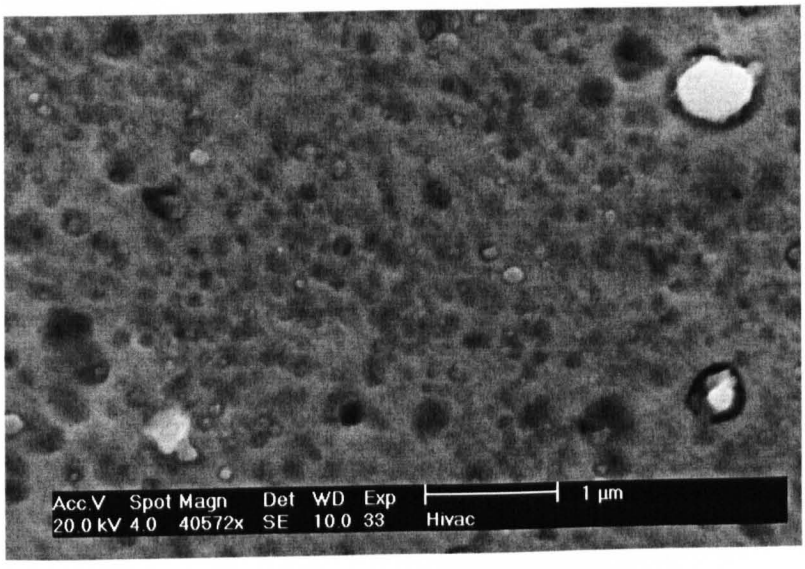

Figure 5-26 The clustered grains.

5.5 Summary.

TLP bonds were made using a Ni-P interlayer with the parent alloy in the fine-grained and recrystallized state, under applied pressure. The grain size of the parent alloy affects the TLP bonding process. Microstructural examination indicated that a thin joint width and less disruption to the parent grain structure was achieved when bonding the ODS alloy in the fine-grained state. The time for isothermal solidification was found to be shorter when compared with bonds made in the recrystallized state. Liquid penetration along grain boundaries of the parent alloy was observed with the parent alloy in the recrystallized state, which was attributed to the greater diffusivity of P along grain boundaries compared to that within the bulk alloys.

When pressure is applied during TLP bonding, the P-rich liquid phase is squeezed out of the joint. This helps to accelerate the isothermal solidification process and reduces the formation of phosphides which could embrittle joints.

High Cr content within the parent alloy plays an important role in bonding the ODS alloy using a Ni-P interlayer. The diffusion of Cr into the liquid interlayer has the affect of raising the solidus temperature, which not only accelerates the isothermal solidification process, but also reduces the extent of parent alloy dissolution.

Post-bond heat treatment homogenizes the microstructure and composition profiles across the joint region. For bonds made with the parent alloy in the fine-grained state, grains within the joint centre-line grew into the parent alloy. When bonds were made with the parent alloy in the recrystallized grain state, observations indicated that grains within the parent alloy grew into the joint.

Chapter 6 Conclusions and recommendations for further work.

6.1 Conclusions.

6.1.1 TLP bonding using a Ni-Cr-Fe-Si-B interlayer.

TLP bonding MA 758 ODS alloy using a Ni-Cr-Fe-Si-B interlayer was conducted at bonding temperatures of 1100 °C and 1200 °C.

The effects of the parent alloy grain structure on the TLP bonding process were significant. Firstly, recrystallization of grains adjacent to the joint centre-line was observed in bonds made with the parent alloy in the fine-grained state but was not found in bonds made with the parent alloy in the coarser-grained state. This was attributed to the stored strain energy within the grains of the alloy in the fine-grained state during the mechanical alloying process and the rapid diffusion of B from the interlayer into the parent alloy. Secondly, a smaller melt-back distance and faster isothermal solidification were achieved in TLP bonding the parent alloy in the fine-grained state. This was attributed to the contribution from the rapid diffusion of solutes in the grain boundaries. Thirdly, homogeneity of the bond was produced by carefully controlling the bonding conditions: 1100 °C with a hold time of 30 minutes followed by a post bond heat treatment at 1360 °C for 120 minutes. The bonding temperature and hold time will affect the recrystallization behaviour during the post-bond heat treatment. In general, a lower bonding temperature and shorter hold time produces a homogeneous recrystallized grain structure across the joint region during post-bond heat treatment.

The effects of the bonding temperature on the TLP bonding process have been observed. A higher bonding temperature produced much larger recrystallized grains adjacent to the centre-line of the joint. This caused the disruption to the parent alloy microstructure. Joining at a higher bonding temperature also enhanced the segregation of oxide dispersoids and therefore produced weaker joints. TLP bonding at a higher temperature (1200 °C) resulted in pore formation within the parent alloy, especially when joining the parent alloy in the recrystallized state. Therefore, TLP

bonding at 1200 °C is not a practical route for achieving good bond properties.

The most promising approach was to TLP bond the alloy in the fine-grained state followed by a post-bond heat treatment.

6.1.2 TLP bonding using a Ni-P interlayer.

MA 758 alloy has been TLP bonded using a Ni-P interlayer with the parent alloy in the fine-grained state and recrystallized states. A pressure was also applied during bonding.

When the alloy was bonded in the fine grain state, a thin bond-line was produced with negligible disruption to the microstructure of the parent alloy. When the alloy was bonded in the recrystallized state, the time required for isothermal solidification was longer and liquid penetration along grain boundaries of the parent alloy was observed.

A pressure applied during TLP bonding rejects the P-rich liquid phase out from the liquid interlayer. This helps to accelerate the isothermal solidification and reduces formation of phosphides.

A high content of Cr within the parent alloy plays a very important role in TLP bonding MA758 alloy using a Ni-P interlayer with respect to the formation of Cr(Ni) phosphides and in raising the solidus temperature of the liquid interlayer. This accelerates isothermal solidification and in turn reduces the degree of melt-back.

Post-bond heat treatment homogenizes the microstructure and composition profiles across the joint region. During the post-bond heat treatment, when the alloy was bonded in the fine-grained state, the grains within the joint centre-line grew into the parent alloy. When the alloy was bonded in the recrystallized grain state, grains within the parent alloy grew into the joint. The best bonds were obtained by joining the ODS alloy in the fine-grained condition and then inducing recrystallization across the joint region.

6.1.3 Particulate segregation during TLP bonding processes.

The results indicated that melting of Ni-Cr-Fe-Si-B interlayer had 3 stages. When bonding MA 758 alloy at 1100 °C, the interlayer was in the semi-solid-state. This can be useful reducing the bonding temperature and decrease the degree of disruption to the microstructure of the parent alloy. Also, it is thought that an increase in viscosity of the liquid interlayer when in the semi-solid state helps to produce segregation free joints.

Although grain size variations affect velocity of the solid/liquid interface, this would be insufficient to change the degree of particulate segregation along the joint interface when considering the ultra-fine Y_2O_3 particles which requires extremely high interface velocity.

When TLP bonding MA 758 alloy using a Ni-P interlayer, the oxide dispersoids remain stationary even when the interlayer melts and dissolution of the parent alloy starts. This confirms the effect of diffusion of Cr into the liquid interlayer resulting in increase in solidus temperature of the liquid interlayer and a very good structural stability of the parent alloy due to the dispersion strengthening of the Y_2O_3 particles. As a result, a segregation-free bond was produced.

6.2 Recommendations for further work.

Bonding MA 758 ODS alloy using a Ni-Cr-Fe-Si-B interlayer can produce a homogenized bond with an even dispersion of the Y_2O_3 strengthening particles. However, this research revealed that intermetallic phases such as Ni(Cr) borides were produced. The formation of these intermetallics is likely to affect the mechanical properties of the joints. It would be useful to carry out stress rupture tests at a high temperature, e.g. 1100 °C in the 'as-bonded condition' and then compare the results with the bonds in the heat-treated conditions.

The earlier reference work on the bonding process, especially on the isothermal solidification stage, yielded results with high values for the time to complete the solidification (especially in Ni/Ni-P/Ni systems containing Cr). However, in this study, much shorter times were observed for solidification and this was attributed to

the formation of intermetallic phases and the increase in the solidus temperature of liquid interlayer due to the diffusion of Cr from the ODS alloy into the liquid interlayer. More modelling work needs to be carried out regarding complicated systems in order to predict such values more accurately.

This research proposes a model for particulate segregation behaviour during TLP bonding. It is not possible to avoid particle segregation by increasing the velocity of the solid/liquid interface during isothermal solidification, by altering either the bonding temperature or the grain size of the parent alloy, because the extremely fine particle size of the dispersoids requires an extremely high interface velocity. This suggested that segregation-free bonds could only be made by increasing the viscosity of the liquid interlayer, using a semi-solid interlayer. Further research is necessary to identify suitable interlayer systems.

References:

1. R.F. Singer and G.H. Gessinger, Metall. Trans., 13A, 1982, 1463.
2. T.E. Howson, D.A. Mervyn, and J.K. Tien, Metall. Trans., 1980, 11A, 1599.
3. T.J. Kelly, in Proc. Conf. on Frontiers of High Temperature Materials, International Nickel Company, New York, 1981.
4. K.H. Holko, T.J. Moore, and C.A. Gyorgak, in Proc. Second Int. Conf. on Superalloys-Processing, MCIC, Seven Springs, Pennsylvania, 1972.
5. K.H. Holko and T.J. Moore, NASA TN D-6493, Sept. 1971.
6. K.H. Holko and T.J. Moore, NASA TN D-7153, Feb. 1973.
7. T.J. Moore and K.H. Holko, Welding J., Research Supplement, 1970, 49, 395s.
8. W.A. Owczarski and D.S. Duvall, in Proc. Conf. New Trends in Mat. Processing, American Society for Metals, Oct., 1974.
9. T.J. Kelly, US Pat. 4444 587, February 1983.
10. T.I. Khan and E.R. Wallach, J. Mater. Sci., 1995, 30, 5151-5160.
11. L.E. Shoemaker, in Proceedings of the International Conference on Trends in Welding Research, ed. S.A. David, ASM International, Gatlinburg, Tennessee, May 1986, 371.
12. R.W. Messler, Joining of Advanced Materials, Butterworth-Heinemann, USA, 1995.
13. T.W. Eager, in Proceedings of the International Conference Held in Montreal, Canada, 1990, Pergamon Press, New York, USA, 3-14.
14. W. Betteridge and S.W.K Shaw, Mater. Sci. & Techn., 1987, 3, 682-694.
15. C.T. Sims and W.C. Hagel (eds.), The Superalloys, IX, 1972, Wiley, New York.
16. J.S. Benjamin, Metall. Trans., 1970, 1, 2943-2951.
17. B.A. Ewing, Superalloys 1980, ed. J.K. Tien *et al.*, American Society for Metals, Metals Park, Ohio, 1980, 169.
18. Y.G. Kim and H.F. Merrick, NASA CR-159493, May 1979.
19. C.J. Burton, S. Baranow, and J.K. Tien, Metall. Trans., 1979, 10A, 1297.

20. M.P. Anderson, J.Y. Koo, and R. Petcovic-Luton, in Proc. American Ceramic Society-AIME Powder Processing Symposium, 1981, 155.
21. G.H. Gessinger, Metall. Trans., 1976, 7A, 1203.
22. R.L. Cairns, L.R. Curwick, and J.S. Benjamin, Metall. Trans. 1975, 6A, 179.
23. G.A.J. Hack, Metals & Mater., 1987, 3, 457-462.
24. J.J. Fischer, J.J. deBarbadillo, and M.J. Shaw, Heat Treating, 1991, 23, (5), 15-16.
25. Powder Metal Technologies & Applications, ASM Handbook, Vol. 7, ASM International, 1998, 85.
26. G.H. Gessinger and R.F. Singer, Powder Metallugy of Superalloys, ed. G.H. Gessinger, Butterworths, London, 1984, 213-292.
27. J.S. Benjamin, Metall. Trans., 1970, 1, 2943.
28. H.S. Ubhi, T.A. Hughes, and J. Nutting, in Frontiers of High Temperature Materials, ed. J.S. Benjamin, Inco MAP, New York, 1981, 33.
29. J.H. Hausselt and W.D. Nix, Acta Met., 1977, 25, 595.
30. W.L. Kimmerle, V.C. Nardone, and J.K. Tien, Metall. Trans. A, 1986, 18A, 1029-1033.
31. J.D. Whittenberger, Metall. Trans., 1981, 12A, 845.
32. R.L. Cairns and J.S. Benjamin, J. Eng. Mat. Techn., 1973, 95, 10.
33. R.J. Henricks, in Frontiers of High Temperature Materials, ed. J.S. Benjamin, Inco MAP, New York, 1981, 63.
34. G.E. Linnert, Welding Metallurgy, Vol. 1&2, American Welding Society, 1967.
35. Welding, Brazing, and Soldering, ASM Handbook, Vol. 6, ASM International, 1993.
36. A.F. Stephen, Machine Design, 1982, 21, 95.
37. L.E. Shoemaker, Proc. An Intern. Conf. Trends in Welding Research: Advances in Welding Sci. & Technol., ed. S.A. David, 1986, Gatlinburg, TN, USA, ASTM.
38. Welding Handbook, R.L. O'Brien (ed.), Vol.2, Amer. Weld. Soc., 1995.

39. D.T. Bushby, Unpublished Research, Wiggin Alloys Limited, Hereford, England.
40. J.E. Franklin, Unpublished Research, Paul D. Merica Research Laboratory/International Nickel Company, Suffern, NY, USA.
41. T.J. Kelly, Proc. 2nd Int. Conf. on Oxide Dispersion Strengthened Alloys by Mechanical Alloying, ed. J.S. Benjamin and R.C. Benn, Inco Alloys International, 1983, 129-148.
42. H.D. Hedrich, H.G. Mayer, G. Haufler, M. Koph, and N. Reheis, ASME 91-GT-411, The International Gas Turbine and Aeroengine Congress and Exposition, Orlando, FL, American Society of Mechanical Engineers, 1991.
43. P.A. Molian, Y.M. Yang, and P.C. Patnaik, J. Mater. Sci., 1992, 27, 2687-2694.
44. J.E. Franklin, Internal Inco Report, August 6, 1976.
45. J.E. Franklin, Internal Inco Report, August 19, 1975.
46. T.J. Kelly, Trends in Welding Research, American Society for Metals, 1982, 16-18.
47. T.J. Moore, Welding J., 1972, 51, 253.
48. I.A. Bucklow, S.B. Dunkerton, and P.L. Threadgill, TWI Report, 1996.
49. C.Y. Kang, T.H. North, and D.D. Perovic, Metall. Mater. Trans. A, 1995, 27A, 4019-4029.
50. T.J. Kelly, Unpublished Research, Paul D. Merica Research Laboratory/International Nickel Company, Suffern, NY, USA.
51. T.J. Moore and T.K. Glasgow, Welding J., 1985, 64, (8), S219-S226.
52. I.A. Bucklow, in Proceedings of the International Conference Held in Montreal, Canada, 1990, Pergamon Press, New York, USA, 299-305.
53. W.D. MacDonald and T.W. Eagar, An Rev. Mater. Sci., 1992, 22, 23-46.
54. D.S. Duvall, W. A. Owcarski, and D.F. Paulonis, Welding J., 1974, 4, 203.
55. A.E.Dary, PhD Dissertation, University of Cambridge, 1985.
56. E.R. Maddrell and E.R Wallach, in Proc. Conf. 'Recent trends in welding science and technology', ed. S.A David. & J.M Vitek, 1990, Materials Park, OH, ASM International.

57. T.J. Moor and J.M. Kalinowski, in MRS Symp. Proc. On 'High temperature ordered intermetallic alloys V', ed. I. Baker *et al.*, 1993, Pittsburgh, PA., Materials Research Society, 288, 1173-1178.
58. M.J. Strum and G.A Henshall, in Proc. Conf. 'Advanced joining technologies for new materials II', ed. N.F. Flore and J.O Stiegler., 1994, Miami, FL, American Welding Society, 76-88.
59. S.V.Orel, L. Parous, and W.F. Gale, ibid., 5-9.
60. R. Thamburaj, W. Wallace, and J.A. Golddak, Int. Met. Rev., 1983, 28 (1), 1-22.
61. X.H. Li, W. Mao, and Y.Y. Cheng, Transactions of Nonferrous Metals Society of China, 2001, 11, 405-408.
62. W.F. Gale, Y. Guan, and S.V. Orel, Int. Mater. Prod. Technol., 1998, 13, 1-12.
63. W.D. MacDonald and T.W. Eagar, The Metal Science of Joining, ed. M.J. Cieslak *et al.*, TMS International, 1992.
64. I. Tuah-Poku, M. Dollar, and T.B. Massalski, Metall. Trans. A, 1988, 19A, 675-686.
65. Y. Zhou and T.H. North, Model. Simul. Mater. Sci. Eng., 1993, 1, 505-516.
66. J.T. Niemann and R.A. Garret, Weld. J., 1974, 52, 175-184.
67. Z. Li, W. Fearis and T.H. North, Mater. Sci. Techn., 1995, 11, 363-369.
68. S.N. Omenyi and A.W. Neumann, J. Applied Physics, 1976, 47, 3956.
69. D.M. Stefanescu, B.K. Dhindraw, S.A. Kacar, and A. Moitra, Metall. Trans. A, 1988, 19A, 675-686.
70. A. Urena, J.M. Gomez De Salazar, and M.D. Escalera, Key Engineering Materials, 1995, 523-540.
71. D. Shanguan, S. Ahija, and D.M. Stefacescu, Metall. Trans. A, 1992, 23 A, 669.
72. D.M. Stefanescu, B.K. Dhindaw, S.A. Kacar, and A. Moitra, Metall. Trans. A, 1988, 19A, 2847.
73. Y. Zhai and T.H. North, J. Mater. Sci., 1997, 32, 5571-5575.
74. A.A. MacFayden, R.R. Kapoor, and T.W. Eagar, Weld. J. (Suppl.), 1990, 11, 339s.

75. Z. Li, Y. Zhou and T.H. North, J. Mater. Sci., 1995, 30, 1075-1082.
76. H. Kokawa, C.H. Lee, and T.H. North, Metall. Trans. A, 1991, 21A, 1627-1631.
77. A. Rabinkin and S. Pounds, Weld. J., 1988, 67, 33-44.
78. R. Dammer, in Beitrag zur Bewertung Mechanischer Eigenschaften Hochtemperaturgelöteter Superlegierungen, Deutscher Verlag für Schweißtechnik (DVS), Düsseldorf, 1986, 61-66.
79. M.S. Yeh and T.H. Chuang, Metall. Mater. Trans. A, 1997, 28A, 1367.
80. A.A. Shirzadi and E.R. Wallach, Trends in Welding Research, Pro. 4th Int. Conf., 5-8 June, 1995, Gatlinburg, Taxas.
81. A.A. Shirzadi and E.R. Wallach, Sci. & Techn. of Welding & Joining, 1997, 2, (3), 89-94.
82. A.A. Shirzadi and E.R. Wallach, Mater. Sci. Techn., 1997, 13, 135-142.
83. N.L. Peterson, Int. Met. Review, 1983, 28, 65-91.
84. K. Ikeuchi, Y. Zhou, H. Kokawa, and T.H. North, Metall. Trans. A, 1992, 21A, 2905.
85. W.W. Mullins, J. Appl. Phys., 1957, 28, 333-339.
86. W.W. Mullins, Trans. AIME, 1960, 218, 354-361.
87. K. Ikeuchi, Y. Zhou, H. Kokawa, and T.H. North, Metall. Trans. A, 1993, 23A, 2905-2915.
88. K.Saida, Y. Zhou, and T. H. North, J. Jpn Inst., Met., 1994, 58, 810-818.
89. W. F. Gale and E.R. Wallach, Metall. Trans., 1991, 22A, 2451–2457.
90. S.V. Orel, L. Parous, and W. F. Gale, Weld J., 1995, 74, 9, 319s–324s.
91. J.R. Askew, Ph.D. Thesis, Brunel University, June 2000.
92. J.R. Askew and T.I. Khan, Mater. Sci. & Techn. 1998, 14, 920-924.
93. Inco Alloys International, Inclonel Alloy MA758, Inclo Alloys International Publications No. IAI-126
94. G.R. Purdy and Y.J.M. Bayananda, 1988, 161-189, Warrendale, PA TMS.
95. K. Aust and B. Chalmers, Metall. Trans., 1970, 1, 1095-1104.
96. T.I. Khan and E.R. Wallach, in proc. Con. On 'Trends in Welding Research', Gatlinburg, TN, USA, June 1992, American Welding Society, 1095-1099.

97. E.A. Brandes and G.B. Brook, Smithells Metals Reference Book, 7th ed., 11-7 to 11-485, Butterworth-Heinemann.
98. T.I. Khan and E.R. Wallach, J. Mat. Sci., 1996, 31, 2937-2943.
99. A. Ekrami and T.I. Khan, Materials Sci. Techn., 1999, 15, 946-950.
100. W. Sha and H. K. D. H. Bhadeshia, J. Mat. Sci., 1995, 30, 1439-1444.
101. J. W. Hinze, J. Appl. Phys., 2000, 88, 2443-2450.
102. M.M. Baloch and H.K.D.H. Bhadeshia, Mat. Sci. Techn., 1990, 6, 1236-1245.
103. C.P. Jongenburger and R.F. Singer, Proc. of DGM Conference on New Materials by Mechanical Alloying Techniques, ed. E. Arzt and L. Schultz, Stuttgart and Erlangen,1988.
104. Z. Zhou, Z. Fan, H.X. Peng, and D.X Li, Mater. Sci. Tech., 2000, 16, 908-912.
105. J. Cermak, Phys. Status Solidi, A, 1990, 120, 351-361.
106. Binary Phase Diagram, ed. B. Thaddeus, *et al.,* American Society for Metals, Metals Park, Ohio, 1986.
107. G. Korb, Proc. of DGM Conference on New Materials by Mechanical Alloying Techniques, ed. E. Arzt and L. Schultz, Stuttgart and Erlangen,1988.
108. Y.G. Kim and H.F. Merrick, in Superalloys 1980, ed. J.K. Tien *et al.,* American Society for Metals, Metals Park, Ohio, 1980, 75.
109. D.F. Pausonis and W.A. Owczarski, in Proc. of The PM Superalloy Technology Seminar, PM80, MPIF/American Powder Metallurgy Institute, June 1980.
110. Y.G. Kim and H.F. Merrick, in Superalloys 1980, ed. J.K. Tien *et al.,* American Society for Metals, Metals Park, Ohio, 1980, 75.
111. J.C. Pivin, D. Delaunay, C. Roques-Carmes, A.M. Huntz, and P. Lacombe, Corrosion Science, 1979, 20, 351-373.
112. E.O. Hall,Proc. Phys. Soc. London, B64, 1951, 747.
113. N. J. Petch, J. Iron Steel Inst., 1953, 174, 25.
114. Z. Li, Y. Zhou, and T.H. North, J. Mat. Sci., 1995, 30, 1075-1982.

115. T. Enzo, K. Ikeuchi, Y. Murakami, and N. Suzuki, Trans. JWRI 16, 1987, 285.

116. M.B.D. Ellis, Int. Mater. Rev., 1996, 41, 2. 41-58.

117. A. A. McFayden, R.R. Kapoor, and T. W. Eager, Weld. J. 11, 1990, 399.

118. D.P. Spencer, R. Mechrabian, and M.C. Flemings, ibid, 1972, 3, 1925-1932.

119. H. Nakagawa, C.H. Lee, and T.H. North, ibid, 1991, 22A, 543.

120. Y. Zhou, W.F. Gale, and T.H. North, International Mater. Reviews, 1995, 40, 5, 181-196.

121. C.W. Sinclair, J. Phase Equilibria, 1999, 20, 361–369.

122. A. Le Blanc and P. Mevrel, in Proc. Conf. 'High temperature materials for power engineering', ed. E. Bachelet *et al.*, 1451–1460, 1990, Dordrecht, The Netherlands.